

# Study on Microwave Propagation through Human Body

著者	LI YANG
学位授与機関	Tohoku University
学位授与番号	11301甲第17745号
URL	<a href="http://hdl.handle.net/10097/00122161">http://hdl.handle.net/10097/00122161</a>

博士学位論文

Study on Microwave Propagation  
through Human Body  
(人体内外間のマイクロ波伝搬に関する  
研究)

Li Yang

李 揚

東北大学大学院 工学研究科  
通信工学専攻

## Abstract

In the dissertation, the microwave propagation through human body is investigated. In order to design wireless capsule endoscope (WCE) system, the propagation loss through human body is studied. Finite-difference time-domain (FDTD) method is used in the numerical analysis. In order to confirm the simulation results, differential-mode S-parameter method is also used in the experiment, good agreement between numerical and experimental results is obtained.

Moreover, transmission factor under the complex-conjugate matching condition is used as an indicator of propagation loss. EM-wave propagate through a human body phantom is investigated in the frequency range 200 MHz to 2 GHz. The transmission characteristics of a dipole to dipole and a loop to loop through the torso-shaped phantom filled with deionized water or human body equivalent liquid (HBEL) are investigated by the numerical analysis and the measurements. It is found that the transmission factor  $\tau$  decreases as the conductivity increases in the case of dipole antenna placed in deionized water. On the other hand, there is a local maximum in the transmission factor  $\tau$  at a frequency in the case of HBEL. The local maximum is caused by the half-wavelength resonant frequency of inside antenna. It is important to choose operating frequency in capsule antenna design. It is found that the media loss is large in the high frequency range, while the antenna efficiency is low in the low frequency range. Operating frequency of wireless capsule endoscope system can be decided by using transmission factor. However, if operating frequency is decided, size of dipole antenna can be changed in order to decrease the propagation loss. The transmission factor in the case of loop to loop is also investigated.

Furthermore, transmission factor through in-homogenous human body phantom is investigated. The effect of high conductivity human body organs is appeared. Compared with homogenous huamn body phantom, some different results are obtained through in-homogenous human body phantom. In wireless capsule endoscope system, select the optimal position and polarization of outside antenna can decrease the propagation loss through human body.

In addition, design of capsule dipole and loop antennas are discussed by using the

transmission factor. A capsule dipole to dipole system and a capsule loop to loop system are compared: for for dipole to dipole the local maximum of transmission factor in the frequency domain is appeared, while for loop to loop the large value of transmission factor in low frequency is appeared. It has been observed that when a dipole or a loop antenna is implemented on the surface of the capsule, it is easy to achieve impedance matching without matching circuits and also has a large value of  $|S_{21}|$ . An inner-layer capsule dipole antenna (ICDA) is proposed to obtain both impedance matching and low propagation loss.

**Key words:** propagation loss, wireless capsule endoscope (WCE), capsule antenna, Finite-difference time-domain (FDTD) method, differential-mode S-parameter method, dipole to dipole, loop to loop, human body equivalent liquid (HBEL), transmission factor, homogenous phantom, in-homogenous phantom, dispersive effect

# Contents

<b>Abstract</b>	<b>i</b>
<b>1 Introduction</b>	<b>1</b>
1.1 Wireless capsule endoscope system . . . . .	1
1.2 Capsule antenna . . . . .	3
1.3 Previous researches on propagation loss through human body . . . . .	4
1.4 Motivation of this research . . . . .	5
1.5 Organization of this dissertation . . . . .	7
<b>2 Simulation and experiment methods</b>	<b>9</b>
2.1 Introduction . . . . .	9
2.2 Numerical analysis: FDTD method . . . . .	10
2.3 Measurement: differential-mode S-parameter method . . . . .	11
2.4 Experiment results and observations . . . . .	11
2.5 Conclusion . . . . .	12

---

<b>3</b>	<b>Propagation loss through homogenous human body phantom</b>	<b>22</b>
3.1	Introduction . . . . .	22
3.2	Numerical analysis and experiment setup . . . . .	24
3.3	Definition of transmission factor . . . . .	26
3.4	Transmission factor through human body: dipole to dipole . . . . .	30
3.5	Transmission factor and antenna radiation efficiency . . . . .	31
3.6	Transmission factor through human body: loop to loop . . . . .	33
3.7	Conclusion . . . . .	50
<b>4</b>	<b>Propagation loss through in-homogenous human body phantom</b>	<b>53</b>
4.1	Introduction . . . . .	53
4.2	Analysis model . . . . .	54
4.3	Numerical analysis and observations . . . . .	56
4.4	Conclusion . . . . .	61
<b>5</b>	<b>Capsule antenna design</b>	<b>65</b>
5.1	Comparison between capsule dipole and capsule loop system . . . . .	65
5.2	Study on the capsule antenna offset . . . . .	68
5.3	Study on the position of antenna . . . . .	68
5.4	Inner-layer capsule dipole antenna . . . . .	70
5.5	Conclusion . . . . .	71

<b>6 Conclusions</b>	<b>85</b>
<b>Bibliography</b>	<b>88</b>
<b>Publications</b>	<b>94</b>
<b>Acknowledgement</b>	<b>96</b>

# List of Tables

1.1	Main existing commercial wireless capsule endoscope. . . . .	3
1.2	Main existing commercial capsule endoscope. . . . .	5
4.1	Generic dispersive fitting data . . . . .	57
4.2	Typical positions and transmission factors of digestive system. . . . .	63
4.3	Comparison between homogenous phantom and in-homogenous phantom. .	64



# List of Figures

1.1	Wireless capsule endoscope for medical diagnostics. . . . .	3
1.2	Propagation loss model. . . . .	6
1.3	Organization of this dissertation. . . . .	8
2.1	Attenuation in media (in the case of plane-wave). . . . .	14
2.2	Reflection on the interface (in the case of plane-wave). . . . .	15
2.3	Analysis model of dipole antenna in deionized water. . . . .	16
2.4	Relative permittivity and conductivity of deionized water. . . . .	16
2.5	Experimental results of dipole antenna with balun structure. . . . .	17
2.6	Experimental setup of differential-mode S-parameter method. . . . .	18
2.7	Reflection coefficient of dipole antenna in deionized water. . . . .	19
2.8	Input impedance of dipole antenna in deionized water. . . . .	20
2.9	$ S_{21} $ from inside dipole through deionized water to the outside dipole. . . . .	21
3.1	Homogenous torso-shaped phantom. . . . .	23
3.2	Relative permittivity and conductivity of HBEL. . . . .	23

---

3.3	Human torso-shaped model with dipole antennas. . . . .	27
3.4	Input impedance of dipole antenna immersed in deionized water. . . . .	28
3.5	Input impedance of dipole antenna immersed in HBEL. . . . .	29
3.6	Calculated $\lambda_g$ and $l_1/\lambda_g$ by using plane wave formula. . . . .	34
3.7	Reflection coefficient $ S_{11} $ . . . . .	35
3.8	$ S_{21} $ from inside dipole through torso-shaped phantom to the outside dipole. . . . .	36
3.9	Reflection coefficient $ S_{22} $ . . . . .	37
3.10	Two-port equivalent circuit. . . . .	37
3.11	Transmission factor of dipole to dipole through torso-shaped phantom. . . . .	38
3.12	Transmission factor of inside dipole immersed in different liquids. . . . .	39
3.13	Calculated transmission factor with change the length of inside dipole. . . . .	40
3.14	Calculated transmission factor with change the length of outside dipole. . . . .	40
3.15	Analysis model of radiation efficiency simulation. . . . .	41
3.16	Numerical analysis results of antenna radiation efficiency. . . . .	42
3.17	Analysis model of transmission factor simulation. . . . .	43
3.18	Numerical analysis results of transmission factor. . . . .	44
3.19	Numerical model and experiment setup of loop to loop antenna. . . . .	45
3.20	$ S_{11} $ of inside loop antenna immersed in deionized water and in HBEL. . . . .	46
3.21	Input impedance of loop antenna immersed in deionized water. . . . .	47
3.22	Input impedance of loop antenna immersed in HBEL. . . . .	48

---

3.23	Reflection coefficient $S_{22}$ and impedance of outside loop antenna $Z_{22}$ . . . . .	49
3.24	$ S_{21} $ from inside loop through torso-shaped phantom to the outside loop. . . . .	51
3.25	Transmission factor of loop to loop through torso-shaped phantom. . . . .	52
4.1	Homogenous phantom and in-homogenous phantom. . . . .	54
4.2	Analysis model of in-homogenous phantom. . . . .	55
4.3	Transmission factor (inside dipole is placed in esophagus). . . . .	58
4.4	Near-field and far-field when the inside dipole is placed in the esophagus. . . . .	59
4.5	Transmission factor (inside dipole is placed in stomach). . . . .	60
4.6	Transmission factor (inside dipole is placed in small intestine). . . . .	61
4.7	Transmission factor (inside dipole is placed in large intestine). . . . .	62
5.1	Geometry of capsule antennas. . . . .	67
5.2	Analysis model of capsule antenna systems. . . . .	73
5.3	Transmission factors of capsule dipole system and capsule loop system through torso-shaped phantom. . . . .	74
5.4	Relative received power from the capsule antenna to the outside antenna. . . . .	74
5.5	Analysis model of capsule antenna $\Delta z$ . . . . .	75
5.6	Transmission factors when position of capsule antenna is offset from the outside antenna in the $-z$ direction (function of frequency). . . . .	76
5.7	Transmission factors when position of capsule antenna is offset from the outside antenna in the $-z$ direction (function of offset $\Delta z$ ). . . . .	77

5.8	Geometry of capsule dipole antennas. . . . .	78
5.9	$ S_{11} $ of capsule dipole antenna in HBEL. . . . .	78
5.10	Input impedance of capsule dipole antenna in HBEL. . . . .	79
5.11	$ S_{21} $ from capsule antenna through torso-shaped phantom to the outside antenna. . . . .	80
5.12	Transmission factor from capsule antenna through torso-shaped phantom to the outside antenna. . . . .	81
5.13	Geometry of proposed ICDA. . . . .	81
5.14	$ S_{21} $ from the proposed ICDA through torso-shaped phantom to the outside antenna. . . . .	82
5.15	Transmission factor from the proposed ICDA through torso-shaped phantom to the outside antenna. . . . .	83
5.16	Relative received power from the proposed ICDA to the outside antenna. . . . .	84

# Chapter 1

## Introduction

### 1.1 Wireless capsule endoscope system

Many countries such as Japan and China experience the effects of an aging population, which results a strong demand of human body healthcare facilities. It is necessary to develop novel biomedical technologies to improve diagnostic services for this demographic. Electrical diagram (ECG) and temperature recording have been used for more than 50 years in medical diagnosis to understand various biological activities [1-3]. EM-wave through human body was also studied [4, 5]. Generally, the electronic pill system can be divided to three types [6]:

Type 1: Traditional electronic sensor

Traditional telemetry systems for the electronic pill technology were performed in [7, 8]. This type devices do not require a high data rate, for the reason that physiological parameters (such as pH-value or temperature) are slowly varying and hence low-frequency signals. Simple modulation schemes, (such as OOK or ASK) with a low data rate are used for low power consumption. In [7], the electronic pill transfers physiological data, including pH-value and temperature. In [8], the electronic pill tests blood pressure sensors and a transmission range of 5 m was reported.

Type 2: Multipurpose robotic system

Multipurpose robotic systems were performed in [9-18]. This type devices has locomotion features or transmitting energy by using wireless power transfer (WPT) technology. In [10], the device can be used for precise drug delivery in the human gastrointestinal tract. Real-time wireless energy transfer via magnetic coupling is necessary for these types of endoscopes to provide mechanical function. In [11], the capsule can be move up and down inside human body by using an electric stimulation technique. Researches on wireless power transfer through human body were performed in [14-18], The purpose of these researches are design capsule robotic system without battery. The SAR in the human body generated by a magnetic resonant WPT system operating above 10 MHz is studied in [14].

### Type 3: Wireless capsule endoscope system

The first commercial wireless capsule endoscope was proposed by G. Iddan and the company Given Imaging [19], the pill uses the Zarlink's radio frequency (RF) chip for wireless transmission in the medical implant communication service (MICS) band (402-405 MHz). The wireless capsule endoscope system uses a wireless transceiver to obtain medical images of the inside of the human body [19-21], as shown in Figure 1, the EM-wave from the capsule propagate through human body and received by the remote antenna outside the human body. This type devices require a high-frequency telemetry link in order to obtain a better resolution. In [21], the devices demonstrated a prototyping system to achieve a high data rate transmission (2 Mb/s) for higher image resolution. This systems enabled an image resolution up-to 15-20 frames/s.

Recently some commercial wireless capsule endoscope systems were proposed [22-25], as shown in Table 1.1. Company Given Imaging [22], MEDIATORS [23], Olympus [24] and JINSHAN [25] are focus on the development of wireless capsule endoscope system. In case Pillcam®SB3 developed by Given imaging, adaptive frame rate technology allows the system to sense when the capsule is moving quickly and automatically increases the image capture rate is 2-6 frames/s [22]. In case MiroCam®developed by MEDIATORS provided 12 hour operation time effectively mitigates this concern, while the image capture rate is 3 frames/s [23]. In case ENDOCAPSULE®EC-10 developed by Olympus sees 10% more mucosa than other capsule endoscopy platforms with a 160 degree wide-angle field of view [24]. From Table 1.1, the results are obtained:

1. Bandwidth of existing capsule antenna is narrow.

2. Frame rate of existing capsule endoscopy is low.
3. It is required to develop efficient antennas for capsule to further improve frame rate.

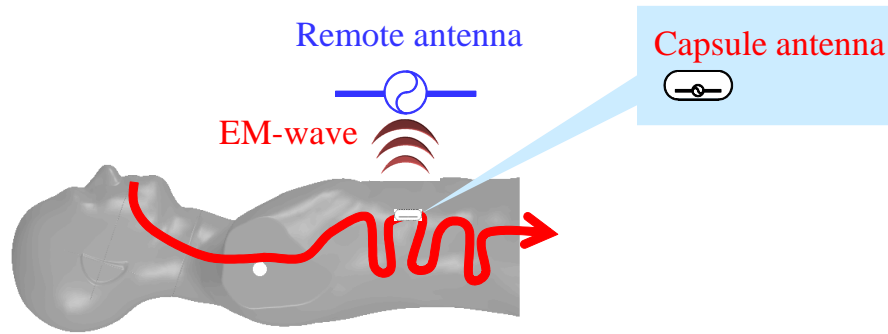






Figure 1.1: Wireless capsule endoscope for medical diagnostics.

Table 1.1: Main existing commercial wireless capsule endoscope.

Name	Frequency [MHz]	Bandwidth [MHz]	Modulation	Operating Time[h]	Dimensions [mm]	Frame Rate [frames/s]
Pillcam® SB 2 	434.1	1.6	MSK	8	$26.3 \times \varphi 11.4$	NA
Pillcam® SB 3 	434.1	6.5	MSK	11	$26.2 \times \varphi 11.4$	2-6
ENDOCAPSULE® 10 	315	2.25	FSK	12	$26 \times \varphi 11$	2
MiroCam® 	NA	NA	NA	12	$24.5 \times \varphi 11$	3

## 1.2 Capsule antenna

High-efficiency antennas for wireless capsule endoscope system have been studied by many researchers [26-40]. Generally, a capsule has a maximum length of 20 mm and a maximum

diameter of 10 mm [19], and it is considered that the transmitting power of antennas is extremely low caused by its physical size. The size of the antenna decides the operating frequency. Furthermore, the absorption of electromagnetic waves by the internal organs is quite large caused by high conductivity of the internal organs with frequency dependent characteristics.

The developed capsule antenna were shown in Table 1.2. From Table 1.2, the results are obtained:

1. Study was limited to single frequency, and frequency dependence on antenna performance was not clarified.
2. Most of proposed antennas are electrically small antennas.
3. For any shape of small antenna, radiation efficiency is proportional to electrical volume [51].

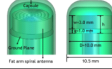
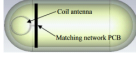

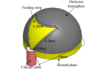
Selection of antenna type such as dipole antenna or loop antenna, is important to decrease propagation loss between the capsule antenna and the antenna outside of the human body. In previous studies, several kinds of antennas were proposed for implantable applications. Operating frequency of antennas is different such as 400-500 MHz in [26-32], the center frequency of 920 MHz in [33], the center frequency of 1.4 GHz in [34, 35], or with the UWB band in [36-38]. Finding a suitable frequency band for high efficiency transmission for the capsule endoscope system is quite important.

### **1.3 Previous researches on propagation loss through human body**

Estimation of the RF-link budget is essential in the capsule endoscope communication systems. Path loss through the human body was presented by several different expressions [41-46]. In [41], the electric field attenuation along the coordinate axes was used to express path loss. The receiving antenna was considered in [42, 43] and  $|S_{21}|$  was used to express the path loss. In [44], the difference of  $|S_{21}|$  with and without the human body was used for the definition of transmission loss.



Table 1.2: Main existing commercial capsule endoscope.

<i>Reference</i>	$f$ [MHz]	$W(D) \times L$ [mm]	$\lambda_0$ [mm]( $c/f$ )	$L/\lambda_0$	$L/\lambda_g$	Small antenna
Lee et. al., 2010 	450	$3 \times 10.1$	667	0.005	0.109	○
See et. al., 2011 	915	$5 \times 4.2$	328	0.015	0.028	○
Izdebski et. al., 2009 	1400	$5.9 \times 9.6$	210	0.058	0.107	○
Wang et. al., 2010 	3500	$5 \times 8.5$	600	0.028	0.156	○

Previous researches focus on the received power while without considering the mismatching in the propagation. The propagation loss is composed of return loss and attenuation in media, as shown in Figure 1.2, Return loss and attenuation in media were not separated for evaluating the antenna performance and loss in media in these researches [41-43]. The return loss of transmitting and receiving antenna were not excluded from the propagation loss.

## 1.4 Motivation of this research

The motivation of this research is to study a methodology to develop a wireless capsule for medical diagnostics with high transmission efficiency.

1. Investigate characteristics of dipole and loop antennas in capsule. In this research, a pair of dipole and a pair of loop antennas were placed inside and outside a torso-shaped phantom used, respectively, and the propagation loss was evaluated by both the numerical and the experimental method to select the suitable antenna type.

2. Investigate propagation loss excluding impedance-mismatching loss. The transmission factor is used as an indicator of propagation loss. The transmission factor is

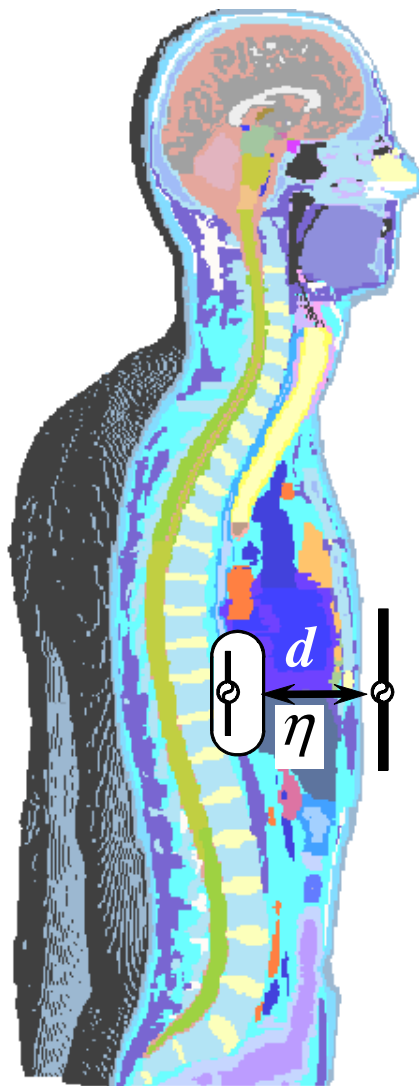


Figure 1.2: Propagation loss model.

the relative maximum received power under the condition that the complex-conjugate matching conditions are satisfied at both transmitting and receiving ports.

3. Investigate propagation loss over a wideband frequency domain to obtain the suitable operating frequency.

4. Investigate propagation loss when capsule is inside some organs. The propagation loss from a dipole antenna placed in a digestive system of a human body to the outside was investigated by using the FDTD analysis.

## 1.5 Organization of this dissertation

The dissertation is organized as follows:

Chapter 1: This chapter presents the introduction of this research. Wireless capsule endoscope (WCE) system is introduced in Section 1.1. Capsule antenna is introduced in Section 1.2. Previous researches on propagation loss through human body are summarized in Section 1.3. The motivation of the dissertation is shown in Section 1.4. The organization of this dissertation is shown in Section 1.5.

Chapter 2: This chapter presents the numerical analysis method and experiment method of this dissertation. The fundamental theories of microwave propagation through human body are introduced in Section 2.1. Numerical analysis by using FDTD method is performed in Section 2.2. Measurement by using differential-mode S-parameter method is performed in Section 2.3. The results of numerical analysis and experiment are compared in Section 2.4. Finally, conclusions are given in Section 2.5.

Chapter 3: This chapter presents the EM analysis and experiment results in homogenous human body phantom. The homogenous human body phantom is introduced in Section 3.1. Numerical analysis and experiment setup are performed in Section 3.2. The concept of transmission factor is performed in Section 3.3. The transmission factor of a dipole to dipole system is presented in Section 3.4. The relationship between transmission factor and radiation efficiency is investigated in Section 3.5. The transmission factor of a loop to loop system is presented in Section 3.6. Finally, conclusions are given in Section 3.7.

Chapter 4: As an addition to Chapter 3, propagation loss of microwave through in-homogenous human body phantom is investigated by numerical analysis. The in-homogenous human body phantom is introduced in Section 4.1. The analysis model is shown in Section 4.2. Some results and analysis are performed in Section 4.3. Finally, conclusions are given in Section 4.4.

Chapter 5: This chapter presents the capsule antenna design. Transmission factors of capsule dipole to dipole and capsule loop to loop are performed and compared in Section 5.1. The transmission factor under the condition that the capsule antenna offset is investigated in Section 5.2. Position of the capsule and the antenna is discussed in

Section 5.3. An inner-layer capsule dipole antenna (ICDA) is proposed in Section 5.4. Finally, conclusions are given in Section 5.5.

Chapter 6: The summary of this dissertation is given.

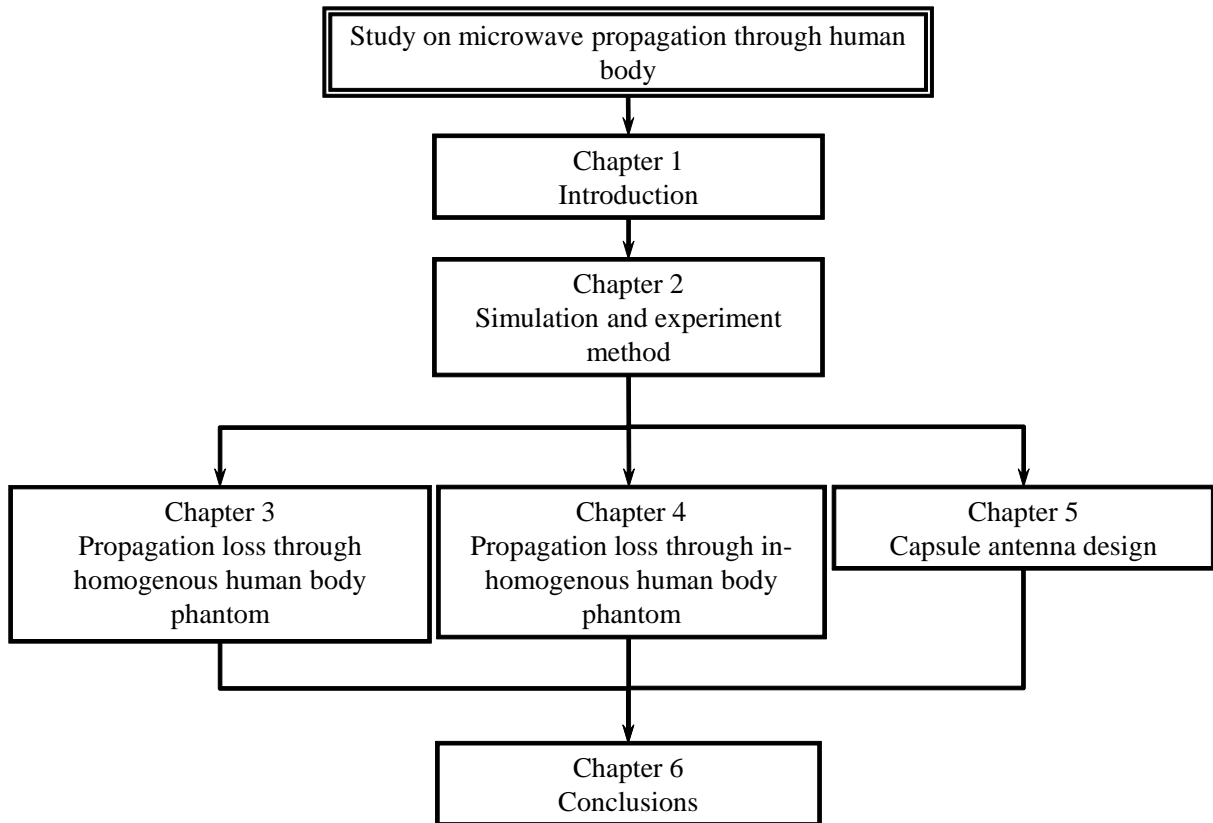


Figure 1.3: Organization of this dissertation.

# Chapter 2

## Simulation and experiment methods

This chapter presents the numerical analysis method and experiment method of this dissertation. The fundamental theory of microwave propagation through human body is introduced in Section 2.1. Numerical analysis: FDTD method is performed in Section 2.2. Experiment differential-mode S-parameter method is performed in Section 2.3. The results of numerical analysis and experiment are compared in Section 2.4. Finally, conclusions are given in Section 2.5.

### 2.1 Introduction

First consider the plane wave case, as shown in Figure 2.1 (a), both inside and outside antennas were placed in human body media, the attenuation can be calculated by using attenuation formulas. The results of skin, muscle and fat were shown in Figure 2.1 (b). For example, in the case of muscle the attenuation is 20 dB/10 cm at 1 GHz.

The plane wave through the interface was shown in Figure 2.2 (a), and the transmit coefficient at the interface was shown in Figure 2.2 (b). For example, in the case of muscle the transmit coefficient is -6 dB at 1 GHz.

Above all, by using plane wave formula, under the conditions: 1) muscle was used as a homogenous media of human body 2) propagation distance is 10 mm inside human body 3) Operating frequency is at 1 GHz, an approximation value of -26 dB was obtained.

## 2.2 Numerical analysis: FDTD method

Because the EM-wave from the actual capsule antenna is not plane wave, the accuracy of calculation by using plane wave formula is not enough. In order to improve the accuracy of the analysis, numerical analysis method is used. Comparing to the frequency domain method such as MoM, the time domain method, for example Finite-difference time-domain (FDTD) method, has advantages of saving calculation time and saving memory. In this search, software SEMCAD based on FDTD method was used.

Finite-difference time-domain is a numerical analysis technique used for modeling computational electrodynamics (finding approximate solutions to the associated system of differential equations). Since it is a time-domain method, FDTD solutions can cover a wide frequency range with a single simulation run, and treat nonlinear material properties in a natural way [47-49]. The FDTD method belongs in the general class of grid-based differential numerical modeling methods (finite difference methods). The time-dependent Maxwell's equations (in partial differential form) are discretized using central-difference approximations to the space and time partial derivatives. The resulting finite-difference equations are solved in either software or hardware in a leapfrog manner: the electric field vector components in a volume of space are solved at a given instant in time; then the magnetic field vector components in the same spatial volume are solved at the next instant in time; and the process is repeated over and over again until the desired transient or steady-state electromagnetic field behavior is fully evolved.

In order to confirm the accuracy of the numerical analysis method, a simple model was considered and experiment method was used to validate. The analysis model is shown in Figure 2.3. The deionized water with temperature of 18 °C was filled in a cubical acrylic case. An inside dipole antenna with the length of  $l_1$  was located in the center of the acrylic case separately and an outside dipole antenna with the length of  $l_2$  was located near the acrylic case with distance of  $D$ . The FDTD method was used for simulation without considering the acrylic cube case, the ohmic loss of antennas was ignored, to simplify the investigation. The relative permittivity and conductivity of deionized water was measured by using the coaxial probe method and was used for FDTD analysis as a curve fitted Debye dispersive material, as shown in Figure 2.4:

$$\epsilon_r = \epsilon_\infty + \frac{\epsilon_s - \epsilon_\infty}{1 + j\omega t_0} \quad (2.1)$$

$\epsilon_\infty$  is the permittivity for  $\omega \rightarrow \infty$ ;  $\epsilon_s$  denotes the relative static ( $\omega \rightarrow \infty$ ) permittivity. In the case of deionized water,  $\epsilon_\infty=4.9$ ,  $\epsilon_s=81.5$ ,  $t_0=1.05\text{e-}11[\text{s}]$  [50].

In the FDTD analysis, the number of cells is  $231 \times 231 \times 234$ , the Gaussian differential pulse is used as an excitation. The cell sizes are  $\Delta x = \Delta y = \Delta z = 1$  mm. 13-layer PML was used as an absorbing boundary condition. To simplify the investigation, the ohmic loss of the antennas were ignored and the material of antennas were considered as perfect electric conductors.

## 2.3 Measurement: differential-mode S-parameter method

The experiment setting and the results of numerical analysis and experiment were shown in Figure 2.5. Disagreement of numerical analysis and experiment was observed. It is considered that the reason is the balun structure affects the accuracy of the experiment. In order to obtain the accurate experiment results in broadband frequency range, the experiment dipole without balun structure should be considered. In order to obtain the reflection and the transmission coefficients in broadband frequency range, the differential-mode S-parameter method [51] was used with four port of VNA. S-parameters of differential mode  $S_{dd11}$ ,  $S_{dd22}$  and  $S_{dd21}$  [51] were measured by using four-port Vector Network Analyzer (Keysight N5224A) in order to compare with the numerical results in the broadband frequency range. In this research, these differential mode S-parameters were indicated as  $S_{11}$ ,  $S_{22}$  and  $S_{21}$ . The experiment setup with differential mode S-parameter method was shown in Figure 2.6.

## 2.4 Experiment results and observations

A dipole antenna with the length of 54 mm and a dipole antenna with the length of 20 mm were considered separately. Figure 2.7 (a) and (b) shows the reflection coefficient of  $l_1=54$  mm and  $l_1=20$  mm dipole antenna in deionized water respectively. Almost good

agreement between calculated and measured values was observed. For  $l_1=54$  mm, several resonances and anti-resonances below 1 GHz were obtained. This phenomenon was caused by the multiple reflection of the cubical water structure (from the wall of the box to the other). For  $l_1=20$  mm, there was a wideband from 1.05 GHz to 1.51 GHz ( $|S_{11}| < -10$  dB) when it was located in the middle of cubic water. Resonances below 1 GHz were smaller compare to  $l_1=54$  mm.

Figure 2.8 (a) and (b) shows the input impedance of  $l_1=54$  mm and  $l_1=20$  mm dipole antenna in deionized water respectively. Good agreement between calculated and measured values was observed. Compare Figure 2.7 and Figure 2.8, for  $l_1=54$  mm, several resonances and anti-resonances below 1 GHz were observed caused by the cubic water. For  $l_1=20$  mm,  $0.5 \lambda_g$  resonant happened at 710 MHz, the resistance was  $8.8 \Omega$  and the reflection was large.  $1 \lambda_g$  anti-resonant happened at 1.3 GHz, the resistance was  $68.7 \Omega$  and the reflection was small.

Figure 2.9 (a) and (b) shows the transmission coefficient  $|S_{21}|$  of  $l_1=54$  mm and  $l_1=20$  mm dipole antenna in deionized water respectively. Good agreement between calculated and measured values was observed. For  $l_1=54$  mm, the maximum value of experiment was -22 dB at 520 MHz. A high transmission with levels of around -30 dB through the 72 mm thick deionized water with wideband characteristics from 300 MHz to 1 GHz was observed. For  $l_1=20$  mm, the maximum value of experiment was -22 dB at 500 MHz. A relatively high transmission with levels of around -25 dB through the 72 mm thick deionized water with wideband characteristics from 300 MHz to 1 GHz was observed.

Above 1 GHz, transmission coefficient decreases for the reason that conductivity increases as frequency increases. A dipole antenna with the length of 20 mm was suitable at 1 GHz nearby for capsule applications. Propagation loss is not too large in case of deionized water. From the results before, the results of the FDTD numerical analysis were reliable.

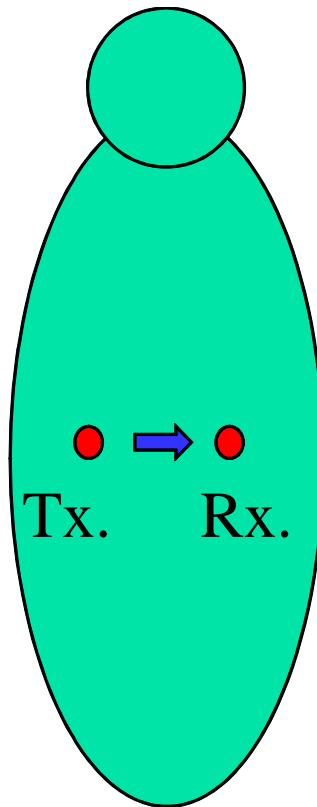
## 2.5 Conculsion

In this chapter, measurement of a dipole antenna located in deionized water was studied and compared with FDTD simulation. Differential mode S-parameter method was used

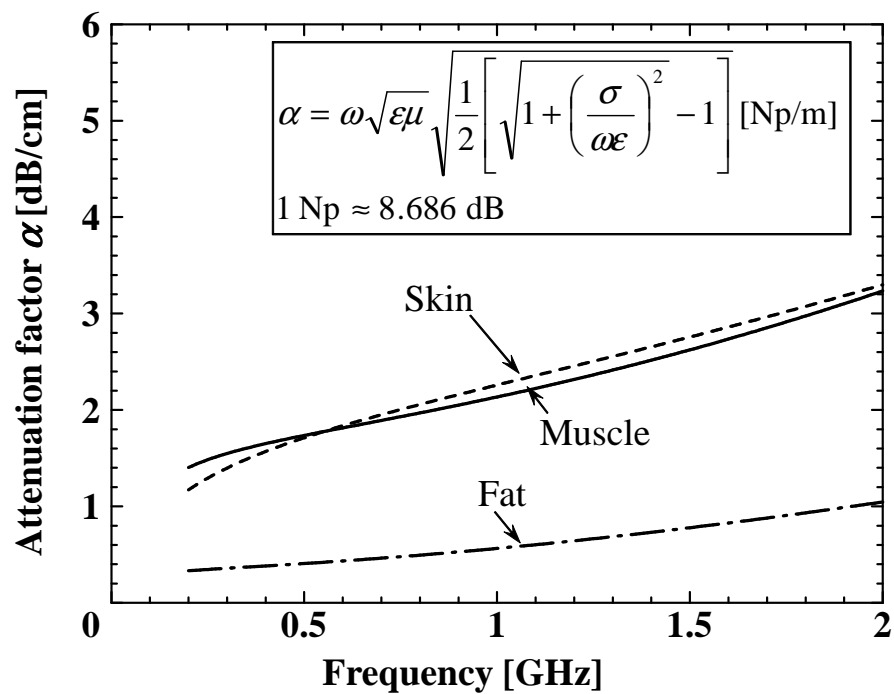


---

to obtain transmission loss in balanced feeding and good agreements between measured and calculated results have been observed. Reliability of both measurements and analysis were confirmed. It is found that the FDTD method is effective when dispersive effect of material is considered. It is also found that differential-mode S-parameter method is effective in broadband frequency range. These methods are useful to the design of capsule antennas.

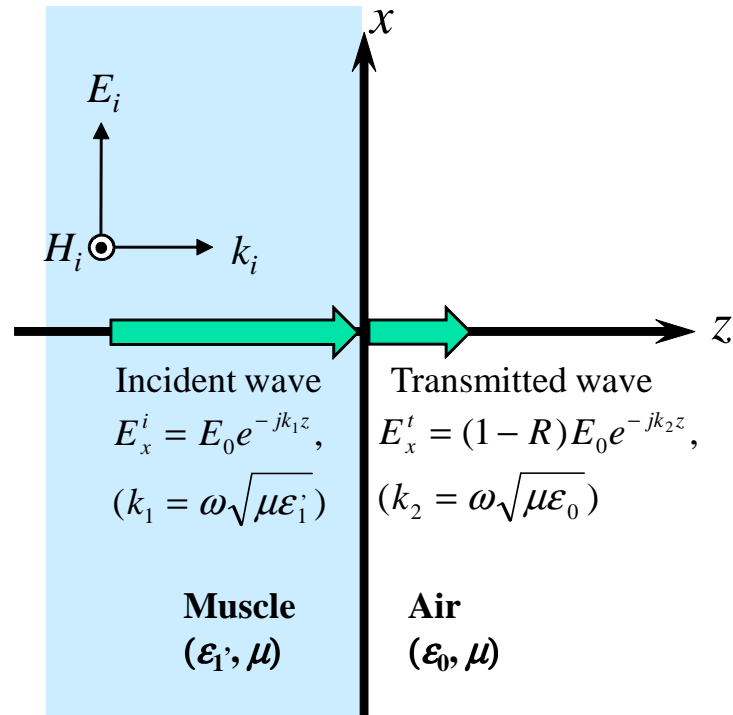


(a) Model.

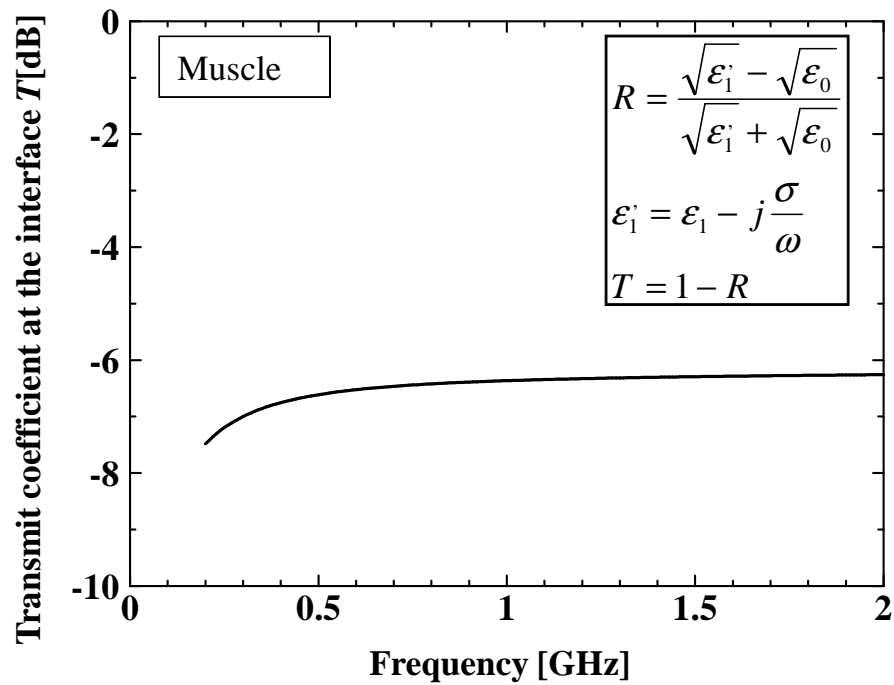


(b) Calculated results.

Figure 2.1: Attenuation in media (in the case of plane-wave).



(a) Model.



(b) Calculated results.

Figure 2.2: Reflection on the interface (in the case of plane-wave).

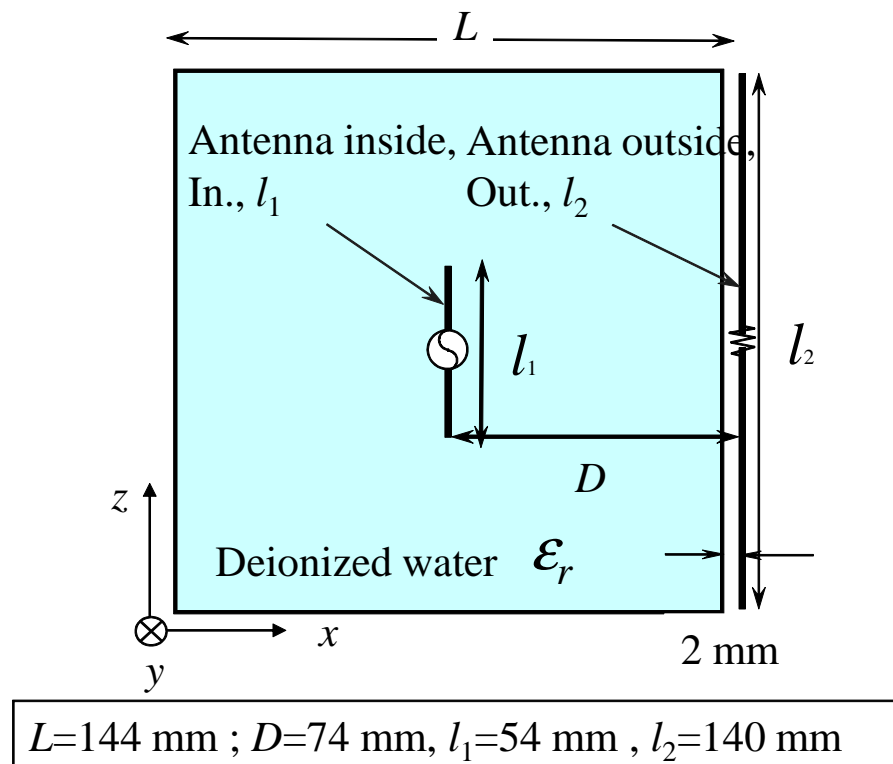


Figure 2.3: Analysis model of dipole antenna in deionized water.

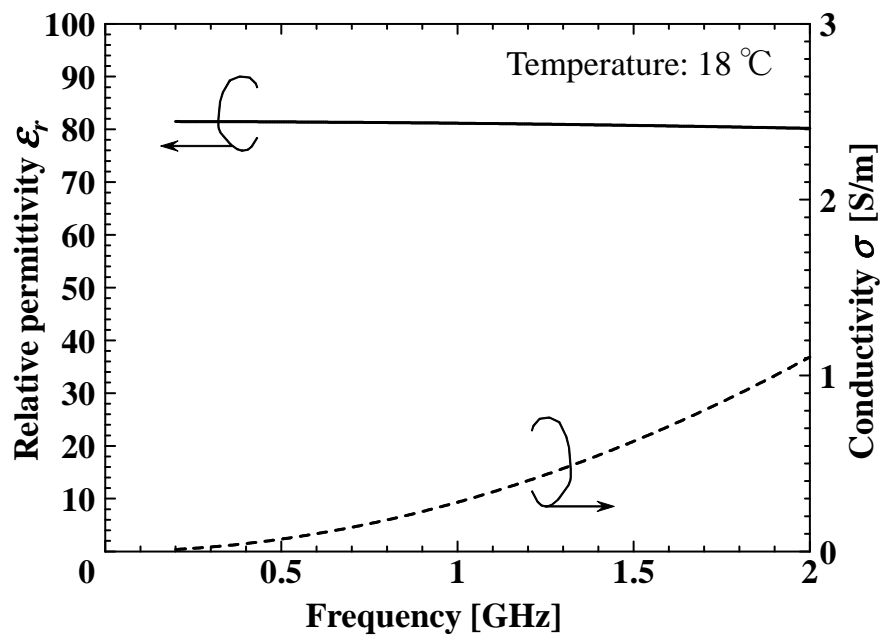
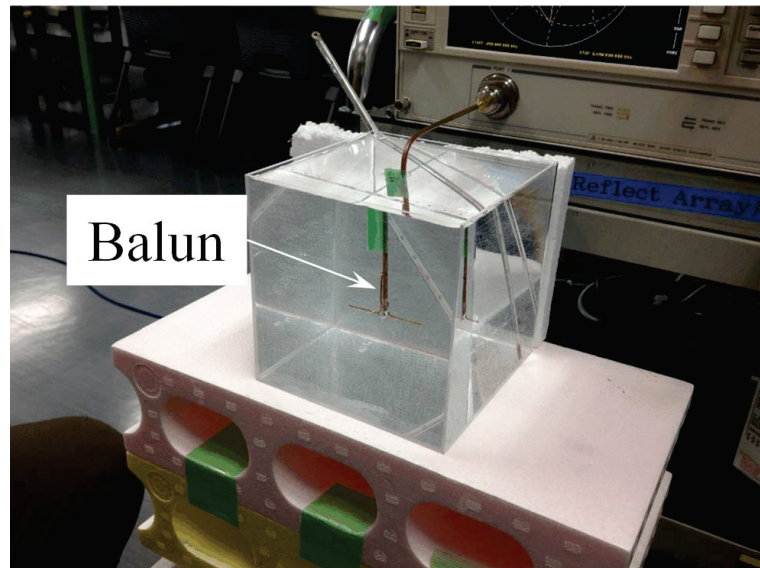
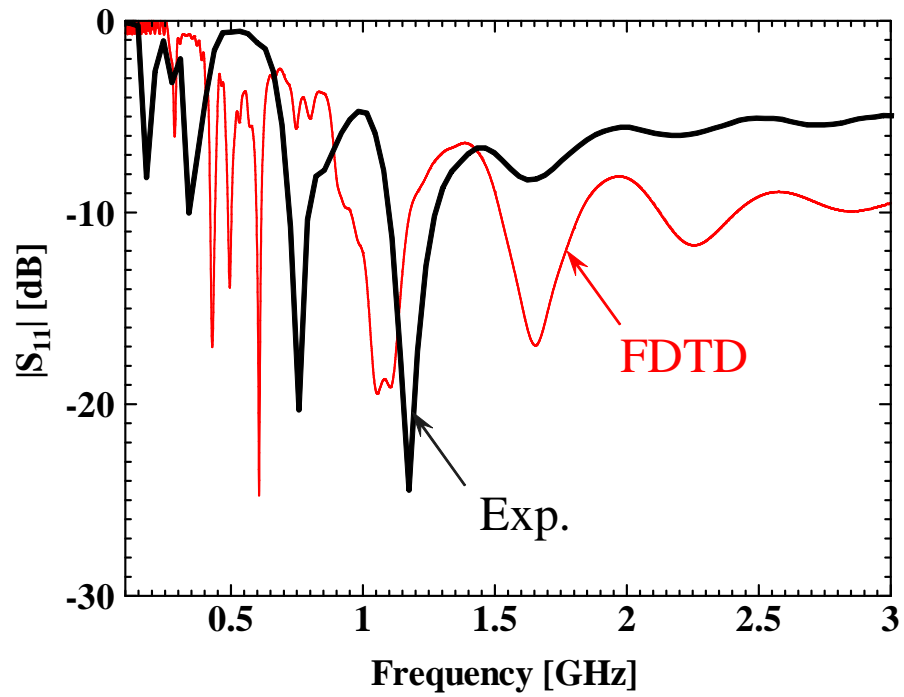


Figure 2.4: Relative permittivity and conductivity of deionized water.



(a) Experiment setup.



(b) Numerical analysis results and experiment results.

Figure 2.5: Experimental results of dipole antenna with balun structure.

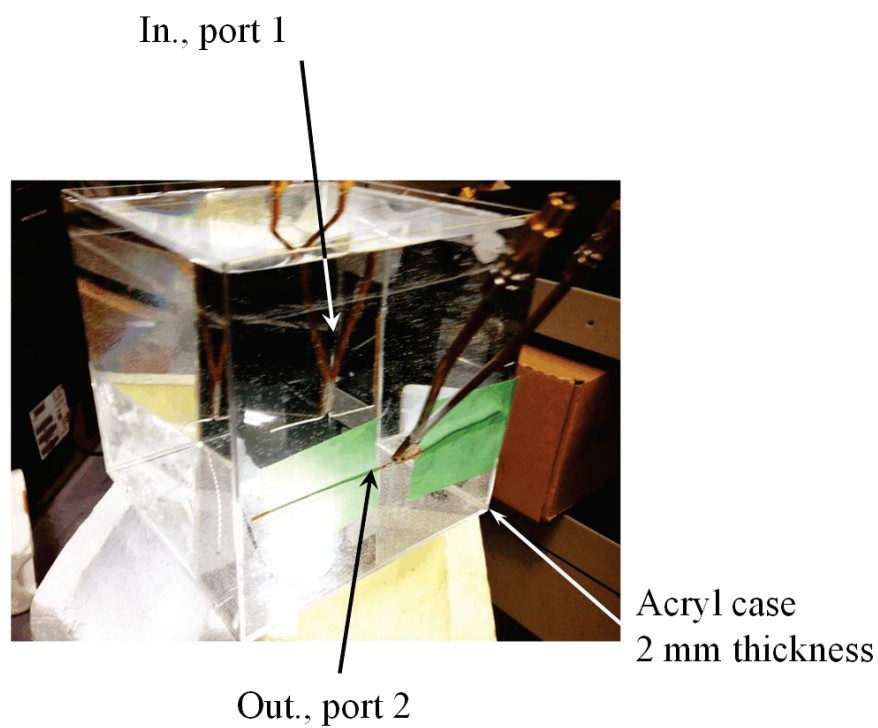
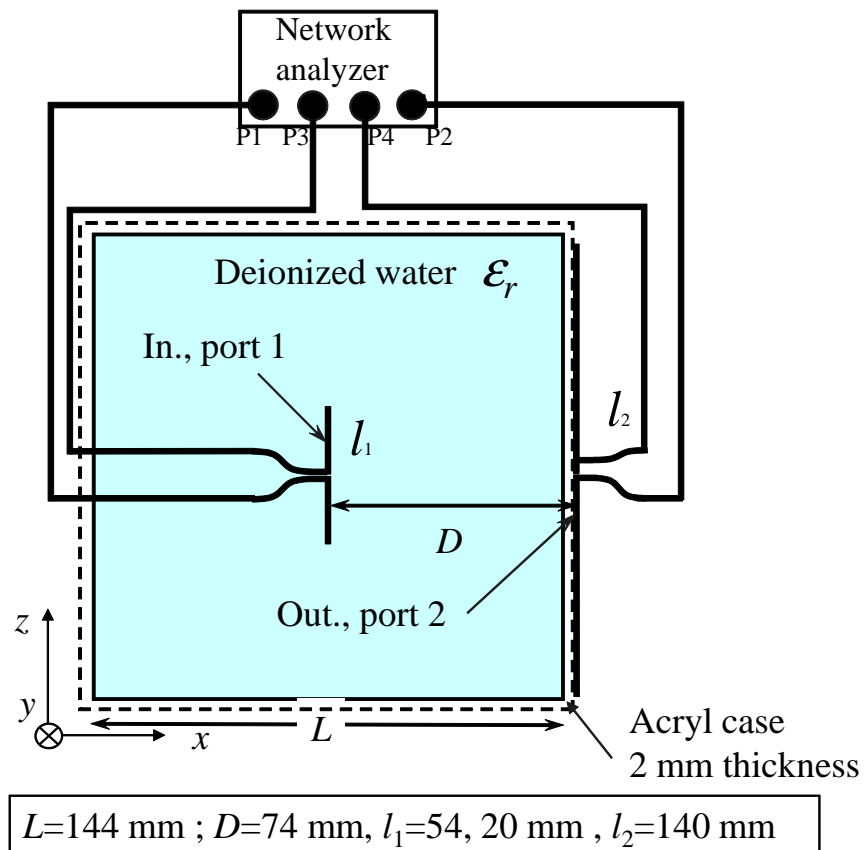


Figure 2.6: Experimental setup of differential-mode S-parameter method.

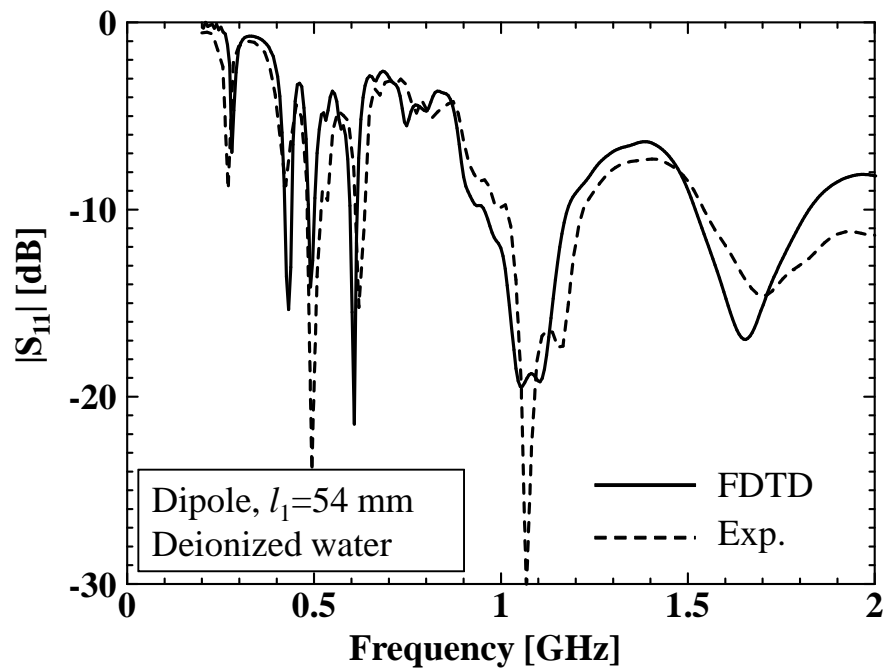
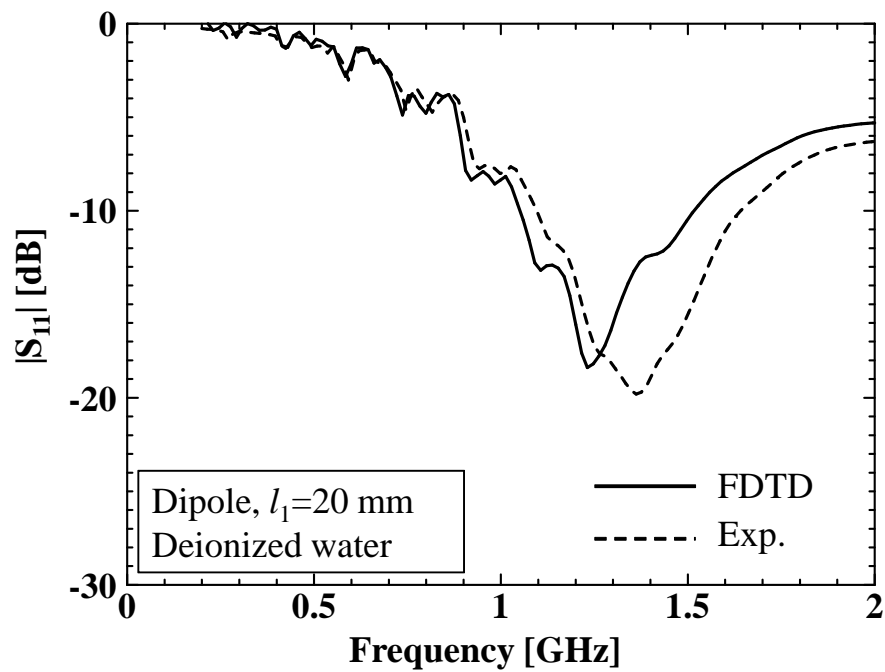
(a)  $l_1=54$  mm.(b)  $l_1=20$  mm.

Figure 2.7: Reflection coefficient of dipole antenna in deionized water.

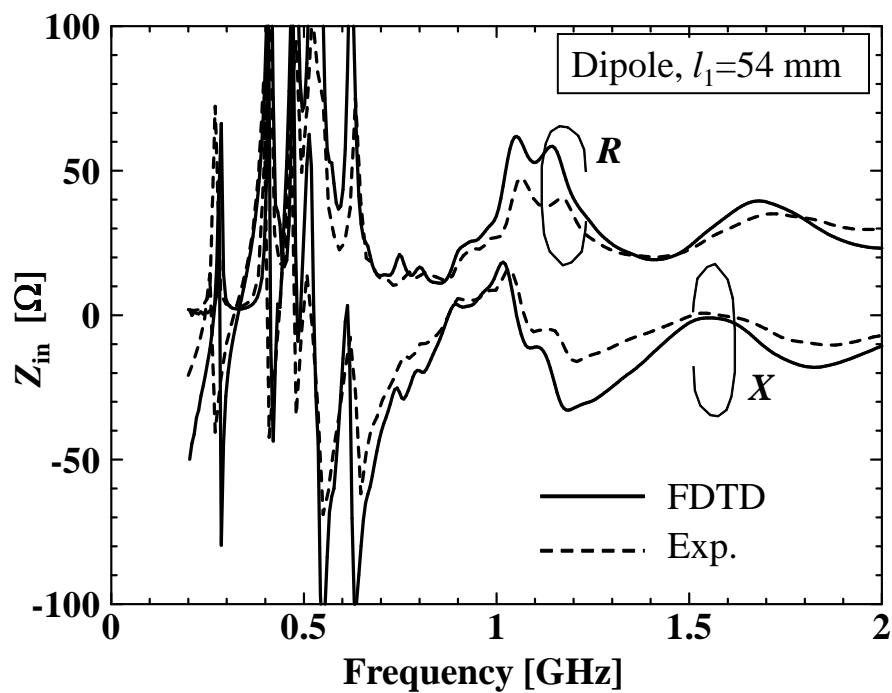
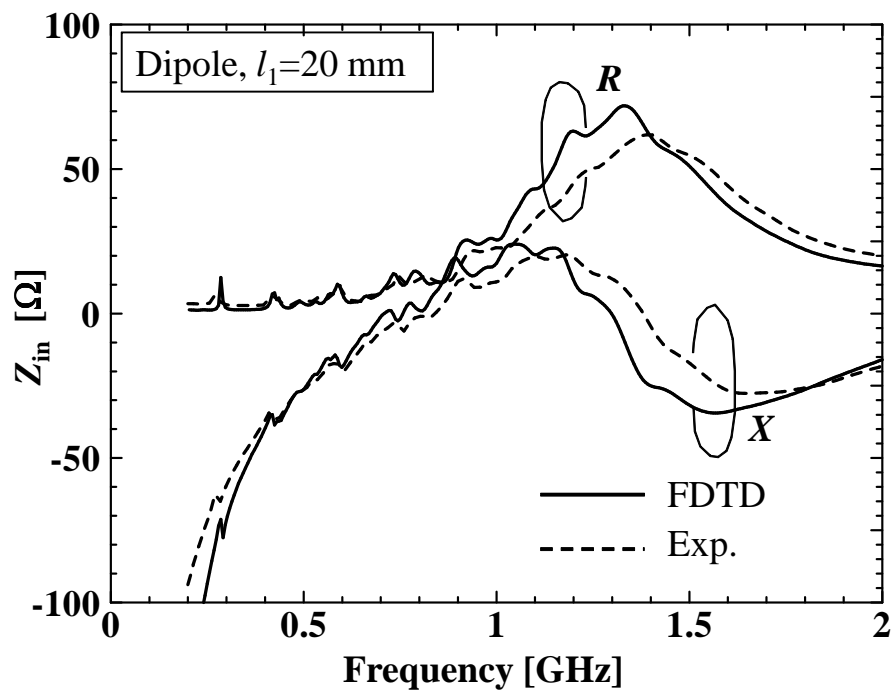
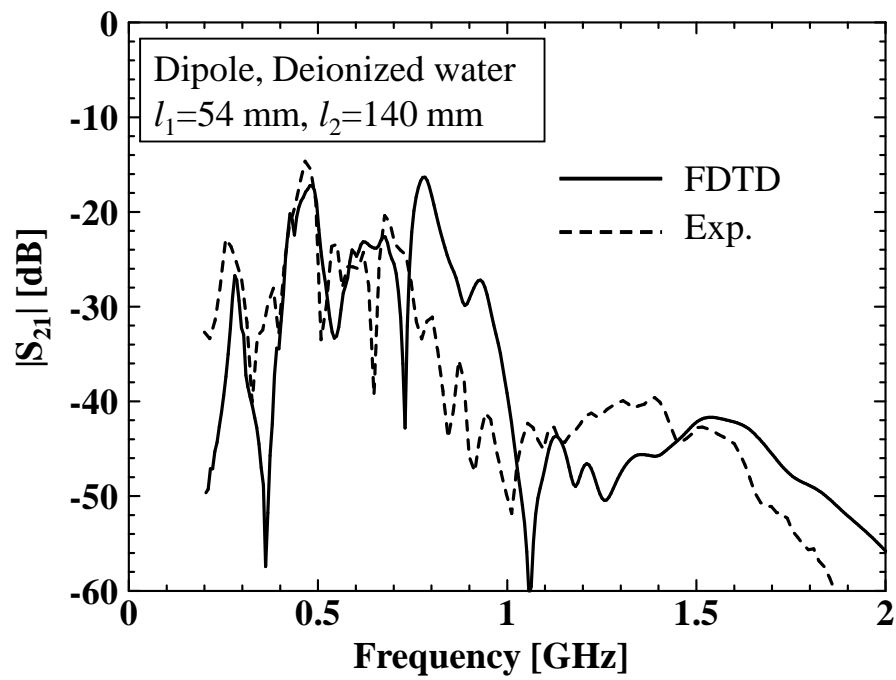
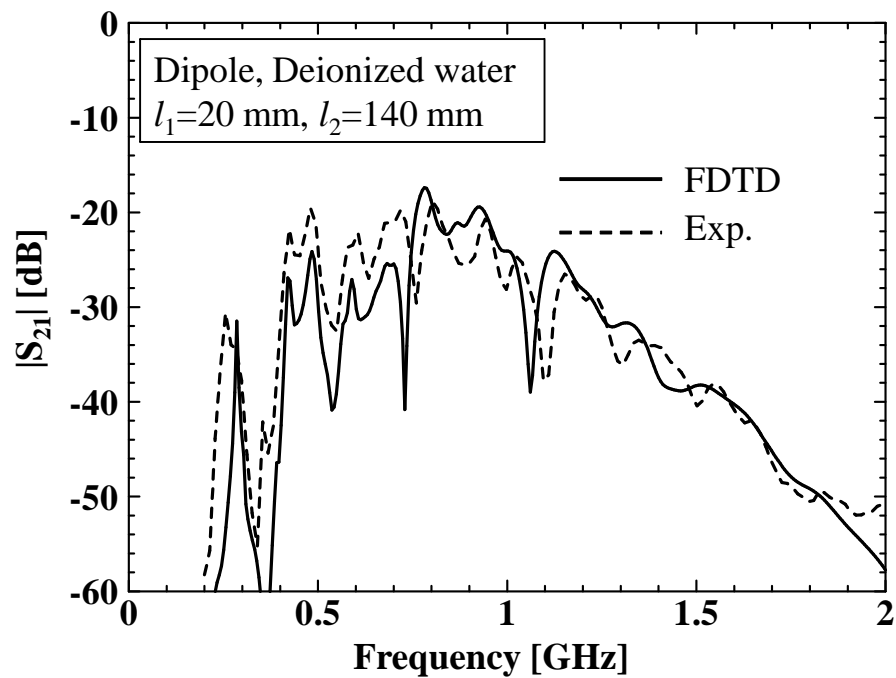
(a)  $l_1=54$  mm.(b)  $l_1=20$  mm.

Figure 2.8: Input impedance of dipole antenna in deionized water.



(a)  $l_1=54$  mm.(b)  $l_1=20$  mm.Figure 2.9:  $|S_{21}|$  from inside dipole through deionized water to the outside dipole.

# Chapter 3

## Propagation loss through homogenous human body phantom

In this chapter, EM analysis and experiment results in homogenous phantom are performed. Homogenous human torso-shaped phantom is introduced in section 3.1. Numerical analysis and experiment setup are performed in section 3.2. The concept of transmission factor is performed in in section 3.3. The transmission factor of a dipole to dipole system is studied in section 3.4. The relationship between transmission factor and radiation efficiency is investigated in 3.5. The transmission factor of a loop to loop system is studied in section 3.6. Finally, some conclusions are summarized in section 3.7.

### 3.1 Introduction

In this chapter, a commercial human torso-shaped phantom developed by SPEAG was used as the container of liquid, as shown in Figure 3.1. The shell of phantom is made of fiberglass ( $\epsilon_r=3.5$ ) and the thickness is around 2 mm [52].

A homogeneous material with relative permittivity and conductivity similar to the muscle, was used as a human body equivalent liquid (HBEL) [52]. In order to study the effect of conductivity on the propagation loss, deionized water was also evaluated. Figure 3.2 shows the measurement results of relative permittivity and conductivity of the

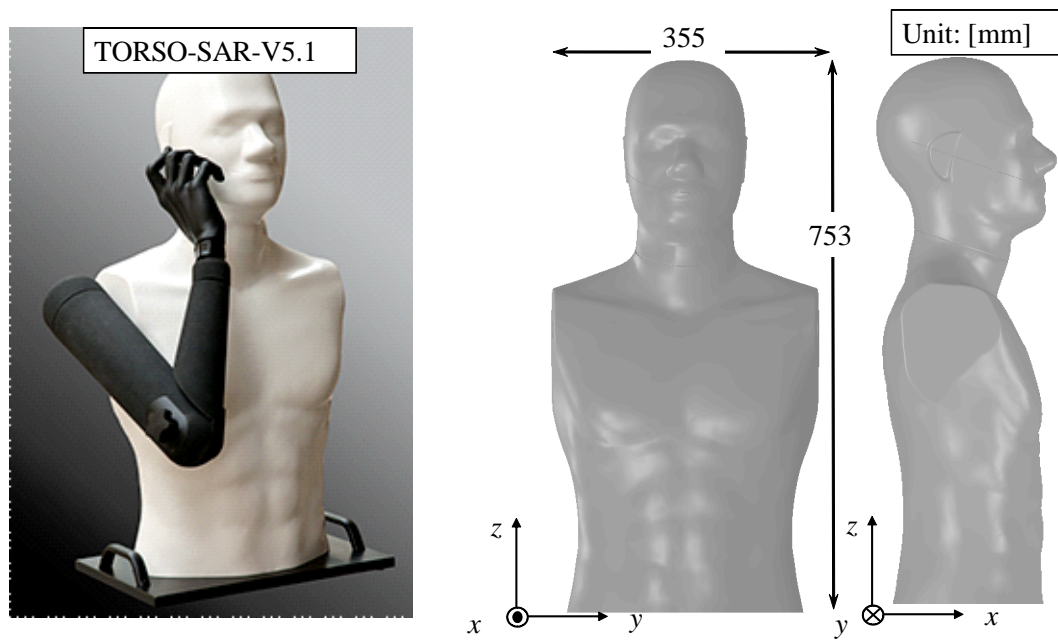


Figure 3.1: Homogenous torso-shaped phantom.

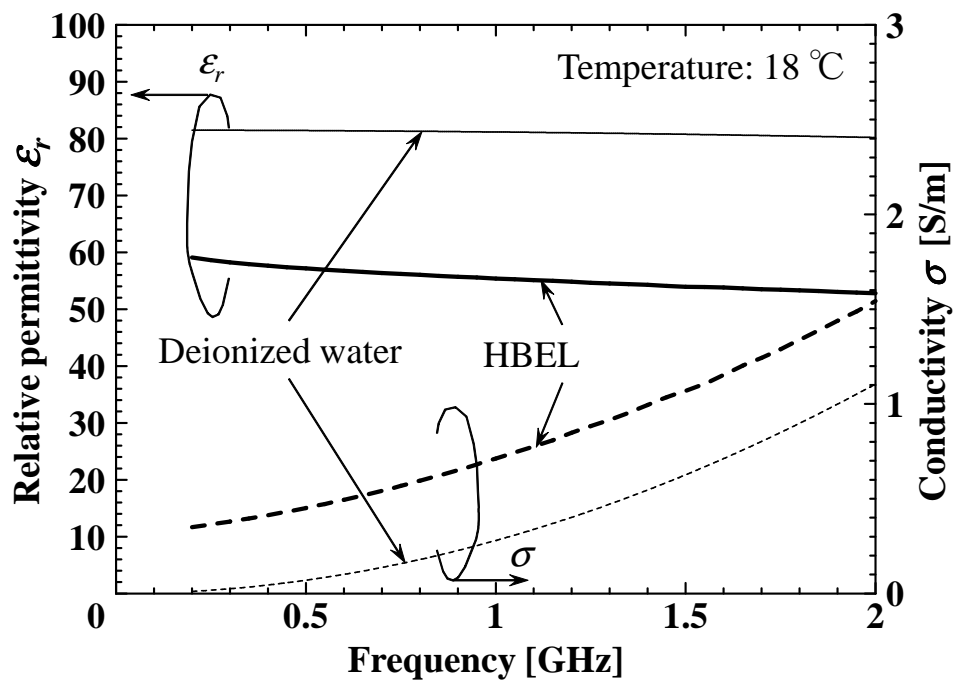


Figure 3.2: Relative permittivity and conductivity of HBEL.

deionized water and HBEL obtained by using the coaxial probe DAK 1.2 provided by SPEAG [52]. In the measurement, the torso-shaped phantom was filled with deionized water or HBEL with a temperature of 18 °C. It is found that:

a) In the frequency range of 200 MHz to 2 GHz, there is no particularly difference between the measured value of HBEL and the measured data of human body tissues provided by S. Gabriel [53, 54].

b) The conductivity of deionized water is lower than that of HBEL in the frequency range of 200 MHz to 2 GHz.

c) The conductivity at the lower frequency of around 200 MHz is almost zero in the case of deionized water and is finite values in the case of HBEL.

## 3.2 Numerical analysis and experiment setup

Figure 3.3 (a) and (b) show the numerical model and the experimental setup, respectively. A dipole antenna with length  $l_1$  was placed inside the torso phantom at the position indicated as Port 1 ( $x_1, y_1, z_1$ ), which is chosen as a typical position of the stomach in the human body. And a dipole antenna with length  $l_2$  was placed outside of the torso-shaped phantom as Port 2. The distance between the antennas was set as to  $D=74$  mm. S-parameters of differential mode  $S_{dd11}$ ,  $S_{dd22}$  and  $S_{dd21}$  [51] were measured by using four-port Vector Network Analyzer (Keysight N5224A) in order to compare with the numerical results in the broadband frequency range. In this study, these differential mode S-parameters were indicated as  $S_{11}$ ,  $S_{22}$  and  $S_{21}$ . The in-homogeneous real human body was studied numerically in [55] a homogeneous material with relative permittivity and conductivity similar to the muscle, was used as a human body equivalent liquid (HBEL) [56]. To compare with the HBEL, deionized water was also used. In the FDTD analysis, the number of cells is  $202 \times 304 \times 462$ , the Gaussian differential pulse is used as an excitation. Subgridding technique was used and the cell sizes are  $\Delta x = \Delta y = \Delta z = 2$  mm for the human torso-shaped phantom and  $\Delta x = \Delta y = \Delta z = 1$  mm for the antennas. 13-layer PML was used as an absorbing boundary condition. To simplify the investigation, the ohmic loss of the antennas were ignored and the material of antennas were considered as perfect electric conductors.

Figure 3.4 and Figure 3.5 show the input impedance of the dipole antenna with  $l_1=20$  mm placed in the cases of deionized water and the HBEL. An agreement between the calculated and the measured values was observed from 200 MHz to 2 GHz. In vacuum, the resonant frequency of the dipole antenna with  $l_1=20$  mm was almost 7.5 GHz. In the deionized water, the half-wavelength ( $0.5\lambda_g$ ) resonance at 710 MHz with resistance of  $8.8 \Omega$  and the wavelength ( $\lambda_g$ ) anti-resonance at 1.3 GHz with resistance of  $68.7 \Omega$  were observed, respectively. In the HBEL, the half-wavelength ( $0.5 \lambda_g$ ) resonance at 913 MHz with resistance of  $19.4 \Omega$  and the wavelength ( $\lambda_g$ ) anti-resonance at 1.6 GHz with resistance of  $65 \Omega$  were observed, respectively.

Figure 3.6 shows the theoretical  $\lambda_g$  and  $l_1/\lambda_g$  by using plane-wave formula.

$$\beta = \omega \sqrt{\mu \varepsilon} \sqrt{\frac{1}{2} \left[ \sqrt{1 + \left(\frac{\sigma}{\omega \varepsilon}\right)^2} + 1 \right]} \quad [rad/m] \quad (3.1)$$

$$\lambda_g = \frac{2\pi}{\beta} \quad (3.2)$$

Considering the wavelength shortening effect, there is an agreement between the measured value and the theoretical value.

Figure 3.7 (a) and (b) show the reflection coefficient of the inside dipole in deionized water and in HBEL.

Figure 3.8 (a) shows the transmission coefficient of the dipole antenna placed in deionized water to the outside. A good agreement between the calculated and the measured values was observed. A relatively high transmission level of around -25 dB through the torso-shaped phantom filled with the deionized water with wide band characteristics below 1 GHz was observed.

Figure 3.8 (b) shows the transmission coefficient of the dipole antenna placed in HBEL to the outside. Agreement between the calculated and the measured values was observed. Because the conductivity of the HBEL was larger than that of the deionized water, a relatively high transmission level of around -31 dB through the torso-shaped phantom filled with the HBEL with wide band characteristics at 920 MHz was observed. The maximum value is -21.4 dB and -28.5 dB at 960 MHz. The transmission coefficients in both the deionized water and the HBEL decreased in the frequency range above 1 GHz

because the conductivity of liquid increases with the frequency, as shown in Figure 3.6 (b).

Figure 3.9 show the reflection coefficient of the outside dipole. It is found that the resonant frequency of outside dipole is 1 GHz and the bandwidth is narrow, this phenomenon causes the maximum value of  $|S_{21}|$  in Figure 3.6. It is considered that it is important to obtain the propagation loss without the effect of antenna mismatching.

### 3.3 Definition of transmission factor

Two-port network equivalent circuit is shown in Figure 3.10 [57-59]. Transmitting antenna is connected to a source with an internal impedance of  $Z_S$ , while receiving antenna is loaded with an internal impedance of  $Z_L$ .  $P_L$  is the power delivered to the load  $Z_L$ ,  $P_{in}$  is the input power,  $P_{inc}$  is the incident power,  $\Gamma_S$  and  $\Gamma_L$  are the reflection coefficients looking toward the source  $Z_S$  and the load  $Z_L$ , respectively, and  $\Gamma_{in}$  and  $\Gamma_{out}$  are the reflection coefficients looking toward Port 1 and Port 2. In this equivalent circuit, there is a relation as

$$\frac{P_L}{P_{inc}} = \frac{1 - |\Gamma_S|^2}{|1 - \Gamma_S \Gamma_{in}|^2} |S_{21}|^2 \frac{1 - |\Gamma_L|^2}{|1 - S_{22} \Gamma_L|^2}. \quad (3.3)$$

where

$$\Gamma_S = \frac{Z_S - Z_0}{Z_S + Z_0}, \Gamma_L = \frac{Z_L - Z_0}{Z_L + Z_0} \quad (3.4)$$

$$\Gamma_{in} = S_{11} + \frac{S_{12} S_{21} \Gamma_L}{1 - S_{22} \Gamma_L}, \Gamma_{out} = S_{22} + \frac{S_{12} S_{21} \Gamma_S}{1 - S_{11} \Gamma_S}. \quad (3.5)$$

If antennas are perfectly matched to the loads with the complex-conjugate impedances at both Port 1 and Port 2 as

$$\Gamma_S = \Gamma_{in}^*, \Gamma_L = \Gamma_{out}^* \quad (3.6)$$

or

$$Z_S = Z_{in}^*, Z_L = Z_{out}^*, \quad (3.7)$$

, there is no reflection at Port 1, the incident power is equal to the input power

$$P_{in} = P_{inc} \quad (3.8)$$



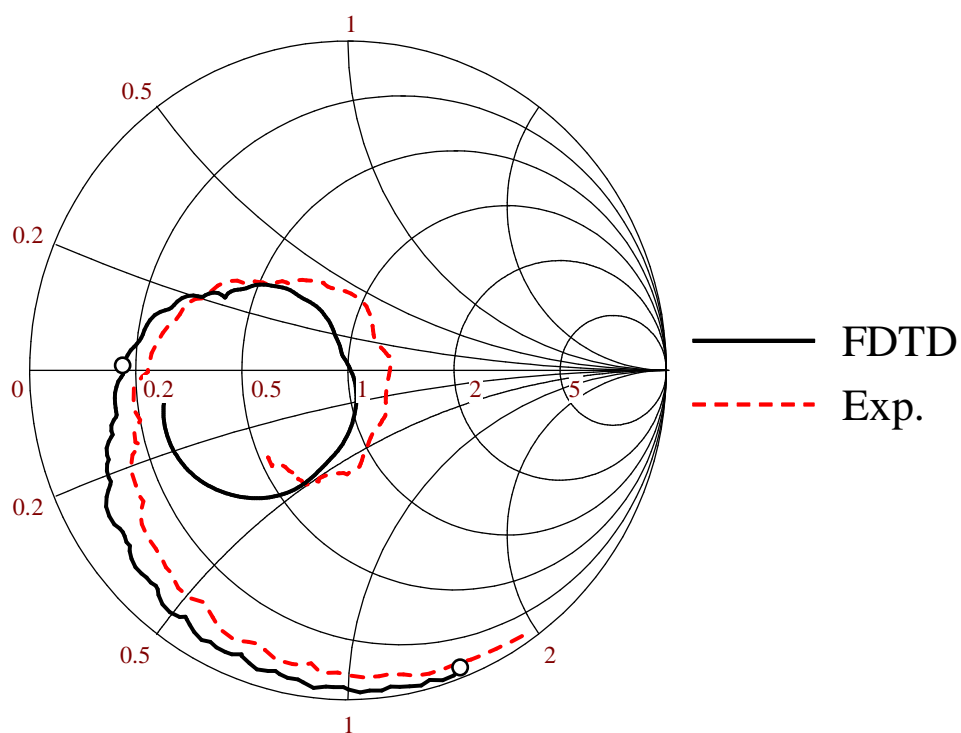
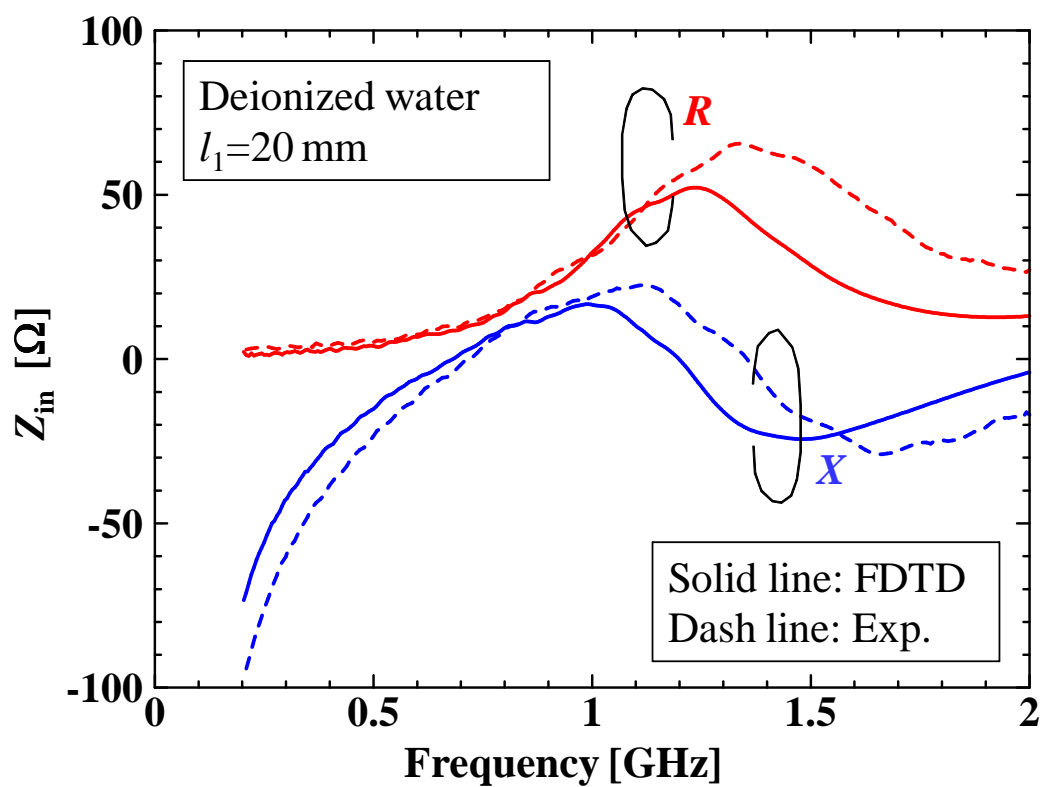


Figure 3.4: Input impedance of dipole antenna immersed in deionized water.



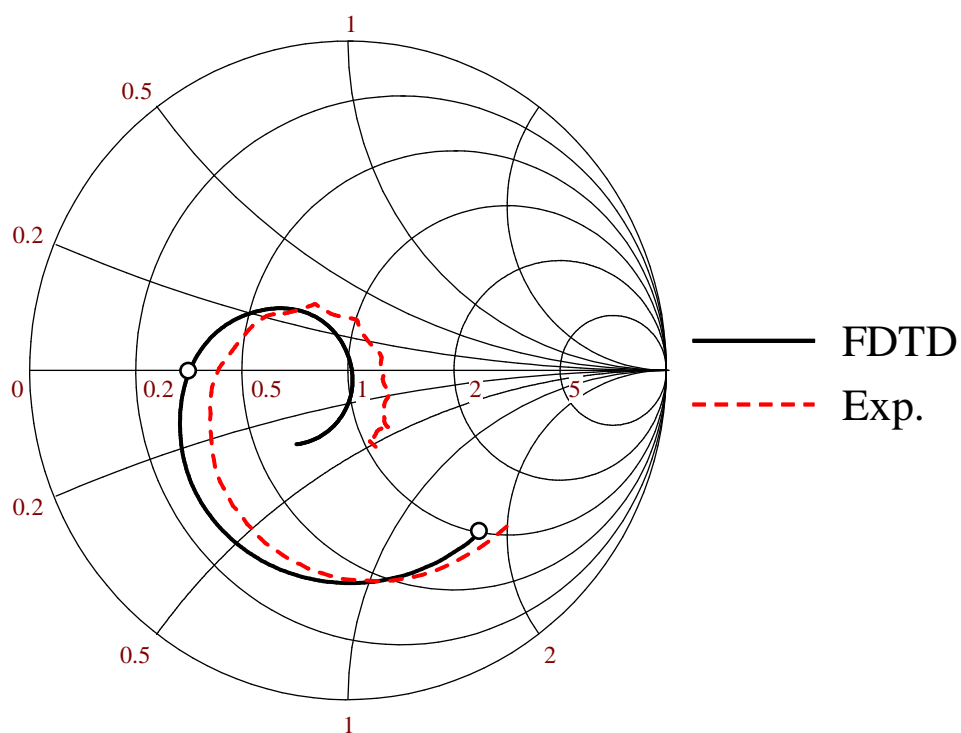
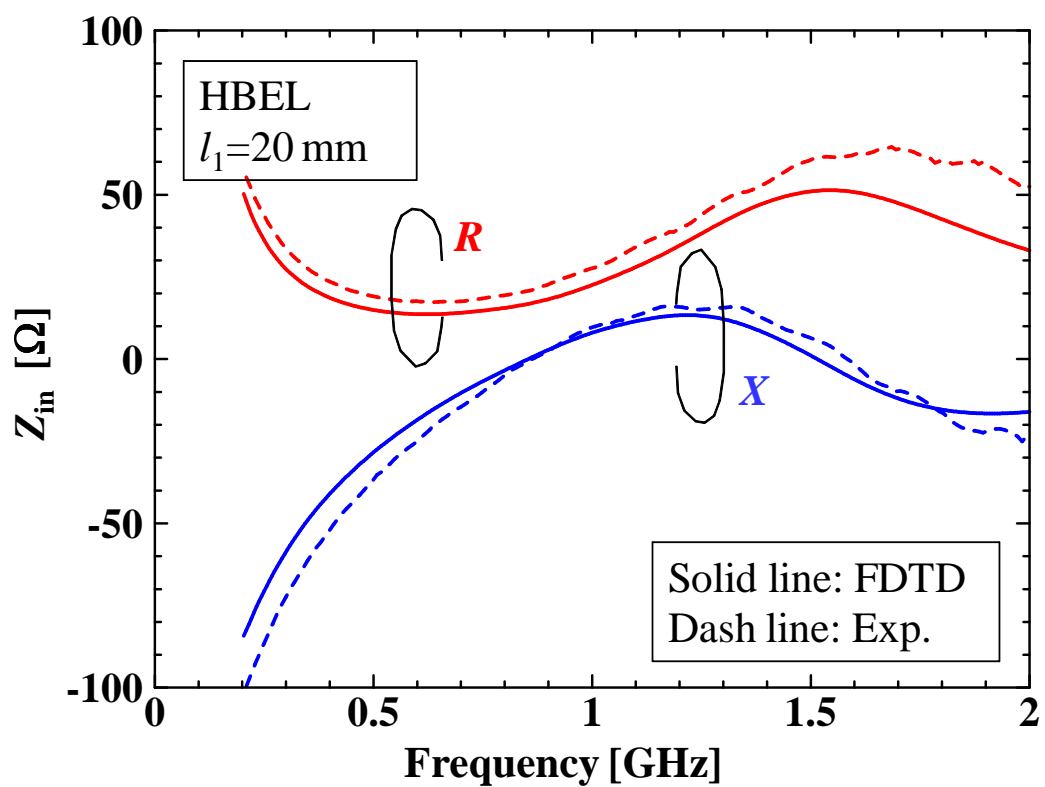


Figure 3.5: Input impedance of dipole antenna immersed in HBEL.

and the transmission factor  $\tau$  is defined by using S-parameters of the circuit as

$$\begin{aligned}\tau &= \frac{P_L}{P_{inc}} \Big|_{Z_S=Z_{in}^*, Z_L=Z_{out}^*} = \frac{P_L}{P_{in}} \\ &= \frac{1}{1 - |\Gamma_S|^2} |S_{21}|^2 \frac{1 - |\Gamma_L|^2}{|1 - S_{22}\Gamma_L|^2}.\end{aligned}\tag{3.9}$$

In the case when  $Z_S=Z_L=50 \Omega$ , the transmission factor  $\tau$  can be written as  $|S_{21}|^2$ . The transmission factor  $\tau$  is the relative, maximum received power which excludes the mismatch effects of the antennas and includes the cases when  $Z_S$  and  $Z_L$  are not equal to  $50 \Omega$ . In this research, the transmission factor  $\tau$  is used as the propagation loss to investigate the transmission characteristics of EM-wave through human body.

### 3.4 Transmission factor through human body: dipole to dipole

Figure 3.11 (a) and (b) show the transmission factor  $\tau$  of dipole antenna through a torso-shaped phantom filled with deionized water or HBEL. In the case of dipole antenna placed in deionized water, it is observed that the transmission factor  $\tau$  decreases as the conductivity increases. In the low frequency range, the conductivity of the deionized water is almost zero and the transmission factor  $\tau$  is quite large (almost -15 dB) with several vibrations caused by the multiple reflections inside a phantom. On the other hand, in the case of HBEL with higher conductivity compared to the deionized water, a local maximum with level of -25.3 dB is observed at 675 MHz corresponding to the half-wavelength resonant frequency ( $l_1=\lambda_g/2$ ) of the dipole antenna immersed in HBEL. The value of  $\tau$  at 675 MHz is -28 dB which is 2.7 dB larger than the value at 1 GHz. Differences between experimental values and FDTD results for both in the case of deionized water and HBEL become larger in the low frequency range, which was caused by the difference between the simulation phantom and the experiment phantom, the setting accuracy of the immersed antenna, and the effect of the conducting jig in the experiment. The transmission factor  $\tau$  is mainly affected by the geometry of a phantom, distance between antennas and conductivity of the liquid.

To study the relationship between the transmission factor  $\tau$  and the conductivity of the liquid, an imaginary numerical material with constant permittivity (MCP,  $\epsilon_r=49$ ,  $\sigma=0.6$  S/m) was supposed to compare with HBEL, as shown in Figure 3.12 (a). Figure 3.12 (b) shows the calculated transmission factor when a dipole antenna is immersed in MCP and is immersed in HBEL. It was observed that the magnitude of transmission factor  $\tau$  replace with a frequency boundary of 850 MHz which is corresponding to the frequency of conductivity boundary as shown in Figure 3.12 (a). This phenomenon demonstrates that a higher  $\sigma$  causes a lower  $\tau$ .

Figure 3.13 shows the calculated transmission factors  $\tau$  in HBEL when the length of inside dipole antenna are changed to  $l_1=20$  mm, 54 mm, and 140 mm, respectively. The maximum value of  $\tau$  increases as the length of antenna increases. These frequency changes of local maximum are considered as the half-wavelength resonant frequency of the dipole antenna. However, in practical application, the length of capsule antenna is limited to 20 mm, and the maximum value of  $\tau$  is considered around -25 dB to -30 dB when a capsule antenna is placed in the middle of a human body.

Figure 3.14 shows the calculated transmission factors  $\tau$  in HBEL when the length of outside dipole antenna are changed to  $l_2=100$  mm, 140 mm, and 180 mm, respectively. The maximum value of  $\tau$  is almost unchanged.

## 3.5 Transmission factor and antenna radiation efficiency

To confirm the local maximum in Figure 3.11 (a), the effect of human torso-shaped phantom on antenna radiation efficiency was studied by using conservation of energy. Here only the inside antenna was considered. According to the view of conservation of energy, we can obtain:

$$P_{in} = P_r + P_l \quad (3.10)$$

The definition of the radiation efficiency is:

$$\eta = \frac{P_r}{P_{in}} \quad (3.11)$$

Here,  $P_{in}$  is the power delivered by the sources;  $P_r$  is the power radiated to the space;  $P_l$  is the power lost to heat in the volume.

Figure 3.15 shows the analysis model of radiation efficiency simulation, Figure 3.15 (a) shows the dipole  $l_1$  without human torso-shaped phantom, while Figure 3.15 (b) shows the dipole  $l_1$  with human torso-shaped phantom. Both these two cases have the same analysis region and the same numbers of cells. Figure 3.16 shows the simulation results: in the case of without human torso-shaped phantom, the radiation efficiency are almost 0 dB in the frequency band; in the case of with human torso-shaped phantom, a local maximum is appereared in the frequency of 700 MHz.

The same analysis method was used to obtain transmission factor. Both inside and outside antennas were considred. Figure 3.17 shows the analysis model of transmission factor simulation, Figure 3.17 (a) shows the dipole to dipole without human torso-shaped phantom, while Figure 3.17 (b) shows the dipole to dipole with human torso-shaped phantom (same as Figure 3.3(a)). Both these two cases have the same analysis region.

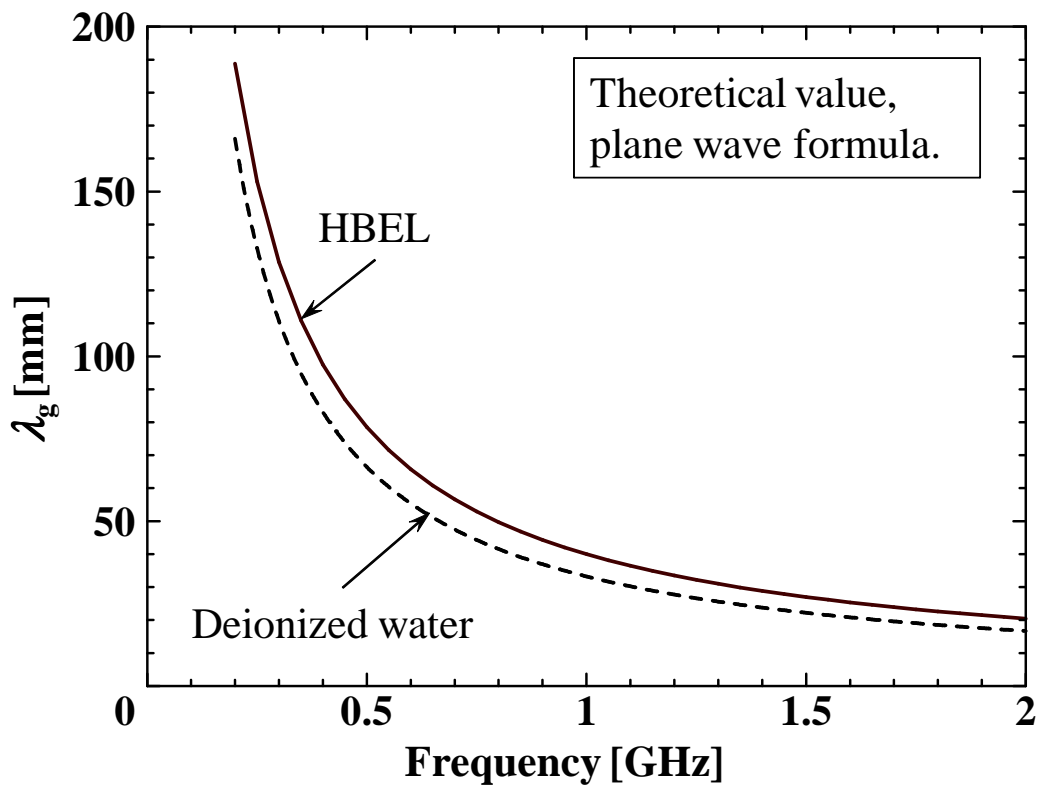
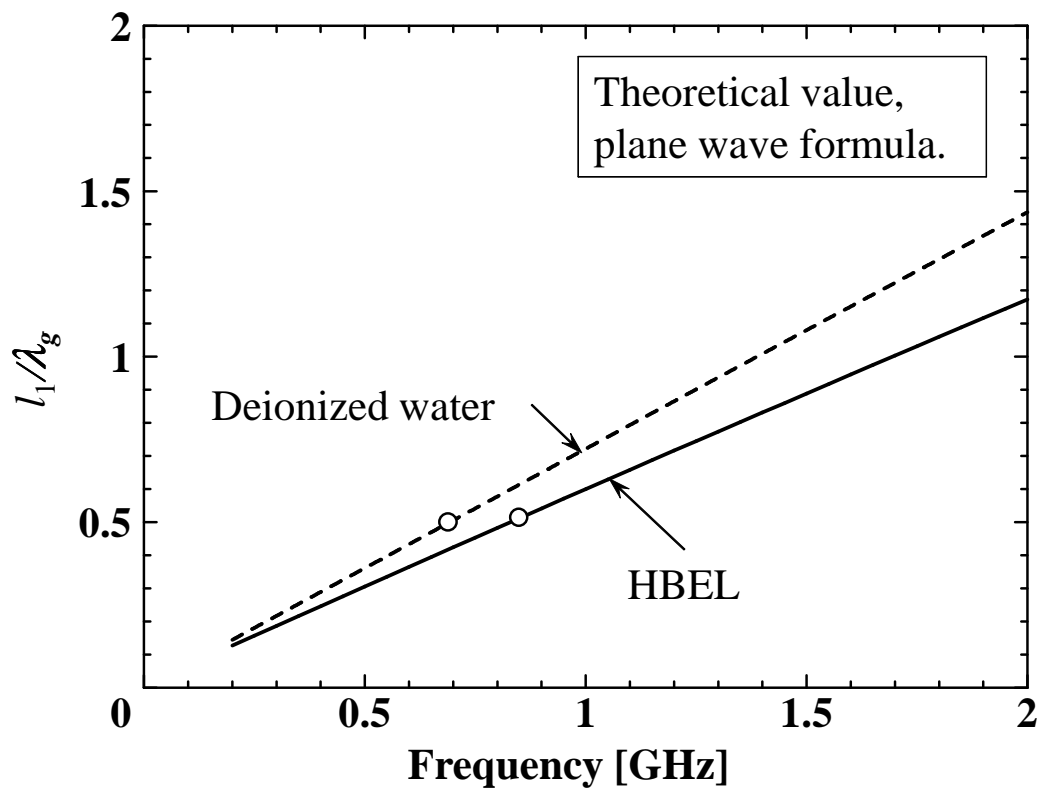
Figure 3.18 shows the results: in the case of without human torso-shaped phantom, the transmission factor decreases as frequency increased; in the case of with human torso-shaped phantom, a local maximum is appereared in the frequency of 700 MHz.

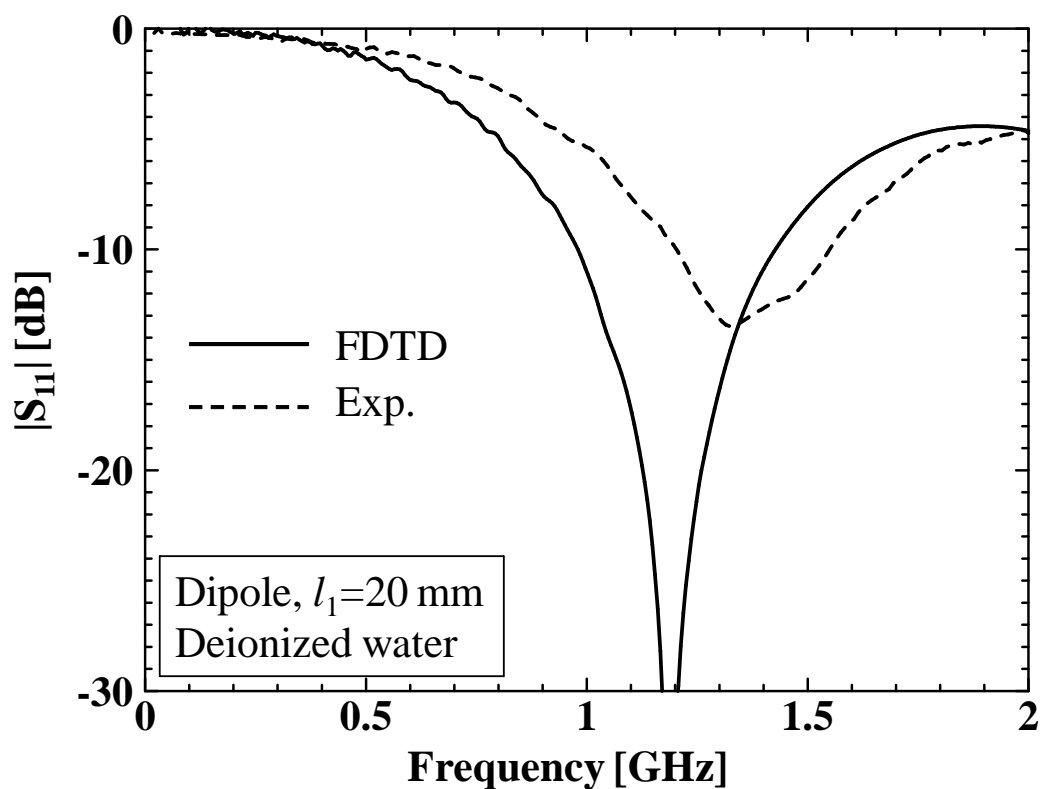
Above all, it is found that the same local maximum frequency band was obtained both in radiation effeicnecy and transmission factor. From Figure 3.11, Figure 3.14 and Figure 3.16, the reason of local maximum in the case of dipole to dipole is clarified: when the inside antenna operating at the half-wavelength resonant frequency, the radiated power to the outside becomes larger, and the local maximum of transmission factor is apperead.

## 3.6 Transmission factor through human body: loop to loop

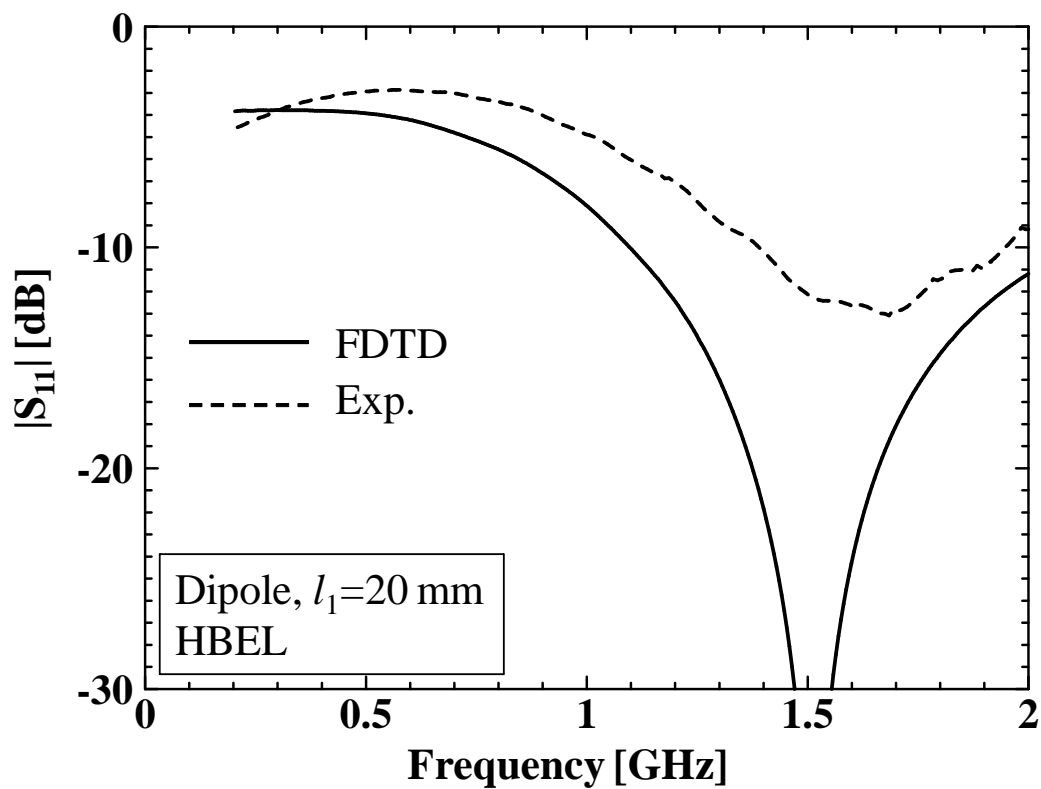
To compare the results of dipole to dipole, it is necessary to consider a loop to loop system. In order to compare with the dipole to dipole system, the same electrical length loop antennas was considered.

The rectangular loop antenna was also studied to compare with the results of dipole antenna. Figure 3.19 (a) and (b) show the numerical model and experimental setup of a torso-shaped phantom with a pair of loop antennas. A rectangular, an 1-turn rectangular loop antenna with loop length of  $L_1=40$  mm was immersed in HBEL as inside antenna (Port 1), and an 1-turn rectangular loop antenna with loop length of  $L_2=280$  mm was placed outside the phantom (Port 2). Figure 3.20 shows the reflection coefficient  $S_{11}$  of inside loop antenna immersed in deionized water and in HBEL. Figure 3.21 shows the input impedance  $Z_{in}$  of inside loop antenna in deionized water. Figure 3.22 shows the input impedance  $Z_{in}$  of inside loop antenna in HBEL. Figure 3.23 shows the reflection coefficient  $S_{22}$  and impedance of outside loop antenna  $Z_{22}$ . Figure 3.24 shows the  $|S_{21}|$  in the case of loop antenna immersed in deionized water and HBEL. It is found that the maximum value was appeared at 1 GHz, the results are similar with the dipole to dipole. Figure 3.25 shows the transmission factor  $\tau$  in the case of loop antenna immersed in deionized water and HBEL. It is observed that the curves of loop to loop are different from dipole to dipole, and it is also found that the transmission factor of loop to loop decreases as frequency increased from 200 MHz to 500 MHz.

(a)  $\lambda_g$ .(b)  $l_1/\lambda_g$ .Figure 3.6: Calculated  $\lambda_g$  and  $l_1/\lambda_g$  by using plane wave formula.

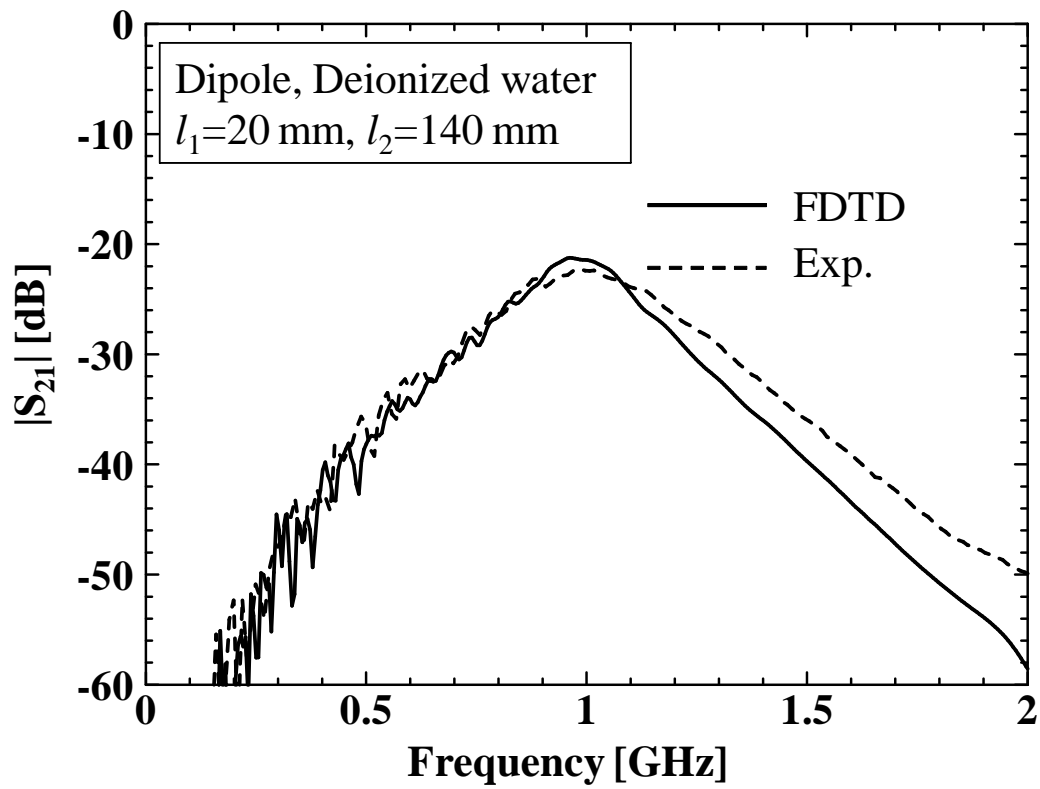


(a) Deionized water.

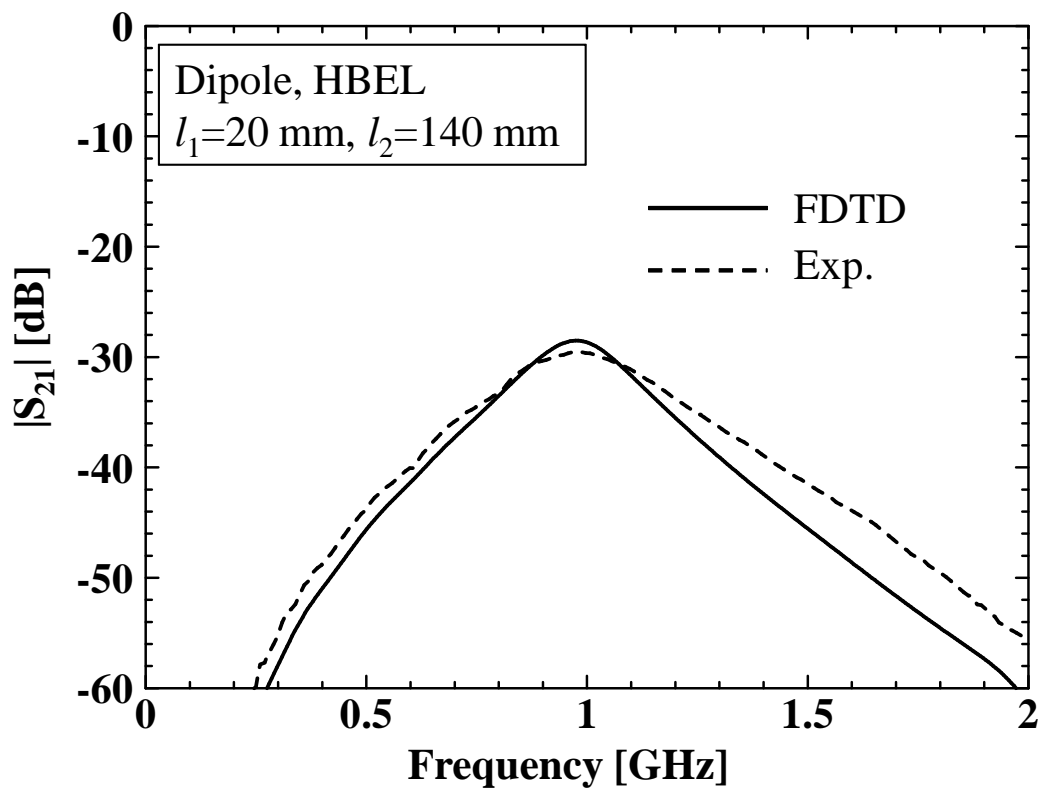


(b) HBEL.

Figure 3.7: Reflection coefficient  $|S_{11}|$ .



(a) Deionzied water.



(b) HBEL.

Figure 3.8:  $|S_{21}|$  from inside dipole through torso-shaped phantom to the outside dipole.



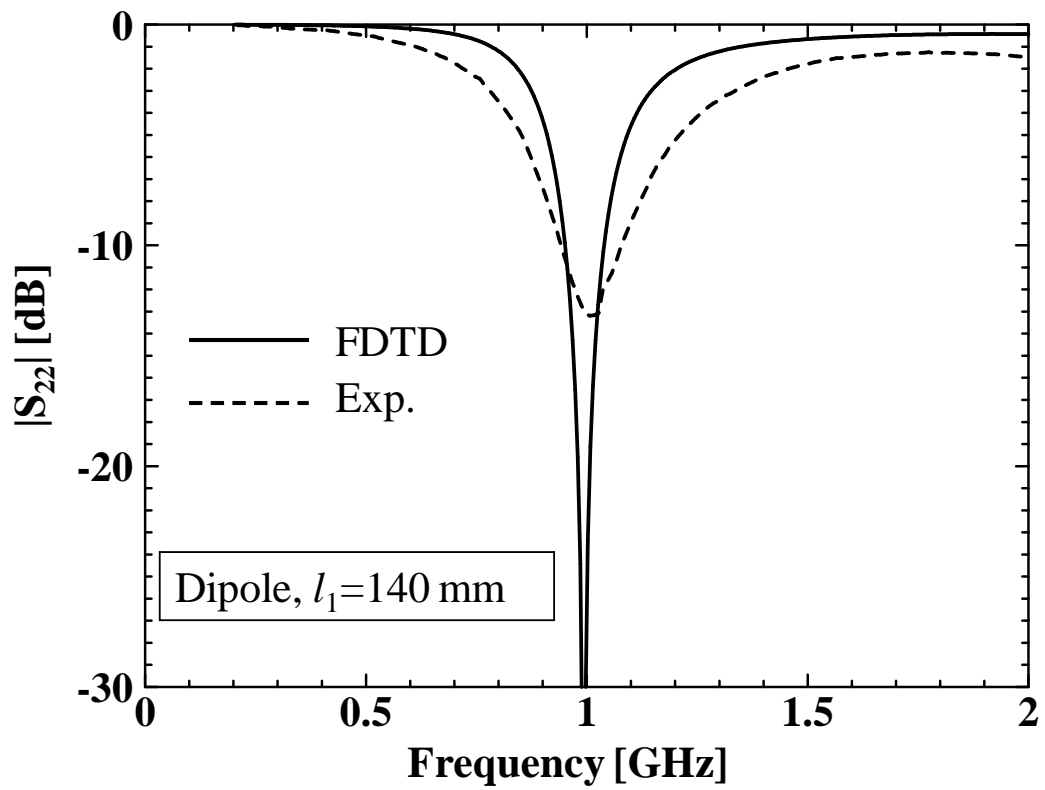
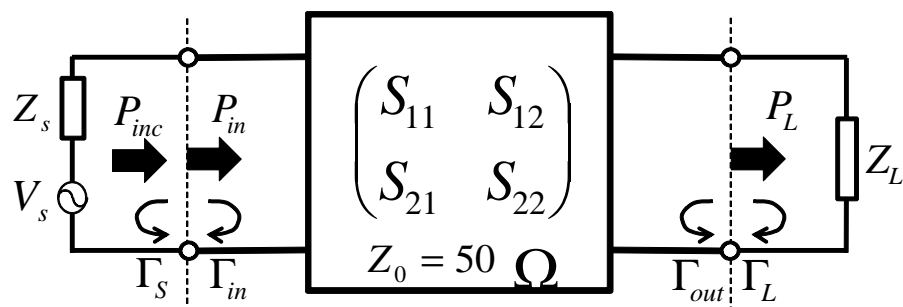
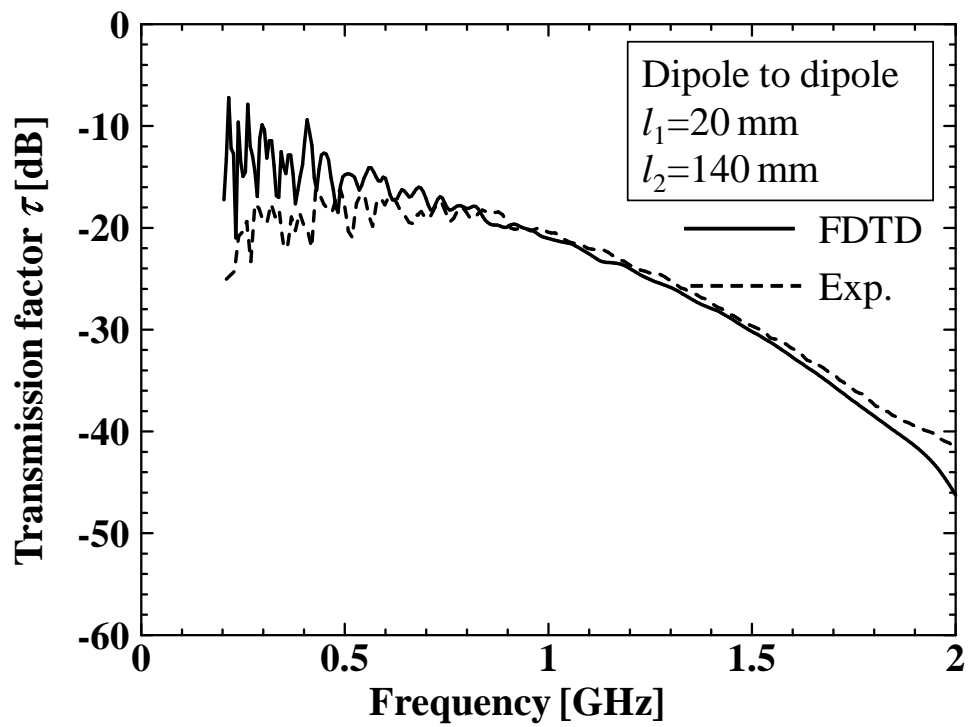
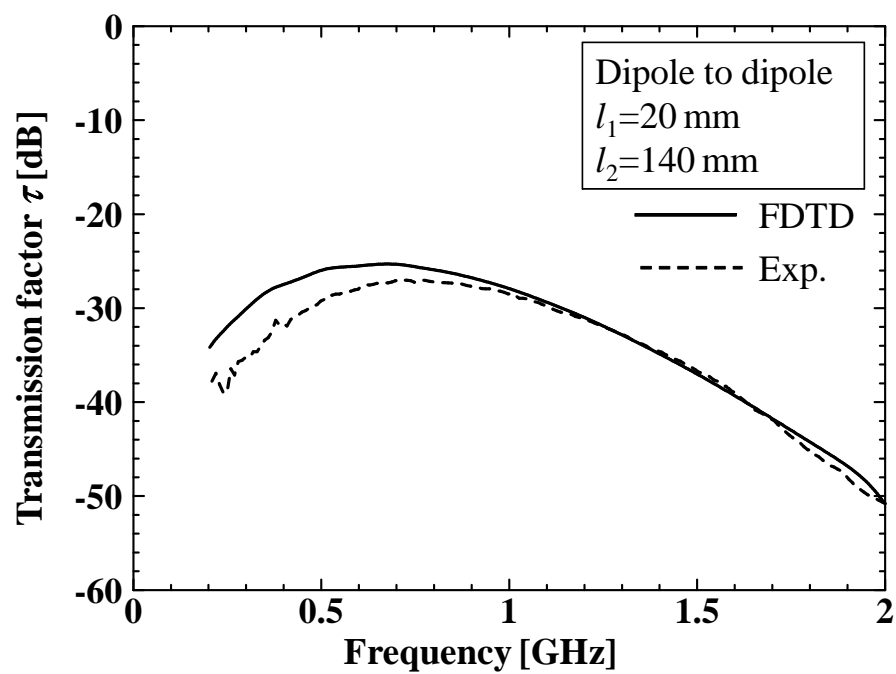
Figure 3.9: Reflection coefficient  $|S_{22}|$ .

Figure 3.10: Two-port equivalent circuit.

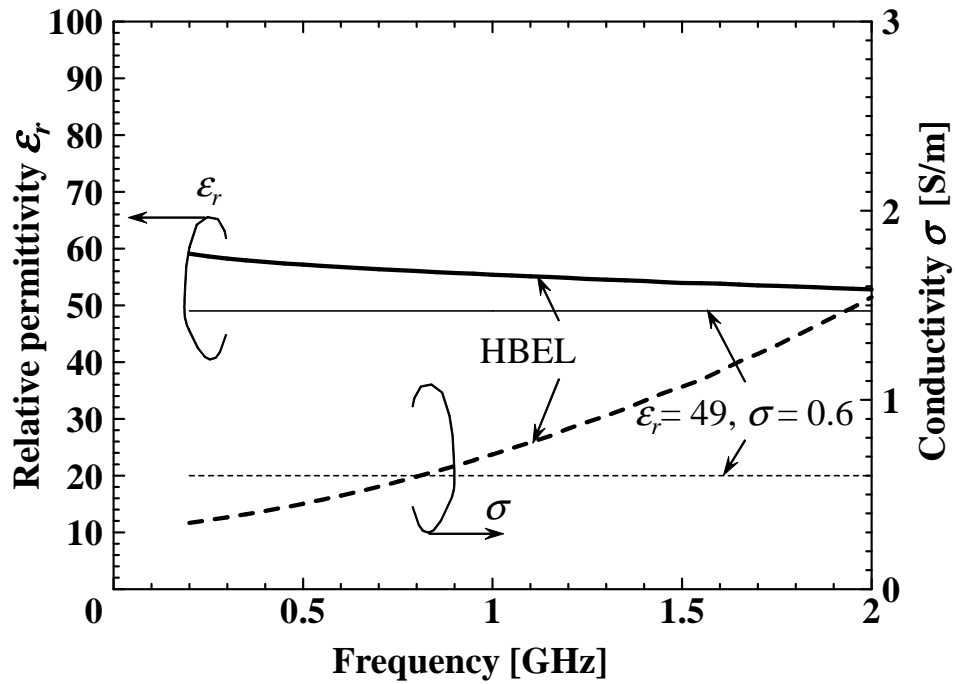


(a) Deionized water.



(b) HBEL.

Figure 3.11: Transmission factor of dipole to dipole through torso-shaped phantom.



(a) Relative permittivity and conductivity of material with constant permittivity (MCP) and HBEL.

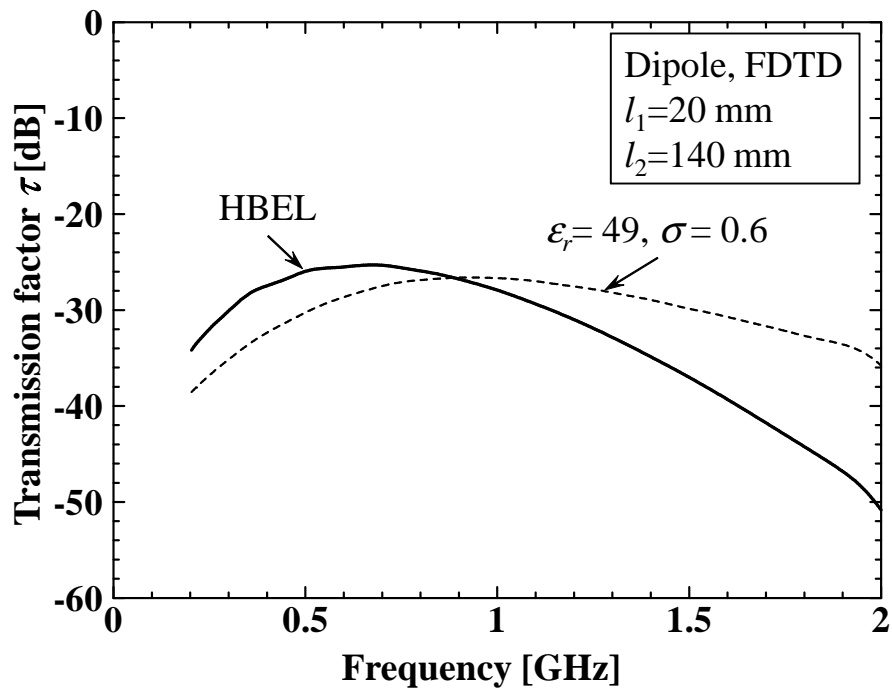
(b) Calculated transmission factor  $\tau$  in the case of dipole to dipole through material with constant permittivity (MCP) and HBEL.

Figure 3.12: Transmission factor of inside dipole immersed in different liquids.

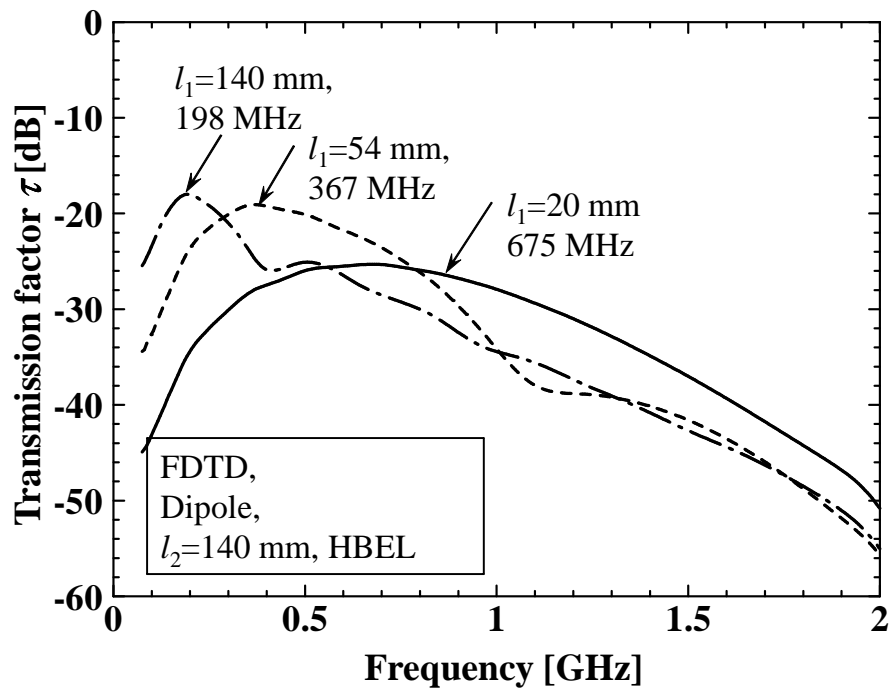


Figure 3.13: Calculated transmission factor with change the length of inside dipole.

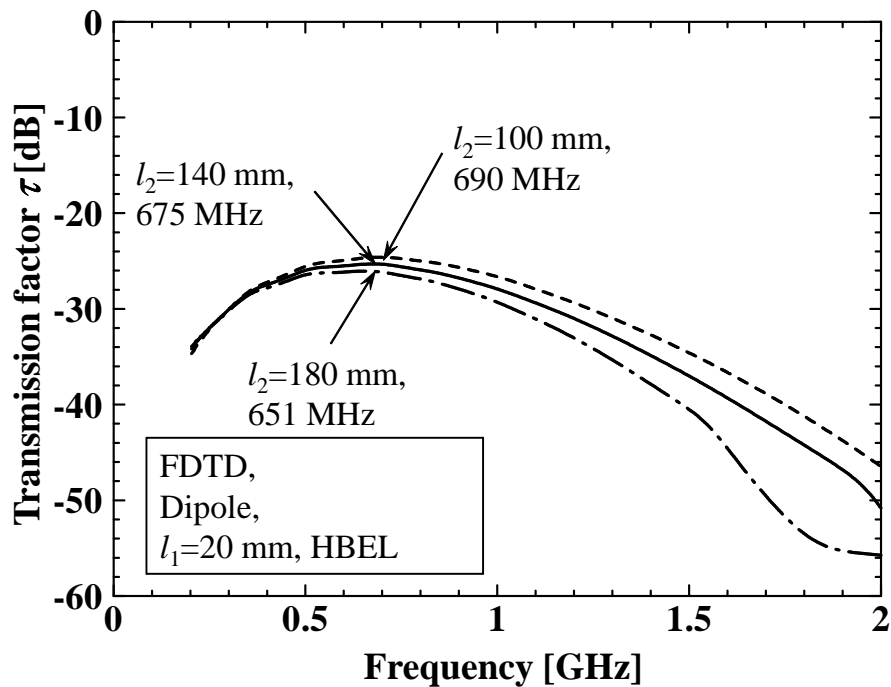
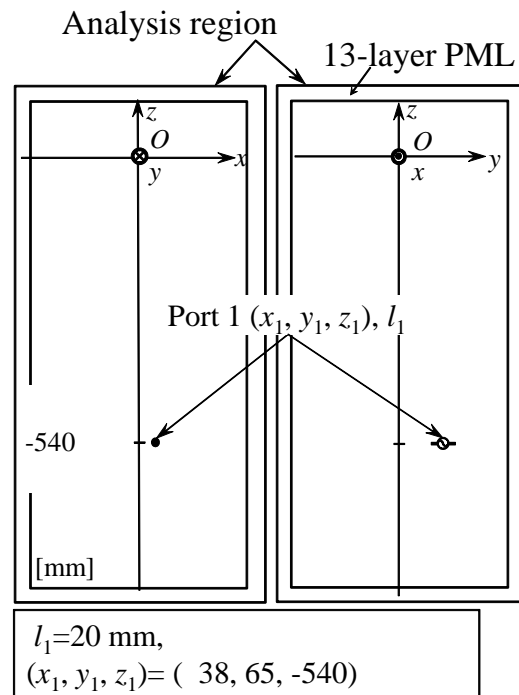
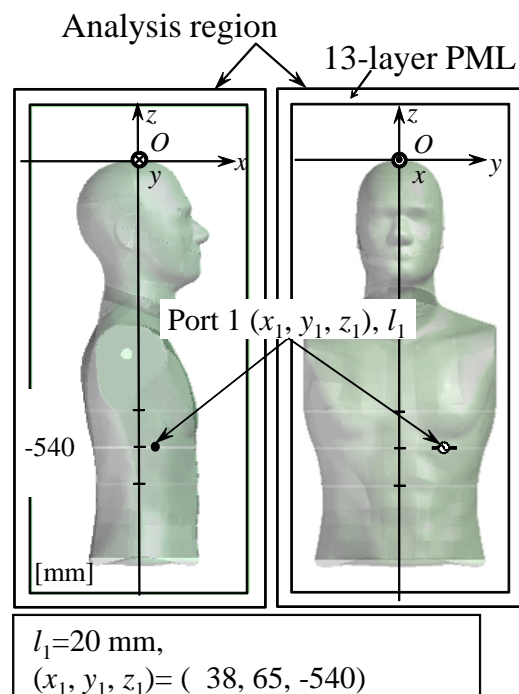


Figure 3.14: Calculated transmission factor with change the length of outside dipole.



(a) Dipole antenna without human torso-shaped phantom.



(b) Dipole antenna with human torso-shaped phantom.

Figure 3.15: Analysis model of radiation efficiency simulation.

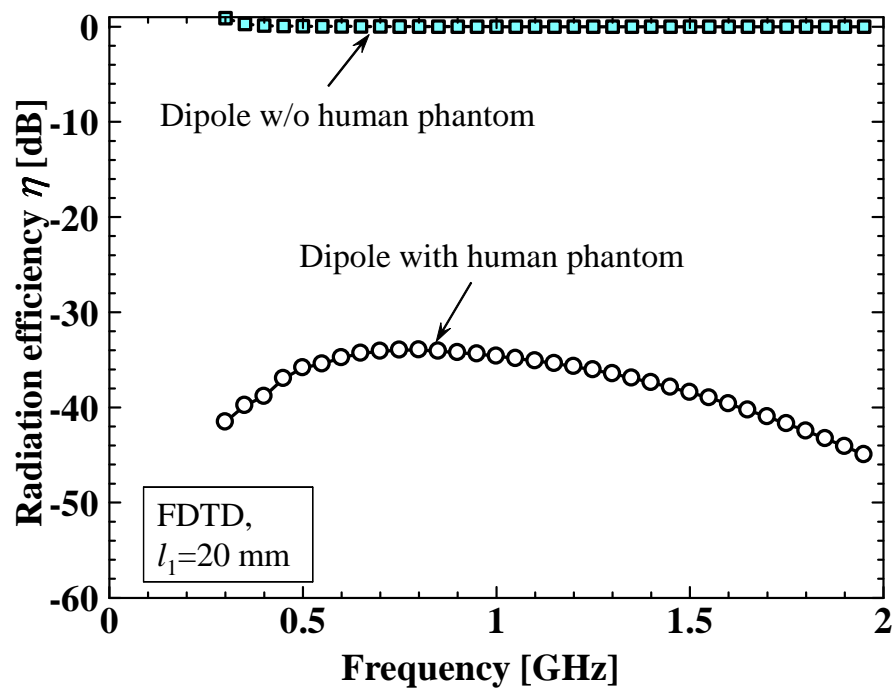
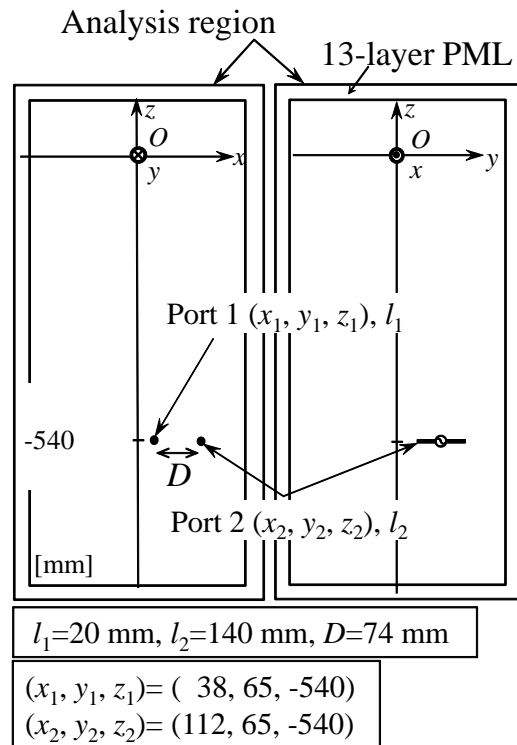
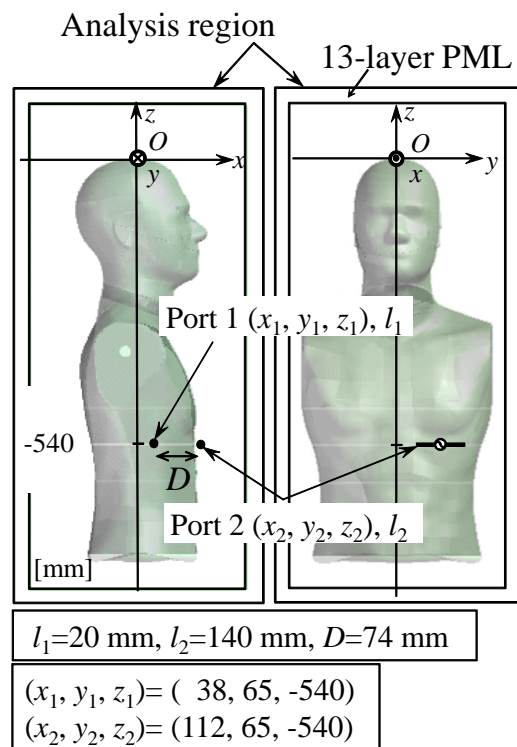


Figure 3.16: Numerical analysis results of antenna radiation efficiency.



(a) Dipole to dipole without human torso-shaped phantom.



(b) Dipole to dipole without human torso-shaped phantom.

Figure 3.17: Analysis model of transmission factor simulation.

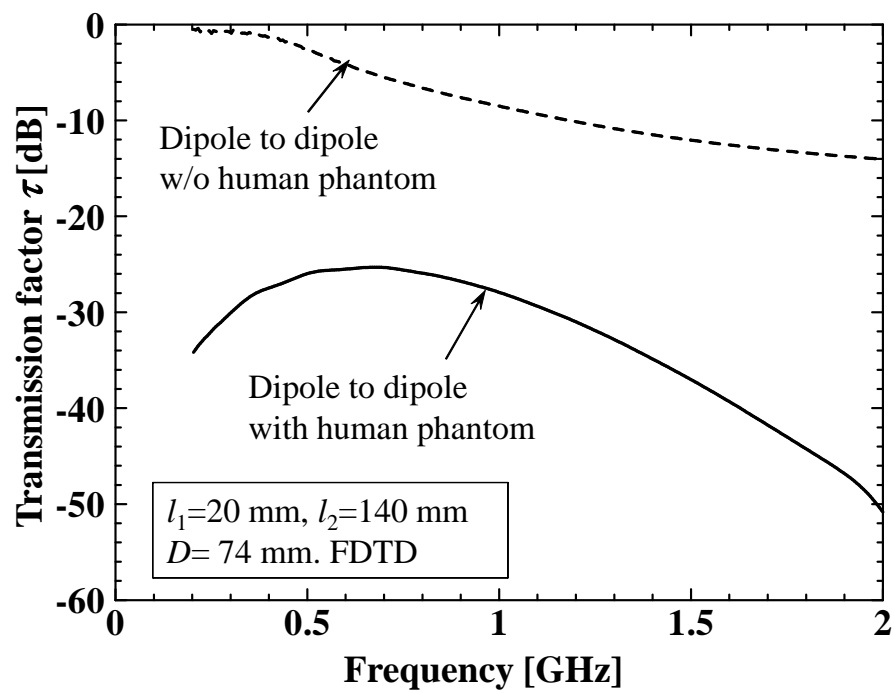
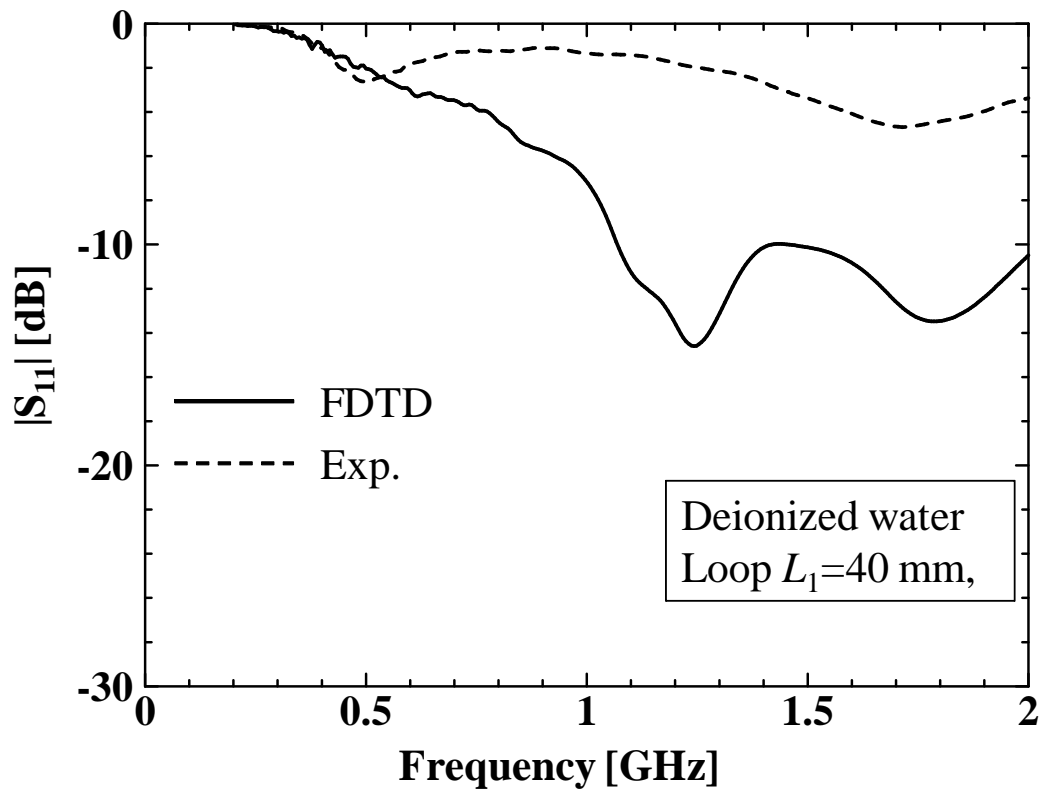


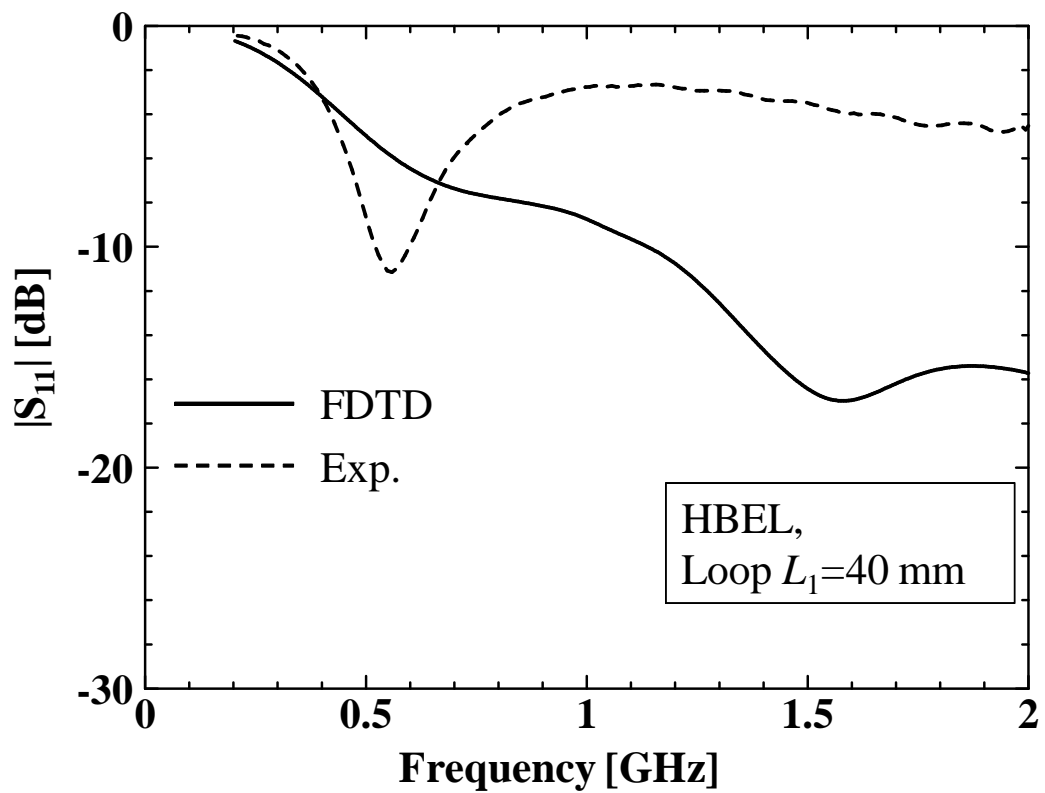
Figure 3.18: Numerical analysis results of transmission factor.







(a) Deionized water.



(b) HBEL.

Figure 3.20:  $|S_{11}|$  of inside loop antenna immersed in deionized water and in HBEL.

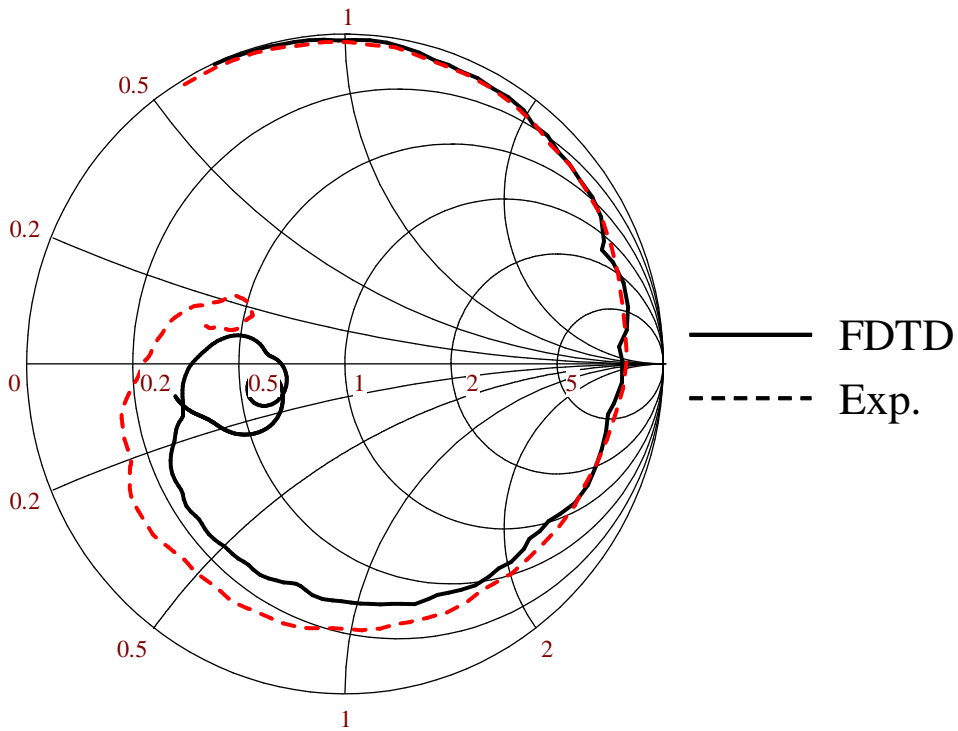
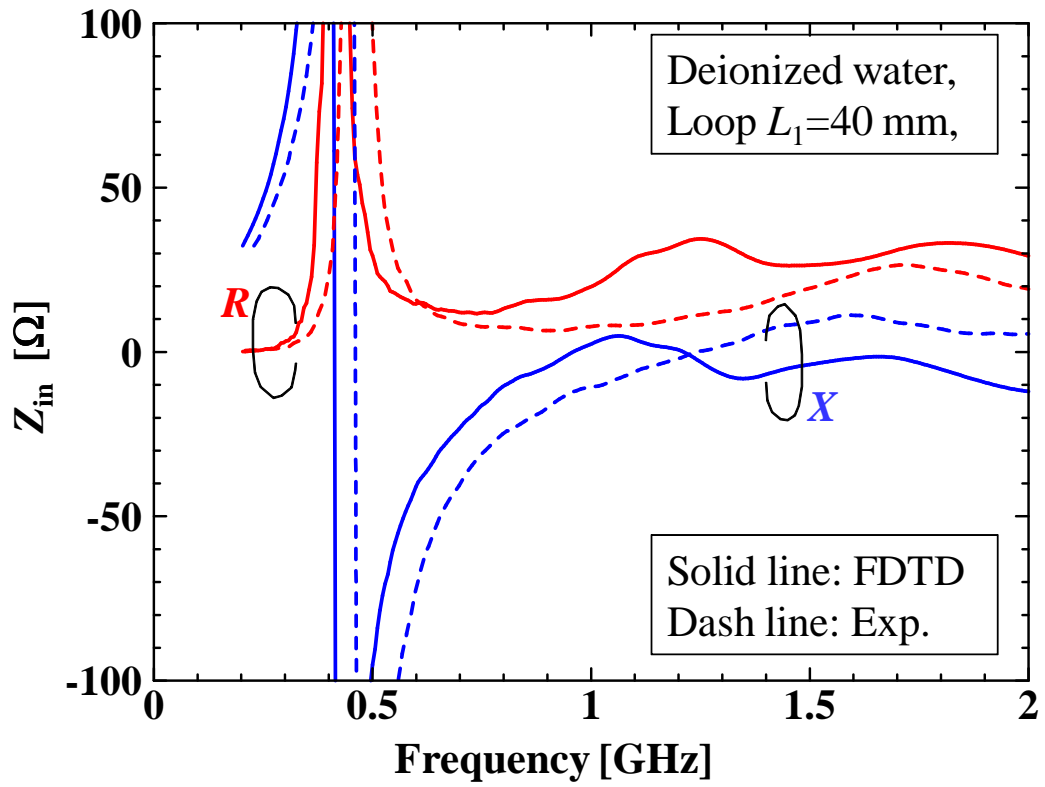
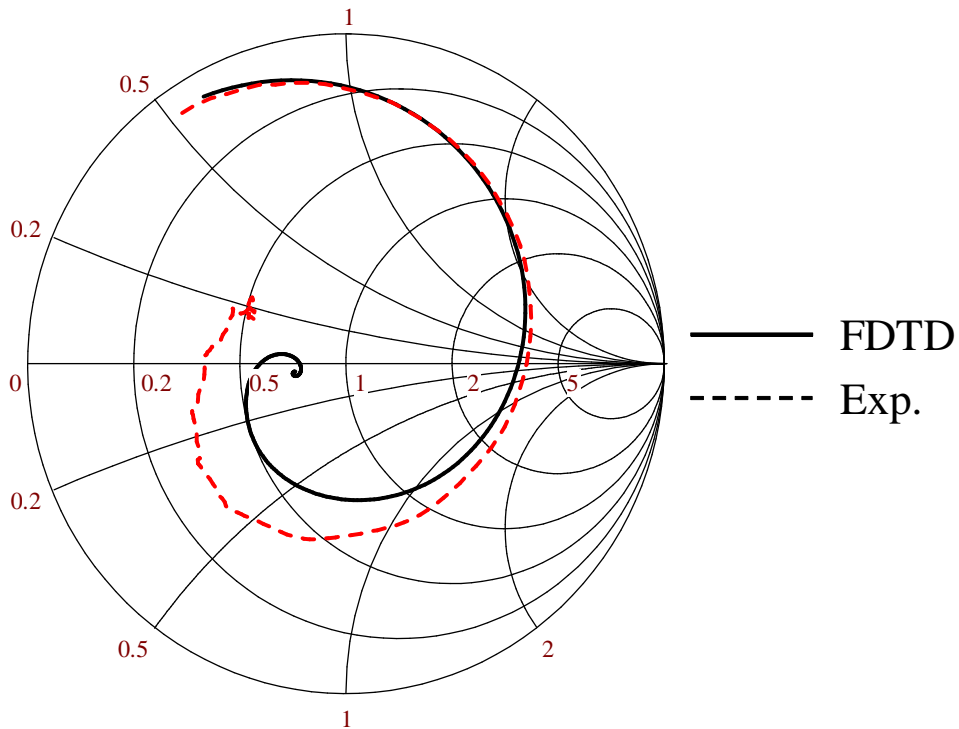
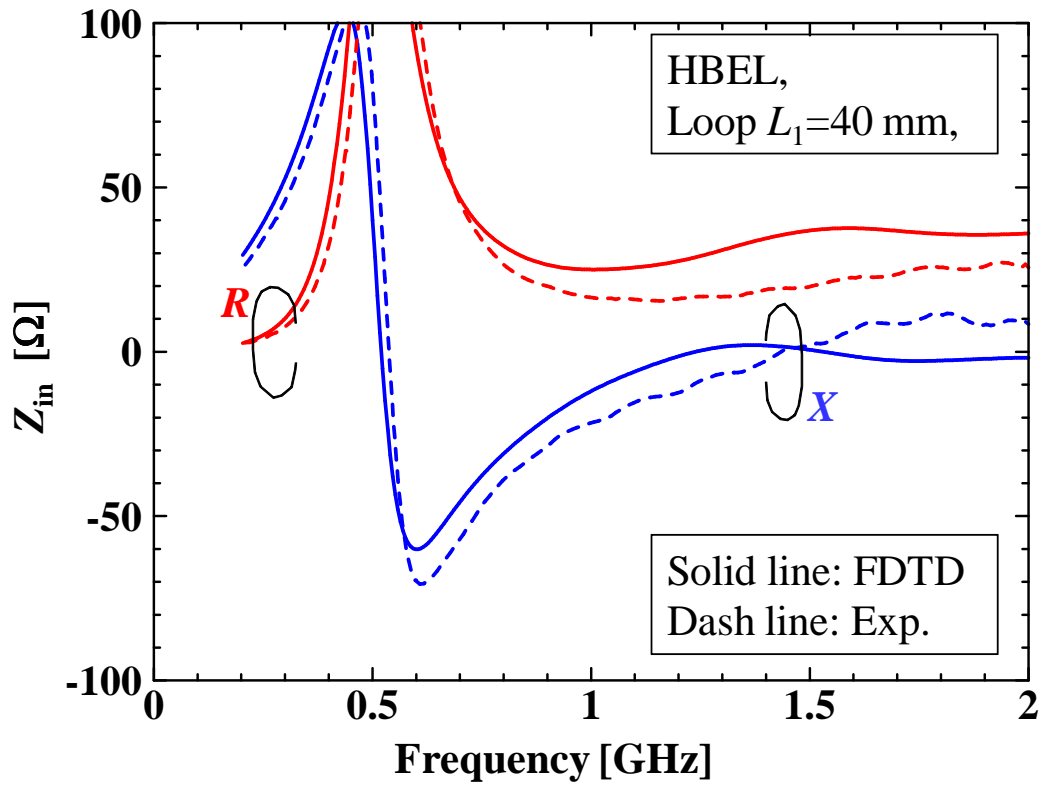
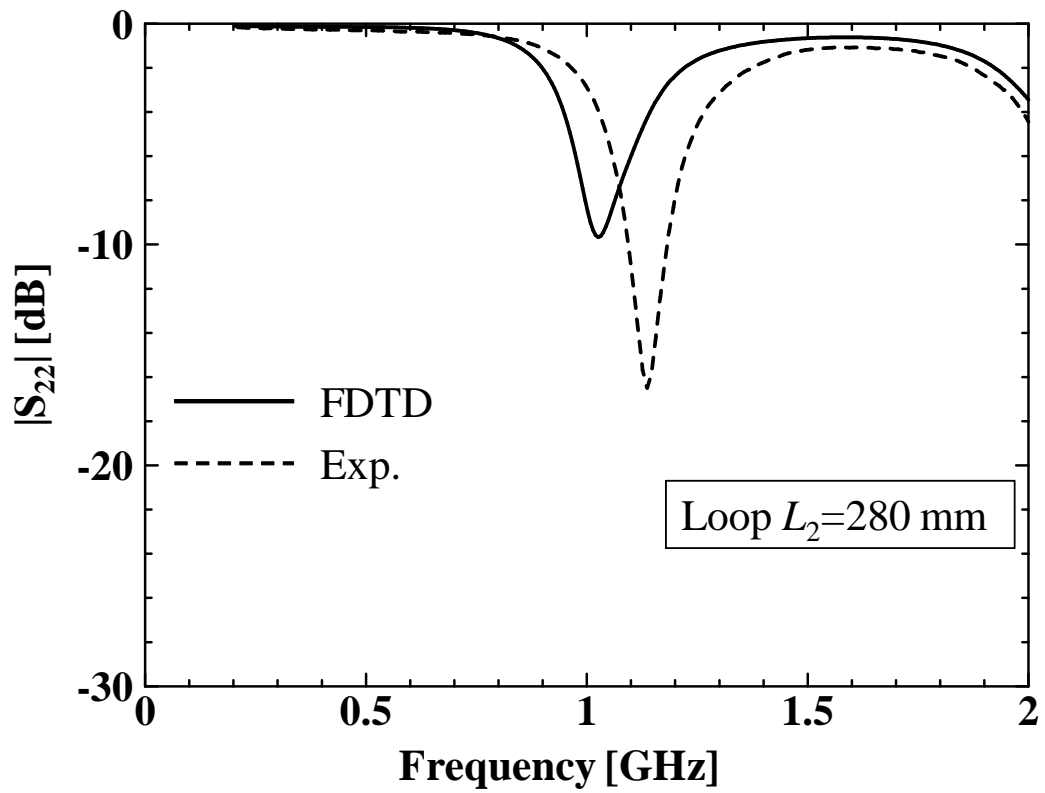
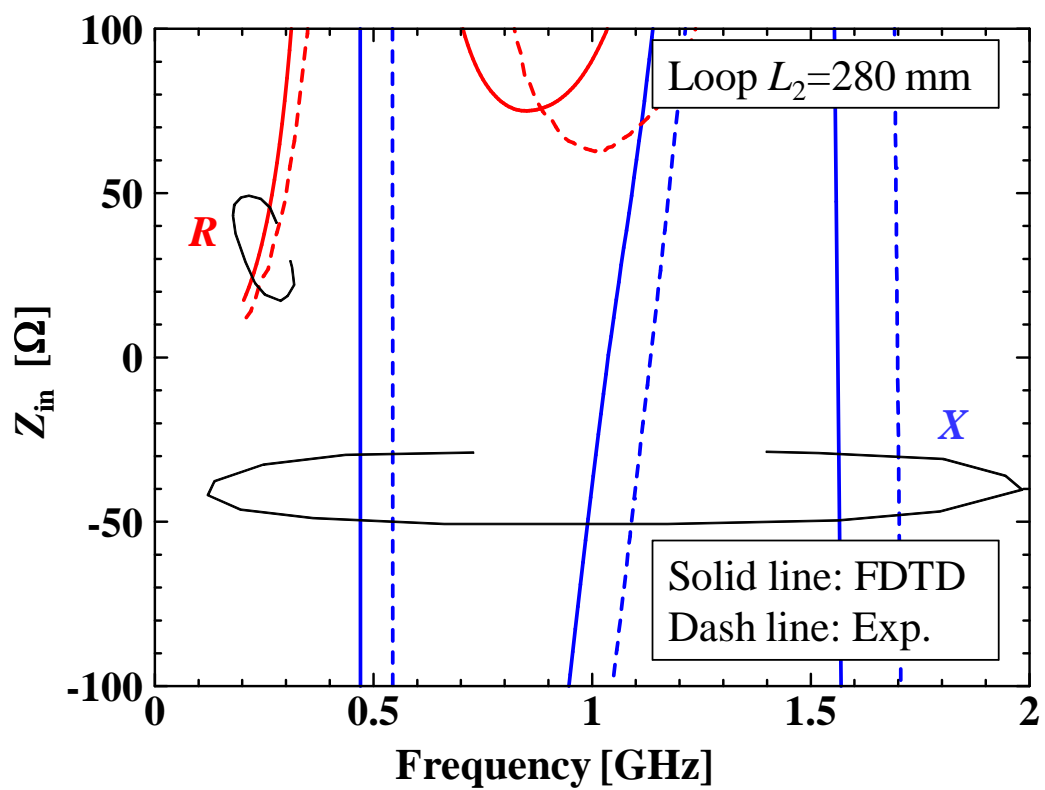


Figure 3.21: Input impedance of loop antenna immersed in deionized water.



(b) HBEL.

Figure 3.22: Input impedance of loop antenna immersed in HBEL.

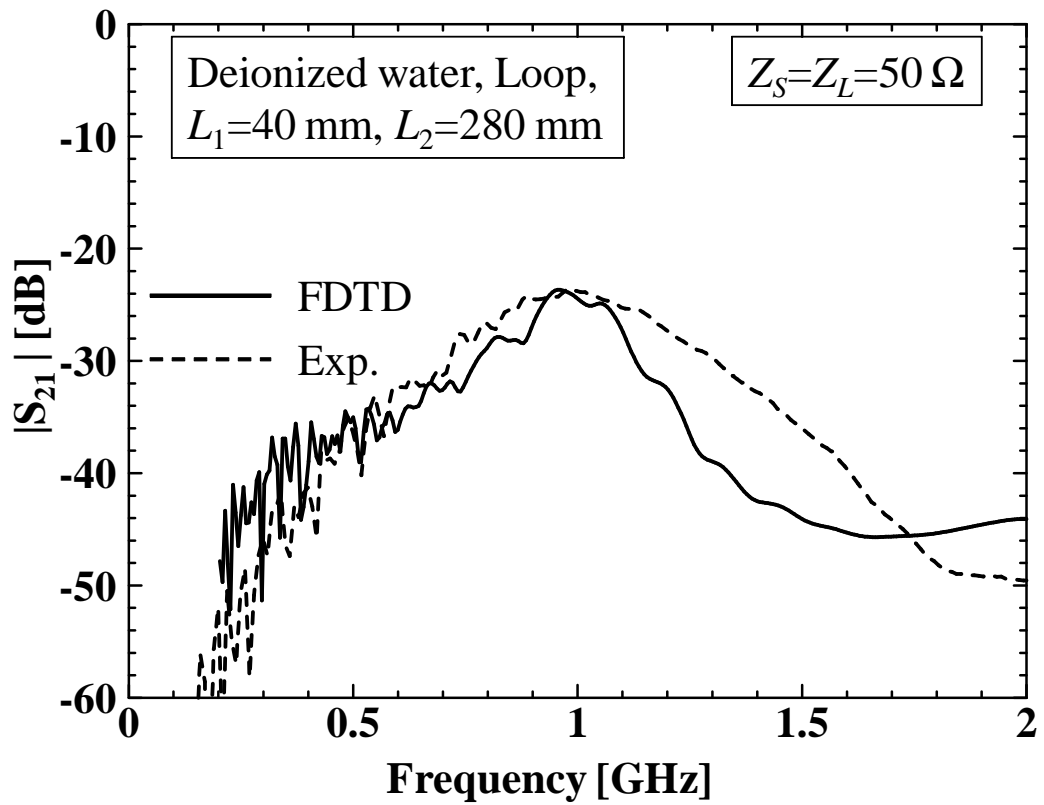
(a)  $S_{22}$ .(b)  $Z_{22}$ .Figure 3.23: Reflection coefficient  $S_{22}$  and impedance of outside loop antenna  $Z_{22}$ .

## 3.7 Conclusion

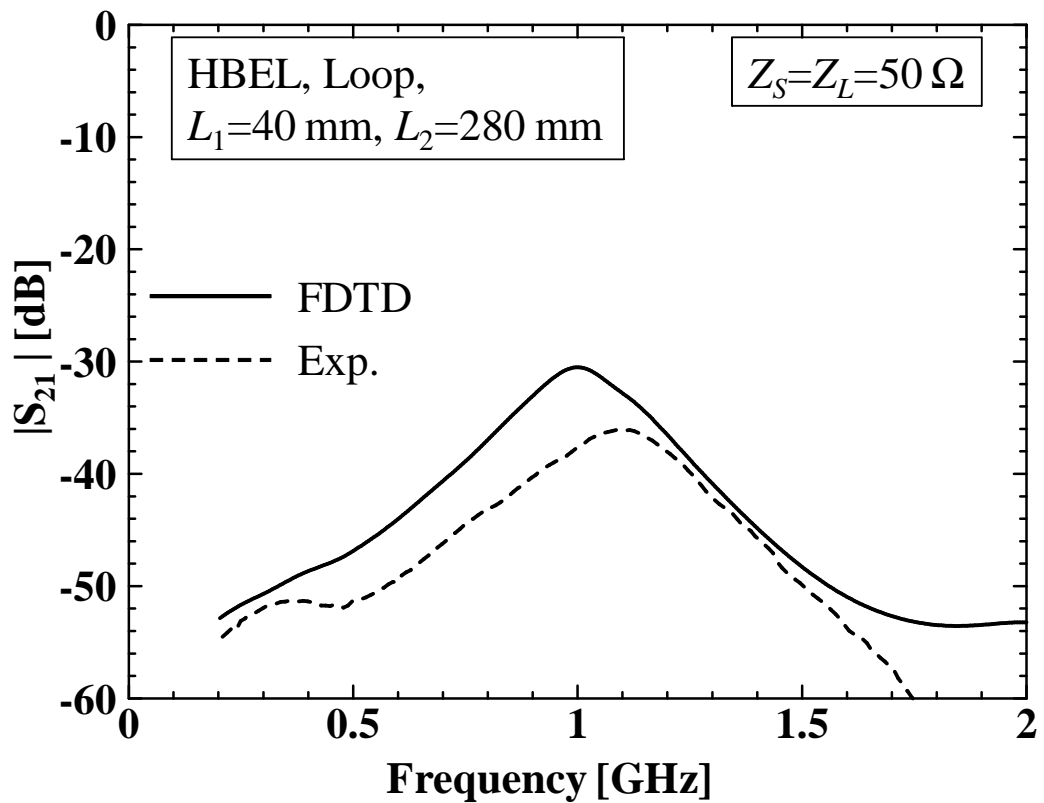
In this chapter, EM-wave propagation through a human body phantom was studied in the frequency range 200 MHz to 2 GHz. The transmission characteristics of a dipole and a loop immersed in the torso-shaped phantom filled with deionized water or human body equivalent liquid were investigated by the FDTD analysis and the measurements.

The transmission factor  $\tau$  was used to evaluate the path loss through the human body phantom. It is found that the transmission factor  $\tau$  decreases as the conductivity increases in the case of dipole antenna placed in deionized water. On the other hand, there is a local maximum in the transmission factor  $\tau$  at a frequency in the case of HBEL. The local maximum is caused by the half-wavelength resonant frequency of inside antenna.

It is important to choose operating frequency in capsule antenna design. From this chapter, it is found that in high frequency range media loss is large, while in low frequency range antenna efficiency is low. Operating frequency of wireless capsule endoscope system can be decided by using transmission factor. However, if operating frequency was decided, size of dipole antenna can be changed in order to decrease the propagation loss.

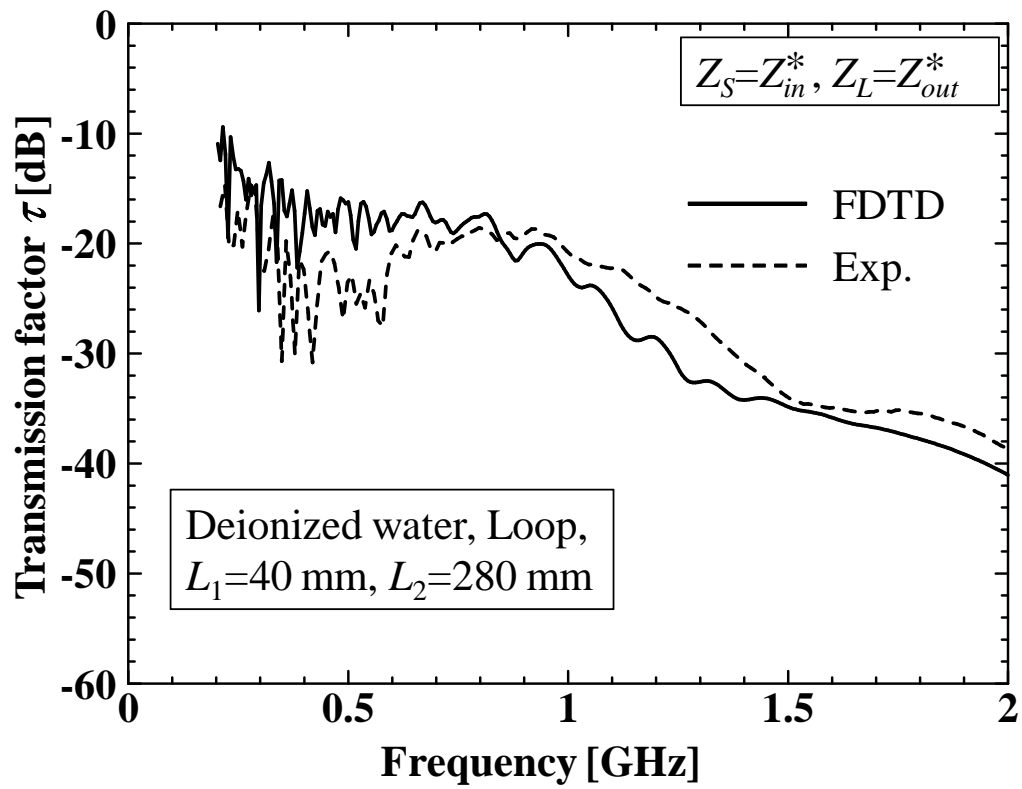


(a) Deionized water.

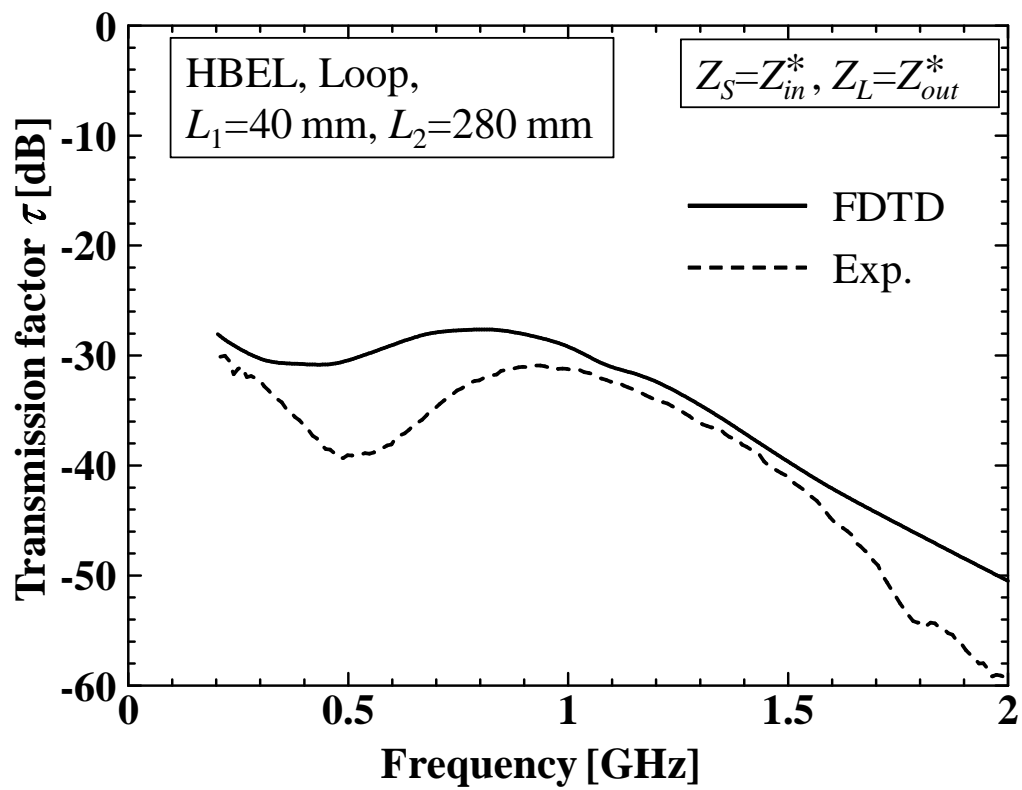


(b) HBEL.

Figure 3.24:  $|S_{21}|$  from inside loop through torso-shaped phantom to the outside loop.



(a) Deionized water.



(b) HBEL.

Figure 3.25: Transmission factor of loop to loop through torso-shaped phantom.



# Chapter 4

## Propagation loss through in-homogenous human body phantom

As an addition to Chapter 3, Propagation loss of microwave through in-homogenous human body phantom is investigated by numerical analysis. The in-homogenous human body phantom is introduced in Section 4.1. The numerical analysis model is shown in Section 4.2. Some analysis results and observations are performed in Section 4.3. Finally, conclusions are given in Section 4.4.

### 4.1 Introduction

In previous chapter, propagation loss through homogenous human body models was studied. When a capsule endoscope passes through various organs of the digestive system, the surrounding environment of the dipole changes and the absorption of EM waves will be changed. In human body organs with different dielectric permittivity, the size of the dipole compared with the wavelength of the operating frequency changes from moment to moment, this phenomenon cannot be obtained with homogenous human body phantom, so it is important to consider the in-homogenous human body phantom. The digestive

system in in-homogenous human body phantom was considered in this chapter, which is composed of the esophagus, the stomach, the small intestine and the large intestine. Until now, few researches focus on the received power from a dipole placed in different parts of the digestive system. In this chapter, transmission factor used in Chapter 3 was also studied as an indicator of propagation loss and was evaluate from different organs of a digestive system.

## 4.2 Analysis model

The FDTD analysis model of a human body “Duke” developed by SPEAG was used which is constructed by using MRI images. It includes 76 kinds of organs and the relative permittivity and conductivity of each organs provided by ITIS [60] were used. Figure 4.1 shows the comparison of homogenous human body phantom and in-homogenous human body phantom.

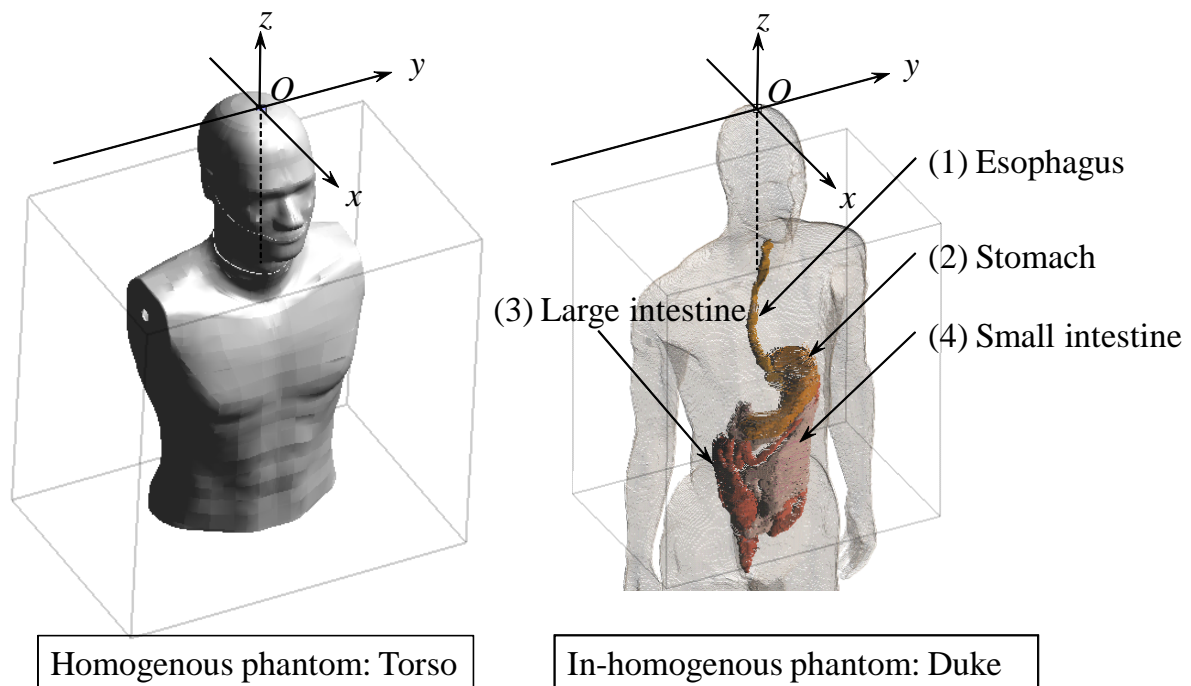


Figure 4.1: Homogenous phantom and in-homogenous phantom.

Figure 4.2 shows the analysis model of in-homogenous human body phantom. The

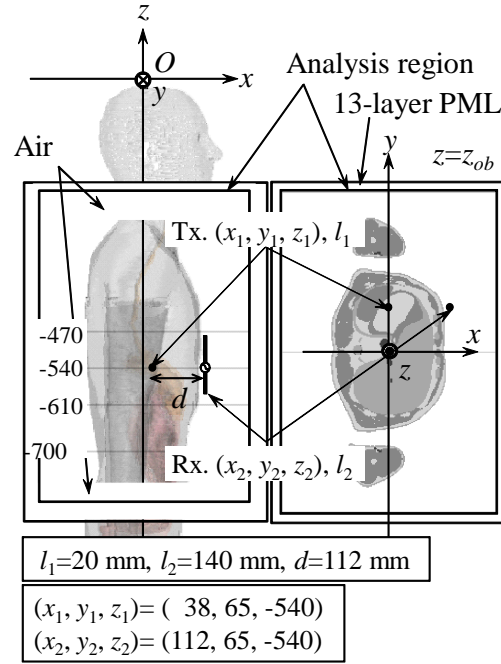


Figure 4.2: Analysis model of in-homogenous phantom.

torso part of a human body was used in the FDTD analysis. Lumina of digestive system were filled with deionized water. The cross section of an analysis model in  $xy$ -plane was shown in Figure 4.2. The origin of coordinates was placed at the top of the head. The inside dipole with a length of  $l_1=20$  mm was placed at  $(x_1, y_1, z_1)$  in the digestive system of a human body and an outside dipole with a length of  $l_2=140$  mm was placed at  $(x_2, y_2, z_2)$  outside of a human body. The position of inside dipole changes along the digestive system as  $z=-470, -540$  and  $-610$  mm which corresponds to the cases when the inside dipole was placed in the esophagus, the stomach, the small intestine and the large intestine. The FDTD method with considering the dispersive effect of complex dielectric permittivity was used for numerical analysis. The fitting data (Debye or generic dispersive) of all 76 kinds of human body tissues are shown in Table 4.1.

$$\epsilon_r = \epsilon_\infty + \frac{\epsilon_s - \epsilon_\infty}{1 + j\omega t_0} \quad (4.1)$$

$$\epsilon_r = \epsilon_\infty - j \frac{\sigma}{\omega \epsilon_0} + \sum_{p=1}^P \frac{A_p}{B_p \omega^2 + C_p j \omega + D_p} \quad (4.2)$$

$\epsilon_0$  is the vacuum permittivity;  $\sigma$  is the conductivity;  $\epsilon_\infty$  is the permittivity for  $\omega \rightarrow \infty$ ;  $\epsilon_s$  denotes the relative static ( $\omega \rightarrow \infty$ ) permittivity;  $P$  is the number of poles;  $A_p$ ,  $B_p$ ,  $C_p$ ,  $D_p$  represent the coefficients for the Generic dispersive model.

An example of the conductivity distribution in the  $xz$ -plane is shown in Figure 4.2. The color indicates the magnitude of conductivity at 1 GHz.

### 4.3 Numerical analysis and observations

When inside dipole passes through the esophagus, the polarization of the inside dipole is vertically placed because the structure of the esophagus is narrow. Both inside dipole and outside dipole were selected as  $z$ -direction. The position of inside dipole is  $(x_1, y_1, z_1) = (20, 0, -470)$  in the esophagus and two cases of the position of outside dipole placed in front of body  $(x_2, y_2, z_2) = (112, 0, -470)$  and at the back of body  $(x_2, y_2, z_2) = (-116, 0, -470)$ , were simulated respectively. The transmission factors are shown in Figure 4.3.

As shown in Figure 4.3(a), in the case of homogenous phantom, the transmission factors are almost same in the condition that the distances are almost same. The local maximum of  $\tau$  is observed at 500 MHz corresponding to the half-wavelength resonant frequency of inside dipole, while  $\tau$  decreases as the frequency increases as the conductivity of HBEL increases.

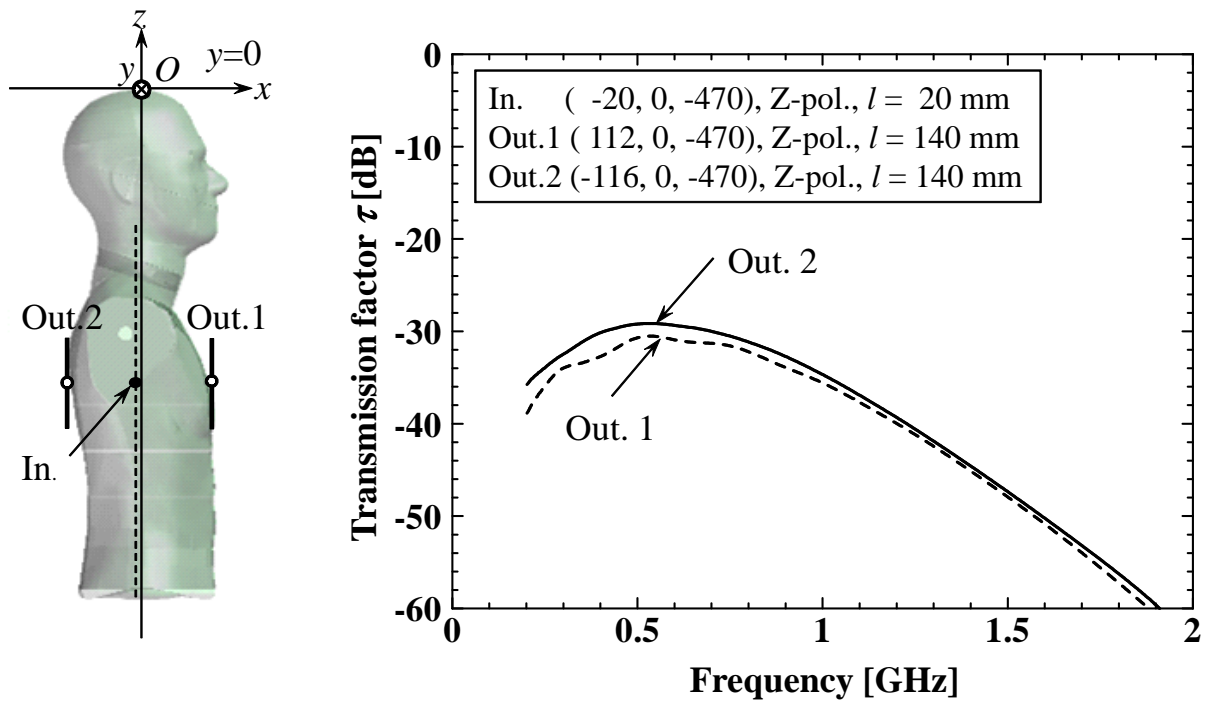
As shown in Figure 4.3(b), in the case of in-homogenous phantom, it is observed that the conductivity of the heart is larger than the other organs. It is also observed that higher  $\tau$  is obtained in the case when the outside dipole is placed at the back of a human body compared to the case when the outside dipole is placed in front of a human body. The reason is the strong reflection caused by high conductivity of the heart.

Figure 4.4 show the  $E$ -field distribution and the radiation pattern when the inside dipole is placed in the esophagus at 500 MHz. From Figure 4.3 we can find electric field in front of body is weaker than back of body because the conductivity of heart is relatively high.

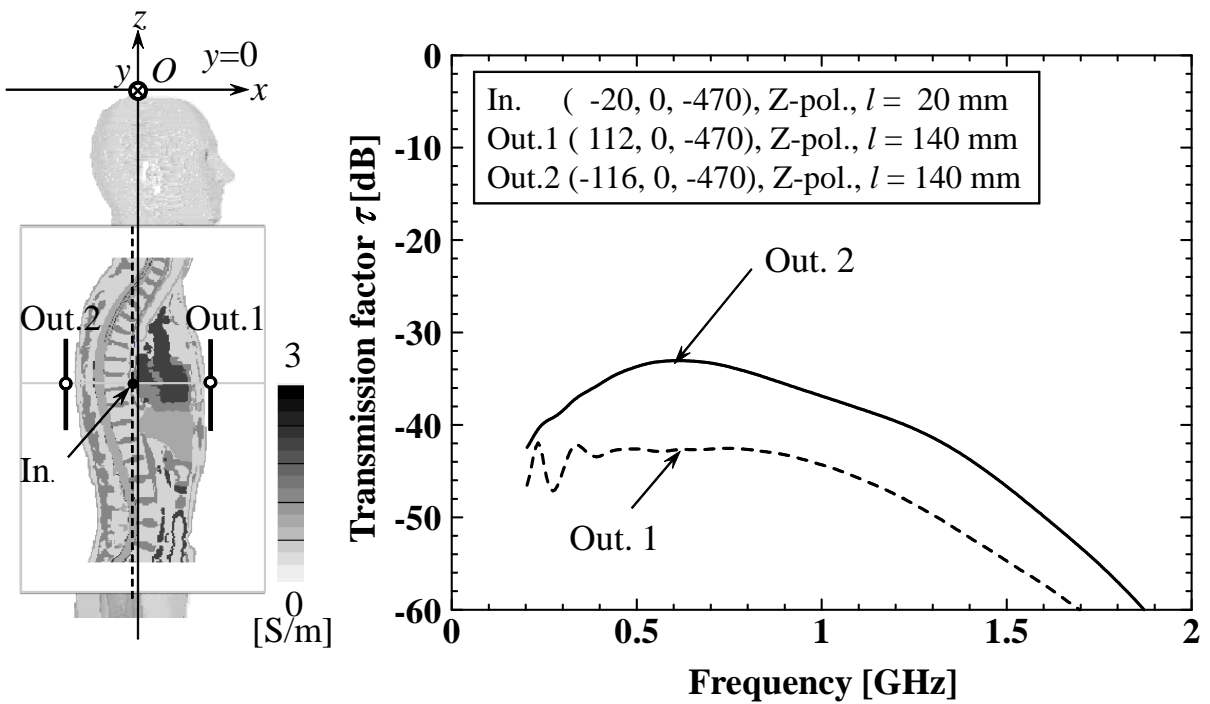
Table 4.1: Generic dispersive fitting data

Name	$\epsilon_0$	$\sigma$	$A_{p1}$	$B_{p1}$	$C_{p1}$	$A_{p2}$	$B_{p2}$	$C_{p2}$	$A_{p3}$	$B_{p3}$	$C_{p3}$	$A_{p4}$	$B_{p4}$	$C_{p4}$
Adrenal_gland	54.6161	1.58121	-1.87E+19	3.86E+08	2.07E+17	-5.50E+19	8.65E+09	2.48E+20	-1.63E+21	1.61E+10	5.93E+17	1.03E+18	1.11E+08	1.28E+18
Artery	15.7355	33.8674	4.00E+19	8.56E+09	1.58E+19	-3.14E+20	8.87E+09	3.87E+12	-3.09E+23	8.48E+10	2.99E+15	-7.28E+18	4.27E+08	1.05E+14
Bladder	10.2257	3.8489	-1.20E+19	2.32E+09	1.38E+12	-1.84E+22	4.64E+10	4.05E+12	0	0	0	0	0	0
Blood_vessel	24.7108	6.45368	1.64E+21	1.15E+06	9.48E+20	-1.83E+19	1.10E+09	7.44E+14	-2.44E+22	3.67E+10	1.62E+13	0	0	0
Bone	7.38404	5.57099	-1.91E+21	1.19E+09	2.32E+16	-3.36E+19	1.08E+08	1.78E+13	-2.95E+22	5.08E+10	9.96E+15	-1.99E+20	9.15E+09	3.57E+17
Bronchi	21.0821	9.56926	3.86E+20	3.45E+10	9.15E+19	-3.11E+18	1.08E+06	1.39E+16	-5.03E+22	4.94E+10	6.21E+13	0	0	0
Cartilage	18.5999	8.28093	-3.20E+22	3.71E+10	8.86E+15	-5.07E+19	3.06E+09	3.45E+16	-4.03E+18	3.07E+06	3.28E+15	0	0	0
Cornea	34.7595	6.87507	2.29E+19	1.65E+09	2.31E+13	-2.11E+22	3.00E+10	1.42E+14	1.21E+21	2.20E+10	1.86E+19	2.59E+19	4.33E+09	3.65E+19
Diaphragm	18.853	26.2669	-2.37E+23	8.28E+10	2.72E+15	-1.11E+20	6.69E+09	6.02E+12	-2.13E+15	3.84E+05	1.79E+18	-1.07E+19	8.94E+08	3.34E+14
Epididymis	30.7815	1.18363	2.91E+23	1.89E+11	1.05E+22	-1.43E+20	6.34E+09	2.02E+12	-1.24E+19	7.56E+08	1.08E+17	0	0	0
Esophagus	28.6486	19.8349	-4.85E+19	3.20E+09	2.15E+15	-4.11E+18	5.81E+05	1.24E+12	8.15E+15	7.19E+06	2.14E+18	-1.27E+23	5.98E+10	1.10E+13
Fat	7.51093	0.87107	-9.76E+17	4.09E+08	1.70E+15	-2.72E+21	3.07E+10	8.39E+16	-7.89E+18	4.68E+09	1.57E+13	1.35E+21	1.65E+10	1.58E+21
Gallbladder	31.501	13.154	-7.41E+22	5.45E+10	1.61E+13	-1.47E+19	8.35E+08	6.66E+15	-1.97E+18	4.46E+05	3.99E+17	2.97E+21	6.97E+09	1.22E+21
Heart_lumen	29.4936	15.5087	-8.21E+22	5.10E+10	8.07E+13	-4.54E+18	3.03E+05	1.86E+15	3.82E+20	2.89E+10	7.46E+19	0	0	0
Heart_muscle	27.2155	4.87444	-7.26E+19	2.17E+09	1.07E+13	-1.02E+22	2.36E+10	6.02E+13	-8.18E+18	3.69E+07	8.76E+15	2.88E+22	4.81E+09	2.24E+21
Interverteb_disc	33.0626	2.70763	-1.12E+18	2.00E+05	4.10E+13	-2.11E+22	1.18E+10	7.29E+13	-1.41E+18	3.32E+07	9.57E+17	3.04E+22	9.93E+09	2.55E+12
Kidney_cortex	33.011	8.26318	-1.36E+19	1.24E+06	5.70E+17	-2.72E+22	3.46E+10	1.91E+18	-1.32E+20	2.60E+09	2.27E+12	-3.33E+19	9.76E+06	4.13E+13
Kidney_medulla	33.0397	8.14429	-2.64E+22	3.40E+10	2.10E+15	-1.03E+19	529870	5.00E+16	-1.22E+20	2.59E+09	4.09E+13	0	0	0
Large_intestine	29.2108	6.62518	7.53E+20	1.10E+10	7.96E+15	1.20E+22	7.61E+07	1.85E+21	-2.00E+22	2.90E+10	1.88E+16	-1.32E+19	3.36E+08	1.74E+12
Larynx	20.8889	6.79903	-2.26E+22	3.24E+10	3.80E+13	-3.69E+19	2.18E+09	4.14E+16	0	0	0	0	0	0
Liver	16.1719	16.8217	-1.18E+23	6.53E+10	4.16E+13	5.91E+16	7.47E+07	1.49E+18	-1.78E+20	5.97E+09	7.82E+15	-2.36E+19	9.51E+08	2.20E+13
Lung	12.3601	3.82719	-6.14E+16	9.27E+07	1.59E+20	-1.65E+22	4.29E+10	3.00E+14	-3.26E+19	2.89E+09	8.78E+15	9.98E+20	238569	2.77E+13
Marrow_red	6.33466	1.50634	-4.51E+21	3.03E+10	2.32E+12	-7.86E+18	2.28E+09	6.56E+13	0	0	0	0	0	0
Medulla_oblongata	22.6185	10.0428	-4.67E+22	4.72E+10	2.35E+17	3.55E+21	2.09E+09	1.70E+21	-1.26E+19	6.92E+06	9.36E+16	-3.92E+19	1.39E+09	2.43E+14
Meniscus	18.5895	8.28619	2.98E+16	2.92E+07	5.66E+19	-3.20E+22	3.71E+10	2.12E+13	-3.91E+18	4.86E+06	2.40E+16	4.55E+17	5.88E+08	6.90E+19
Mucosa	60.9409	2.59266	8.18E+22	3.76E+09	1.67E+21	-4.94E+16	2.97E+07	7.78E+19	-1.50E+23	1.82E+06	2.33E+21	-1.70E+19	1.38E+09	2.94E+13
Muscle	29.3341	12.7152	-2.25E+19	4.36E+07	1.24E+14	-3.70E+19	2.90E+09	9.75E+14	-7.17E+22	5.35E+10	1.44E+18	-1.48E+19	4.16E+06	2.28E+17
Nerve	18.7215	5.12158	-7.12E+19	2.13E+07	6.64E+16	6.76E+19	1.09E+07	2.51E+14	-2.12E+22	4.08E+10	6.52E+15	-5.19E+19	3.02E+09	1.75E+17
Pancreas	40.3556	0.91562	6.40E+22	9.59E+10	3.41E+21	-3.79E+19	2.85E+09	2.69E+15	0	0	0	0	0	0
Patella	7.38404	5.57099	-1.91E+21	1.19E+09	2.32E+16	-3.36E+19	1.08E+08	1.78E+13	-2.95E+22	5.08E+10	9.96E+15	-1.99E+20	9.15E+09	3.57E+17
Prostate	27.8966	16.89	-5.25E+18	6.23E+07	5.04E+13	-1.01E+23	5.66E+10	7.69E+15	-5.30E+19	3.08E+09	8.53E+13	0	0	0
SAT	5.13539	3.94833	-8.73E+19	1.21E+10	1.16E+16	-5.39E+17	6.76E+06	1.68E+17	-8.59E+17	8.18E+06	7.96E+15	-3.26E+22	7.58E+10	1.67E+17
Skin	25.4051	5.15318	2.55E+21	1.56E+10	1.91E+13	4.71E+20	1.91E+10	7.84E+19	-1.40E+20	1.69E+08	9.68E+14	-1.89E+22	2.80E+10	2.32E+12
Small_intestine	36.6625	6.59178	-1.36E+22	2.61E+10	1.87E+18	-5.59E+19	5.33E+06	6.60E+14	6.63E+19	6.48E+08	1.73E+13	-1.18E+20	1.21E+09	8.86E+12
Spinal_cord	10.3566	14.9617	-4.85E+18	5.24E+06	7.59E+14	-1.63E+20	8.04E+09	7.44E+17	-1.32E+23	8.16E+10	1.16E+16	-2.22E+19	1.64E+09	2.98E+12
Spleen	32.6756	7.61242	-2.52E+22	3.47E+10	1.18E+12	1.20E+19	1.93E+06	1.43E+15	7.32E+20	1.82E+09	6.54E+20	-1.06E+20	3.36E+09	2.60E+15
Stomach	30.4541	18.0526	-1.34E+16	3.22E+07	2.11E+19	-5.20E+19	3.27E+09	3.48E+14	-1.09E+23	5.69E+10	1.92E+12	-1.75E+18	5.75E+06	1.05E+18
Tendon_Ligame	12.6737	17.4215	-4.72E+18	5.31E+08	1.66E+17	-8.02E+19	6.41E+09	2.38E+13	-1.12E+23	5.88E+10	7.40E+14	-3.92E+18	3.16E+09	3.36E+20
Thymus	48.1418	1.43796	-4.14E+19	4.33E+09	2.53E+14	-1.66E+18	2.73E+08	1.29E+14	-1.87E+21	2.36E+10	1.28E+17	0	0	0
Trachea	21.1305	9.66304	-1.02E+19	1.15E+07	3.85E+17	-4.38E+19	3.14E+09	1.53E+17	-5.12E+22	5.05E+10	4.33E+17	0	0	0
Ureter_Urethra	22.386	8.15215	2.32E+21	2.75E+06	1.21E+21	-3.67E+22	4.30E+10	1.72E+15	-2.47E+19	2.20E+09	2.05E+14	-4.60E+18	263679	2.16E+15
Vein	15.7355	33.8674	4.00E+19	8.56E+09	1.58E+19	-3.14E+20	8.87E+09	3.87E+12	-3.09E+23	8.48E+10	2.99E+15	-7.28E+18	4.27E+08	1.05E+14
Vertebrae	4.64206	3.67118	-4.92E+18	2.14E+09	3.61E+17	-1.02E+18	3.29E+07	4.64E+12	-2.27E+22	5.80E+10	5.91E+12	-1.44E+20	1.09E+10	2.89E+13

When the inside dipole moves in the stomach, the dipole will rotate and it is necessary to consider the  $x$ ,  $y$  and  $z$  direction polarization of the inside dipole. An example of  $\tau$  when the inside dipole is placed in the stomach is shown in Figure 4.5. The polarization



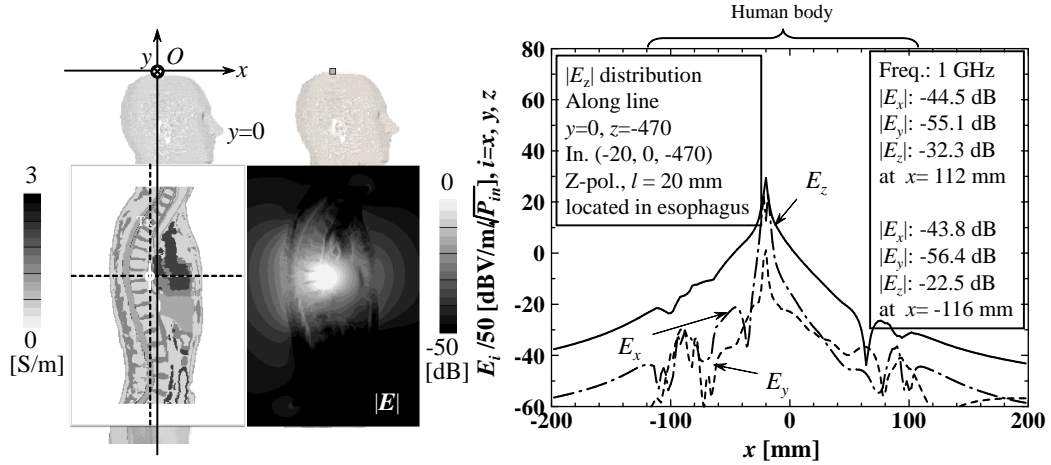
(a) Homogenous human body phantom.



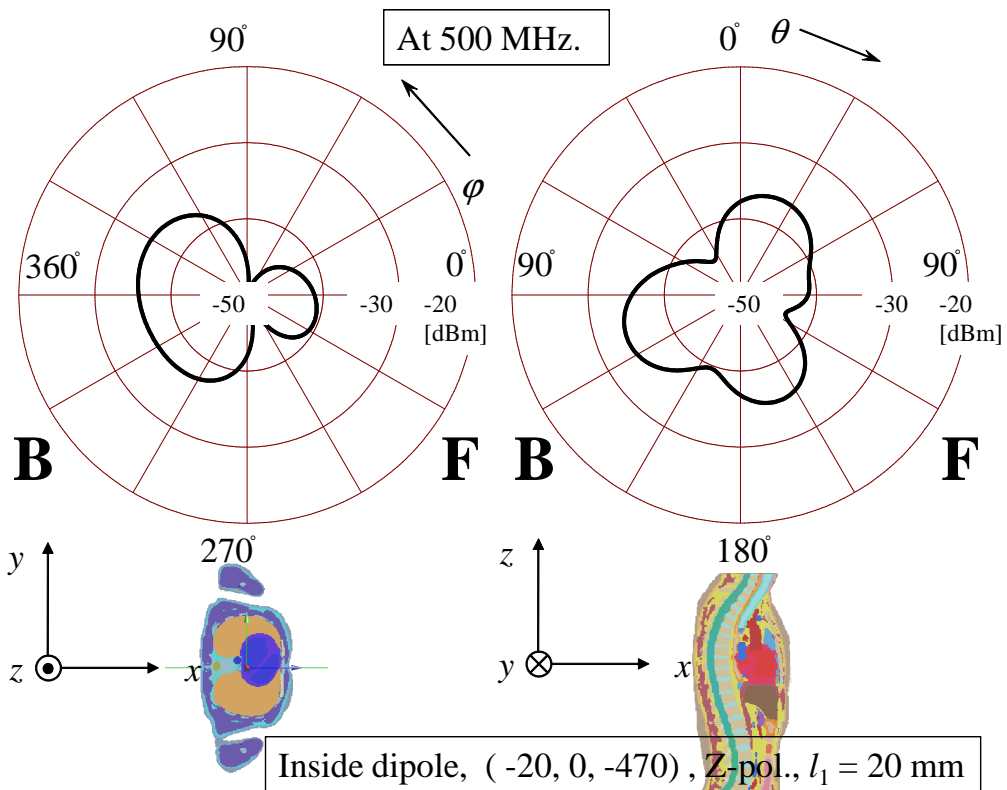
(b) In-homogenous human body phantom.

Figure 4.3: Transmission factor (inside dipole is placed in esophagus).

values of the inside dipole in  $x$ ,  $y$  and  $z$  directions were calculated at  $(x_1, y_1, z_1)=(0, 65, -540)$ , while the polarization values of the outside dipole were settled in the  $z$ -direction at  $(x_2, y_2, z_2)=(112, 65, -540)$ . It is observed that a relatively higher  $\tau$  was obtained when the inside dipole and the outside dipole have the same polarization.



(a)  $E$ -field distribution in the case of in-homogenous human body phantom.



(b) Radiation pattern in the case of in-homogenous human body phantom.

Figure 4.4: Near-field and far-field when the inside dipole is placed in the esophagus.

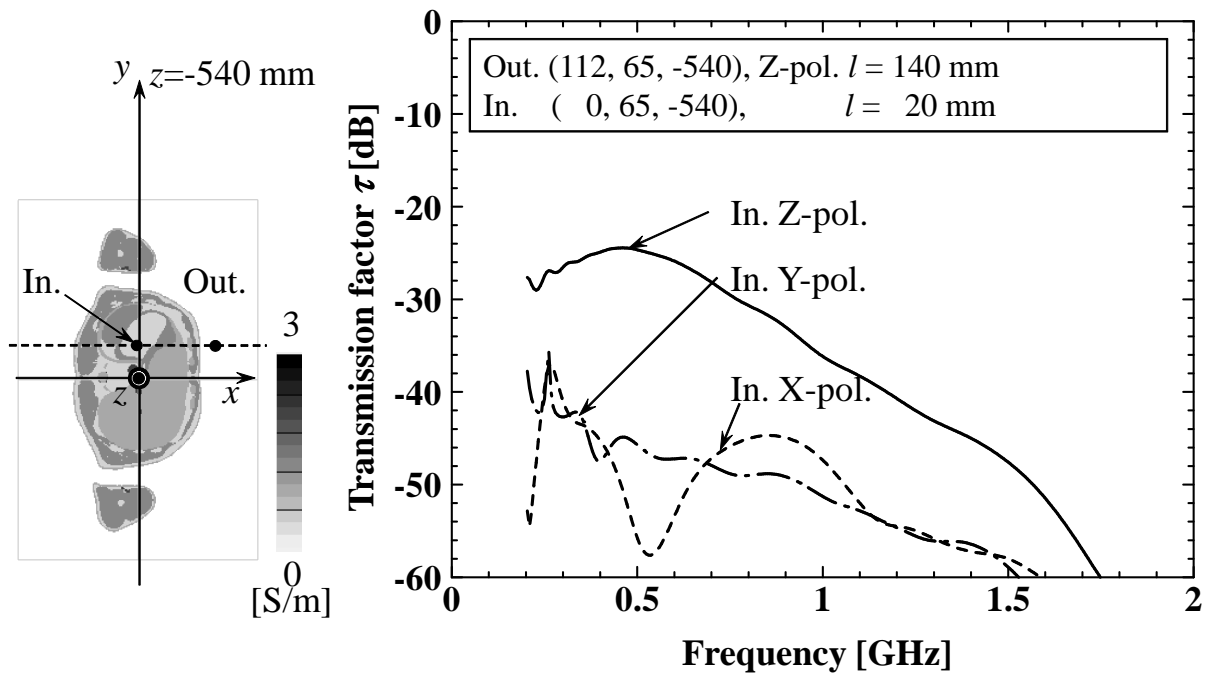


Figure 4.5: Transmission factor (inside dipole is placed in stomach).

When the inside dipole is placed into the small intestine, because the small intestine is very long and coiled in a large area in the middle of the abdomen irregularly, a set of outside dipoles should be considered. For example, under the condition that the inside dipole was placed at  $(x_1, y_1, z_1) = (20, 65, -610)$  in  $z$  direction polarization, three outside dipoles were placed in front of the body with the same coordinate in  $z$  direction and a distance of 40 mm in  $y$  direction. Figure 4.6 shows the results: compared to the case of minimum distance Out.1, there is no obvious decrease in the case of Out. 2 (at a distance of 40 mm from Out.1): in the case of Out. 2 the value is a little larger than the value of Out.1 in a frequency range of 500 MHz to 1 GHz, which is caused by the high conductivity of the small intestine. However, with a distance of 80 mm, the difference is larger than 10 dB, so another outside dipole is necessary to ensure a high value of the transmission factor. The numbers and positions of the outside dipoles used for the small intestine can be determined.

The large intestine surrounds the small intestine. Most of the large intestine is located at the sides of the human body, so it is considered that locating the outside dipole at the sides can obtain a small distance and a high transmission factor. For example, under the



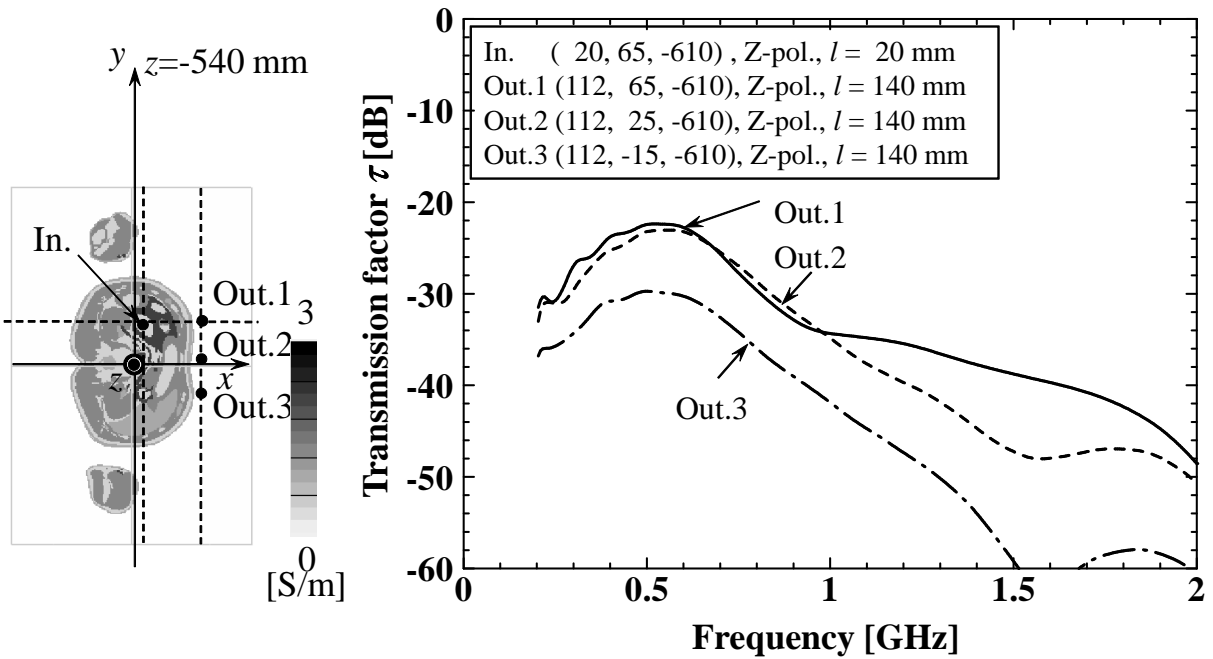


Figure 4.6: Transmission factor (inside dipole is placed in small intestine).

condition that the inside dipole was placed at  $(x_1, y_1, z_1) = (15, 110, -610)$ , as shown in Figure 4.7, when the outside dipole was placed in the left or right side of the human body, the  $\tau$  is 10-15 dB higher than that when the outside dipole was placed at the front of the body.

Table 4.2 shows the typical positions of digestive system the transmission factor in these positions. The positions of inside dipole in digestive system and the distance are performed, it is found that comparing to the esophagus and the stomach, in the case of small and large intestine relatively large value of transmission factor can be obtained for the reason that the distance is short.

## 4.4 Conclusion

In this chapter, the transmission factor from a dipole placed in a digestive system of a human body to the outside was investigated using the FDTD analysis. The effect of human body organs on the propagation loss was investigated and the different results

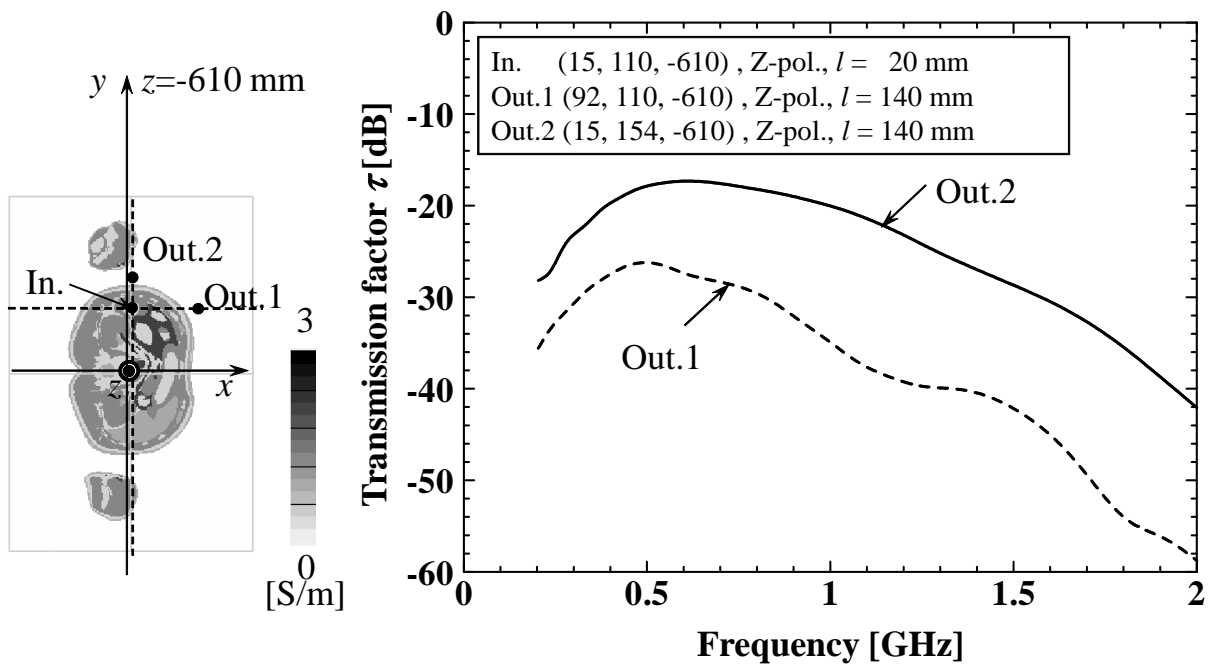


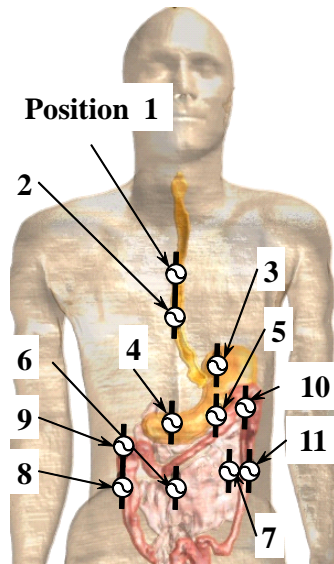
Figure 4.7: Transmission factor (inside dipole is placed in large intestine).

between the homogenous and in-homogenous phantoms were performed and discussed.

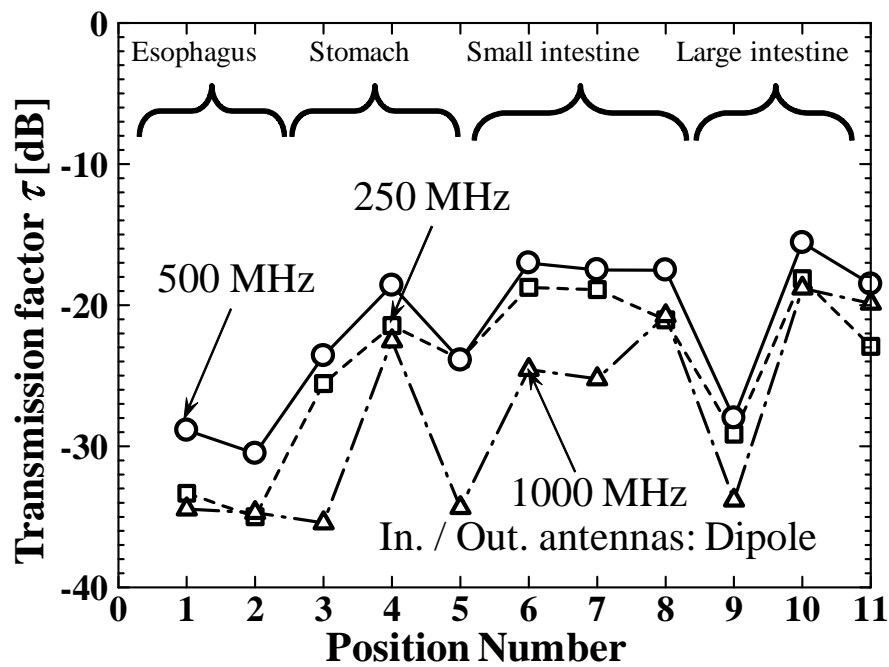
It was found that the peak values of the transmission factor were observed in the frequency range of 400-600 MHz for different organs of the digestive system when the inside dipole and outside dipole have the same polarization. The comparison between homogenous phantom and in-homogenous phantom was shown in Table 4.2.

Compared with homogenous phantom, some different results were obtained in in-homogenous human body phantom. High conductivity organ (such as the heart) reflects EM-wave. It is necessary to consider optimal position of dipole outside body in order to obtain a low propagation loss. In wireless capsule endoscope system, select the optimal position and polarization of outside antenna can decrease the propagation loss through human body.

Table 4.2: Typical positions and transmission factors of digestive system.  
 Typical positions of digestive system



Position No.	Name of tissues	In. (x, y, z) [mm]	Out. (x, y, z) [mm]	Distance d [mm]
1	Esophagus 1	(-15,0,-400)	(-116,0,-400)	101
2	Esophagus 2	(-20,0,-470)	(-116,0,-470)	96
3	Stomach 1	(0,65,-540)	(112,65,-540)	112
4	Stomach 2	(62,0,-610)	(112,0,-610)	50
5	Small intestine 1	(20,65,-610)	(112,65,-610)	92
6	Small intestine 2	(60,0,-720)	(112,0,-720)	52
7	Small intestine 3	(50,65,-700)	(112,65,-700)	62
8	Large intestine 1	(6,-80,-720)	(6,-156,-720)	76
9	Large intestine 2	(26,-40,-650)	(26,-156,-650)	116
10	Large intestine 3	(15,110,-610)	(15,154,-610)	44
11	Large intestine 4	(-12,106,-700)	(-12,156,-700)	50



Transmission factors.

Table 4.3: Comparison between homogenous phantom and in-homogenous phantom.

<b>Phantom</b>	<b>Advantage</b>	<b>Disadvantage</b>
Homogenous	Easy to experiment	Cannot show effects of organs and positions
In-homogenous	Can show effects of organs and positions	Hard to experiment

# Chapter 5

## Capsule antenna design

In this chapter, a capsule dipole to dipole system and a capsule loop to loop system are compared in section 5.1. The results of capsule position offset are performed in section 5.2. The position of antenna and capsule is discussed in section 5.3. An inner-layer capsule dipole antenna is proposed in section 5.4. Finally, conclusions are given in Section 5.5.

### 5.1 Comparison between capsule dipole and capsule loop system

In this chapter, an example of capsule antenna design by using the transmission factor  $\tau$  is presented. The antennas were enclosed by the rectangular column capsule as shown in Figure 5.1. Generally, the capsule has chamfered shape. Under the condition that the antenna is placed inside the capsule, the effect of the shape of the capsule can be ignored. The results of the chamfered shape capsule were proposed previously [56], and the results are the same with the rectangular shaped capsule. In this section, the rectangular shaped capsule was used because it is simple and easy to make voxels in the FDTD analysis. Dimension of the rectangular column capsules are with length of 30 mm and width of 10 mm. To simplify the investigation, relative permittivity of capsule is set as the air ( $\epsilon_r=1$ ).

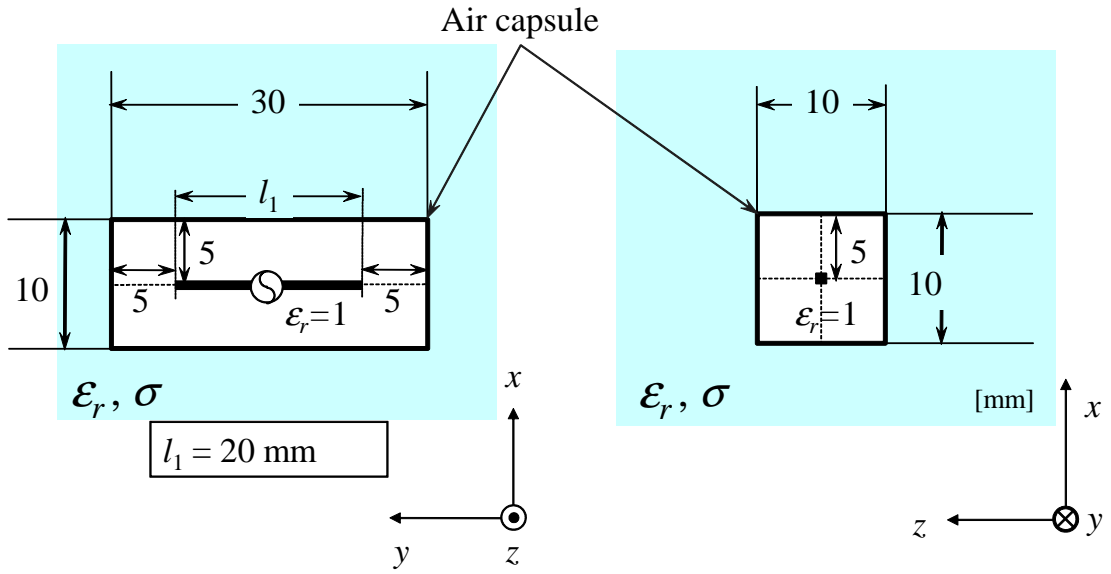
In the case of capsule dipole to dipole system, the antennas and the phantom are

with the same structure as shown in Chapter 3, except for the presence of a rectangular column capsule. A dipole antenna with a length of  $l_2=140$  mm was placed outside the phantom. A capsule dipole antenna with a length of  $l_1=20$  mm was placed in the phantom as shown in Figure 5.1 (a).

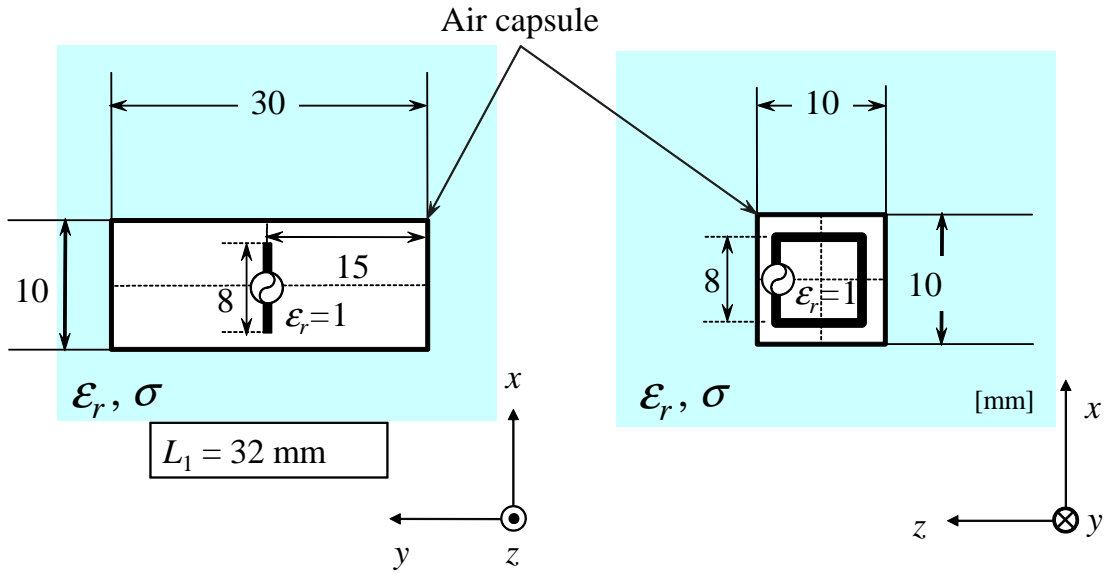
In the case of capsule loop to loop system, the antennas and the phantom are with the same structure as shown in Chapter 3, except for the presence of a rectangular column capsule. A rectangular loop antenna with a loop length of  $L_2=280$  mm was placed outside the phantom. A rectangular capsule loop antenna with a loop length of  $L_1=32$  mm was placed in the phantom as shown in Figure 5.1 (b). The analysis models were shown in Figure 5.2. The dipole and loop antenna have the same electrical length.

Figure 5.3 shows the transmission factor  $\tau$  and Figure 5.4 shows the relative received power of capsule dipole antenna and capsule loop antenna through torso-shaped phantom, respectively. In the case of capsule dipole antenna, it has been found that there is a local maximum of the transmission factor  $\tau$  at a frequency, which is also observed in the case without the capsule enclosure. As an example of the internal impedances,  $Z_S=4.91+j2248.6 \Omega$  and  $Z_L=18.6+j467.2 \Omega$  can be selected and it can be used as the external matching circuits. It is noted that large value of  $\tau = -21.6$  dB at 490 MHz is observed which is 3.7 dB larger than the case without capsule at 695 MHz. This increment of the transmission factor  $\tau$  is considered that the feeding point of dipole antenna is not contact to the lossy liquid by the presence of a capsule enclosure.

In the case of capsule loop antenna, the transmission factor  $\tau$  is quite large especially in the low frequency range. Under the conditions  $Z_S=0.03-j19 \Omega$  and  $Z_L=14.9-j370 \Omega$ , a large value of  $\tau=-14.7$  dB has been obtained at the lowest frequency of 200 MHz. This will be caused by the strong magnetic-coupling between two loop antennas in the near-field region, while this phenomenon was not appeared between two dipole antennas. In our previous research, the power-transmission efficiency could approach very high if the loop was small and the distance between antennas was short enough in the air [51]. In capsule antenna applications, because in a conductive medium the average magnetic field energy density is larger than the average electric field energy density, a magnetic type antenna such as a capsule loop antenna, having a smaller electric field than an electric type antenna in the near-field region in the low frequency region, is preferred to obtain a large relative received power. In the case of capsule dipole antenna, a local maximum of



(a) Capsule dipole antenna.



(b) Capsule loop antenna.

Figure 5.1: Geometry of capsule antennas.

transmission factor is observed at frequency domain. In the case of capsule loop antenna, the transmission factor decreases as frequency increases monotonously. The transmission factor of capsule loop antenna is larger than that of the capsule dipole antenna in the low frequency region, while the performances of both two systems are almost the same in the high frequency region.

## 5.2 Study on the capsule antenna offset

To confirm the phenomena in Figure 5.3, it is important to consider the transmission factors through torso-shaped phantom under the condition that the capsule antenna and the outside antenna are located in an offset position.

Figure 5.5 shows the analysis model transmission factors when the position of capsule antenna is offset from the outside antenna in the  $-z$  direction with the offset value  $\Delta z$ , and Figure 5.6 shows the transmission factors as a function of frequency. In the case of dipole to dipole, the null of transmission factor appeared:  $\Delta z=50$  mm at 1.5 GHz;  $\Delta z=90$  mm at 700 MHz and 1.4 GHz. In the case of loop to loop,  $\Delta z=90$  mm the transmission factor decreases seriously at 800 MHz.

Figure 5.7 shows the transmission factors as a function of the offset value  $\Delta z$ . Two frequencies of 80 MHz and 402 MHz were observed as lower and higher frequency. The transmission factor decreases as  $\Delta z$  increases in a broadband frequency range. In the case of 80 MHz, it is found that the transmission factor of the loop to loop is larger than that of the dipole to dipole, while the transmission factor is reduced in the range of  $\Delta z=30$  mm to  $\Delta z=90$  mm. In the case of 402 MHz, the transmission factor of the dipole to dipole is almost the same as that of the loop to loop and the results in Figure 5.7 are confirmed.

## 5.3 Study on the position of antenna

In this section, the positions of the dipole antenna and the capsule are considered. Geometries of two kinds capsule antennas are investigated as shown in Figure 5.8: (a) the dipole antenna is placed inside the capsule with a distance  $d=4$  mm to the center axis, the antenna is isolated from the human body liquids so it can be called “Isolated type antenna”; (b) the dipole antenna is placed on the interface of the capsule with a distance  $d=5$  mm to the center axis, the antenna is surface touched to the human body liquids so it can be called “Surface type antenna”.

Figure 5.9 shows the reflection coefficient of capsule dipole antennas in the cases of isolated type ( $d=4$  mm) and surface type ( $d=5$  mm) capsule antennas. It is found that in



the case of isolated type antenna ( $d=4$  mm), the reflection coefficient is very large in the frequency range of 200 MHz to 2 GHz, the  $|S_{11}|$  is almost 0 dB. However, in the case of surface type antenna ( $d=5$  mm), the reflection coefficient is relatively small from 1 GHz to 2 GHz.

Figure 5.10 shows the input impedance of capsule dipole antennas in the cases of isolated type ( $d=4$  mm) and surface type ( $d=5$  mm) capsule antennas. In the case of isolated type antenna ( $d=4$  mm), the dipole antenna with a length of 20 mm is an electric small antenna (comparing to the wavelength) in the simulation frequency range. Resistance is quite small ( $R_{in} < 20 \Omega$ ), while reactance is capacitive ( $X_{in} < 0$ ). In the case of surface type antenna ( $d=5$  mm), resistance becomes large as compared to the separated type antenna capsule antenna. Also, it is observed that the reactance is 0 at 1.2 GHz and 2.1 GHz. The wavelength in dielectric liquid becomes small. Assuming that the effective dielectric permittivity of  $\lambda_g = (\epsilon_r + 1)/2$  when the dipole is implemented on the surface of the capsule, the effective wavelength  $\lambda_g$  at 1.2 GHz becomes 50 mm when  $\epsilon_r = 49$ , which is closer to the twice of the length of dipole  $l_1 = 20$  mm.

Figure 5.11 shows the  $|S_{21}|$  from capsule antenna through torso-shaped phantom to the outside antenna. In the case of surface type antenna ( $d=5$  mm), high transmission coefficient of -28.9 dB at 1 GHz was obtained. On the other hand, the maximum value in the case of isolated type antenna ( $d=4$  mm) is -57.4 dB, the value is small comparing to the case of surface type antenna. These results show that large value of transmission coefficient is obtained when the dipole antenna is implemented on the surface of the capsule, and it is considered that the effective electric length increases with the presence of liquid. The half-wavelength resonant frequency of the receiving antenna at Port 2 is 1 GHz; the local maximum of  $|S_{21}|$  in the frequency domain can be changed to other frequencies by changing the operating frequency of the receiving antenna. Also, it is observed that the transmission coefficient were almost the same between the case of without the capsule (Chapter 3) and on the surface of the capsule (Figure 5.8, surface type antenna ( $d=5$  mm)), and it is considered that a dipole antenna implemented on the surface of the capsule has almost the same transmission characteristics as the case of dipole antenna immersed in the HBEL without the capsule.

Figure 5.12 shows the transmission factor from capsule antenna through torso-shaped phantom to the outside antenna. It is found that there is a local maximum in the fre-

quency domain. Because the conductivity loss becomes large when the dipole antenna was touched to the liquid, the value of  $\tau$  in the case of surface type antenna ( $d=5$  mm) is smaller than that in the cases of isolated type antenna ( $d=4$  mm). In the case of isolated type antenna ( $d=4$  mm), under the conditions  $Z_S=3.02+j2467.22 \Omega$  and  $Z_L=18.62-j467.14 \Omega$  a large value of  $\tau=-20.0$  dB is obtained at 500 MHz. Briefly summarize, in the case of dipole antenna implemented inside the capsule (surface type antenna), the value of transmission factor is large while the impedance matching condition is not good, additional matching circuits are necessary. In the case of dipole antenna implemented on the surface of the capsule (isolated type antenna), the impedance matching condition is good while the value of transmission factor is small. The relative permittivity of material surrounding the antenna affects the matching condition and the conductivity of material surrounding the antenna affects the transmission factor.

## 5.4 Inner-layer capsule dipole antenna

To obtain a capsule antenna has both the good impedance matching performance such as surface type antenna ( $d=5$  mm), also has the small conductivity loss (high  $\tau$ ) such as isolated type antenna ( $d=4$  mm), an inner-layer capsule dipole antenna (ICDA) is proposed as shown in Figure 5.13. Dimension of the rectangular column capsules are with length of 30 mm and width of 10 mm. The relative permittivity of capsule is set as the air ( $\epsilon_r=1$ ). An inner-layer with thickness of 2 mm was made inside the capsule. The dipole antenna was placed at the same position as that in the case of isolated type antenna ( $d=4$  mm). Deionized water was used to fill the inner-layer for the reason that its relative permittivity is large and conductivity is small as compared to the HBEL.

Figure 5.14 shows the results of  $|S_{21}|$  (matching to  $50 \Omega$ ) from the proposed ICDA through torso-shaped phantom to the outside antenna. Figure 5.14(a) shows the results when the outside antenna with length of  $l_2=140$  mm (operating frequency: 1GHz): in the case of ICDA, a relatively high value of  $|S_{21}|=-26.6$  dB was obtained; while in the case of isolated type antenna ( $d=4$  mm), the maximum value is -53.8 dB at 980 MHz. Figure 5.14(b) shows the results when the outside antenna with length of  $l_2=280$  mm (operating frequency: 500 MHz): in the case of ICDA, a relatively high value of  $|S_{21}|=-30.4$  dB was obtained; while in the case of separated type antenna ( $d=4$  mm), the maximum value

is -61.6 dB at 500 MHz. Comparing to the case of without inner-layer (isolated type antenna), the impedance matching condition becomes better and large value of  $|S_{21}|$  is obtained.

Figure 5.15 shows the results of transmission factor  $\tau$  from the proposed ICDA through torso-shaped phantom to the outside antenna. Comparing to the isolated type antenna ( $d=4$  mm) and surface type antenna ( $d=5$  mm), the transmission factor  $\tau$  of ICDA has the most high value, especially around 500 MHz. The high conductivity loss of HBEL has been eliminated.

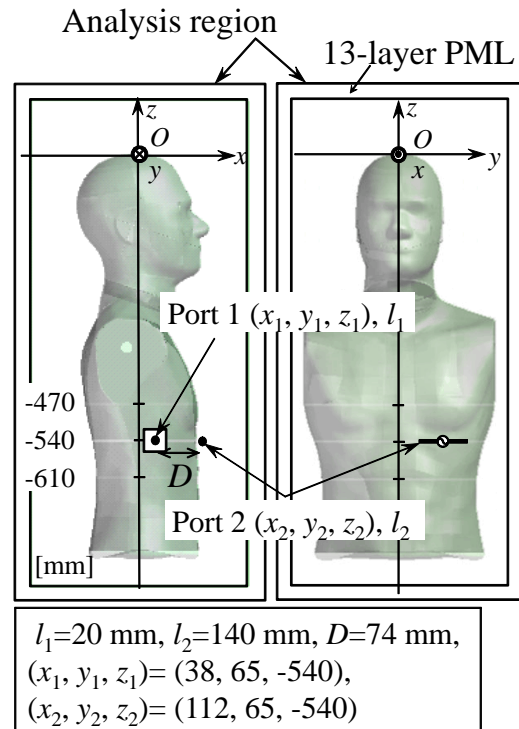
Figure 5.16 shows the results of the relative received power at the outside antenna. In the case of isolated type antenna ( $d=4$  mm), under the conditions  $Z_S=10.2+j2306 \Omega$  and  $Z_L=18.9+j480 \Omega$ , a large received power of -24.7 dBm is obtained at 500 MHz and the 3dB bandwidth is 28 MHz. In the case of proposed ICDA, under the conditions  $Z_S=50 \Omega$  and  $Z_L=50 \Omega$ , an acceptable power of -30.4 dBm is obtained at 500 MHz and a wide 3dB bandwidth 90 MHz is obtained. Above all, the proposed ICDA has an acceptable impedance matching performance to  $50 \Omega$  in the frequency range of 500 MHz to 1GHz.

## 5.5 Conclusion

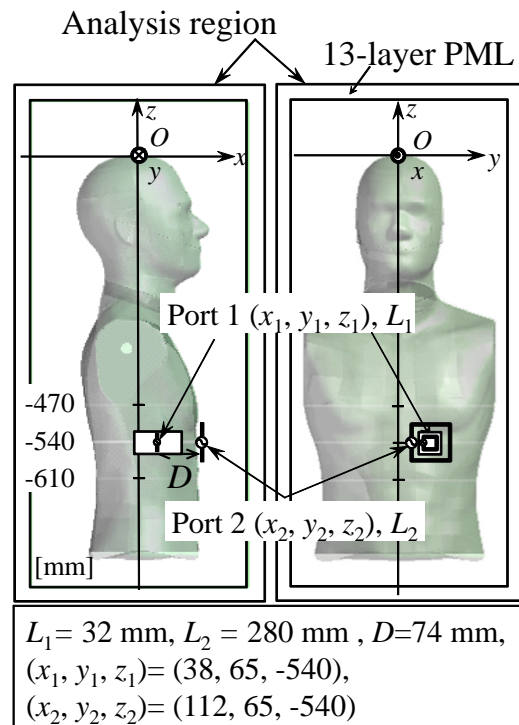
In this chapter, capsule antenna design was investigated. EM-wave propagation characteristics of capsule dipole to dipole system and capsule loop to loop system were performed and compared in the frequency range 200 MHz to 3 GHz. In the case of capsule dipole to dipole system, it is observed that there is a local maximum in the transmission factor at 490 MHz. In the case of capsule loop to loop system, the value of transmission factor is large in low frequency range: under the conditions  $Z_S=0.03-j19 \Omega$   $Z_L=14.9-j370 \Omega$  a large value of  $\tau=-14.7$  dB has been obtained at the lowest frequency of 200 MHz. The position of antenna and capsule was discussed. In the case of the antenna is separated from the human body liquids “Isolated type antenna”, the conductivity loss is small while the impedance matching is bad in the frequency range of 200 MHz- 2 GHz. In the case of the antenna is touched to the human body liquids “Surface type antenna”, the impedance matching is good in the frequency range of 1 GHz-2 GHz, while the conductivity loss is large. In practical applications, if the size of a capsule is strictly limited, the antenna can be implemented on the surface of the capsule to save space, and matching circuits are not

---

required. Otherwise, if high transmission factor is required, antenna implemented inside the capsule with matching circuits is preferred: for dipole antennas the local maximum of transmission factor in the frequency domain should be used, while for loop antennas, the large value of transmission factor in low frequency should be used. An inner-layer capsule dipole antenna (ICDA) was proposed, it has both good impedance matching performance  $50 \Omega$  and the small conductive loss in the frequency range of 500 MHz to 1GHz. Although conical models of the antennas were used in the numerical analysis models, these results and observations are general and fundamental. They can provide theoretical insight on how to design capsule antennas by using transmission factor. In practice, the antenna geometry can be designed to be very complex and the results in this study are still applicable.



(a) Capsule dipole to dipole system.



(b) Capsule loop to loop system.

Figure 5.2: Analysis model of capsule antenna systems.

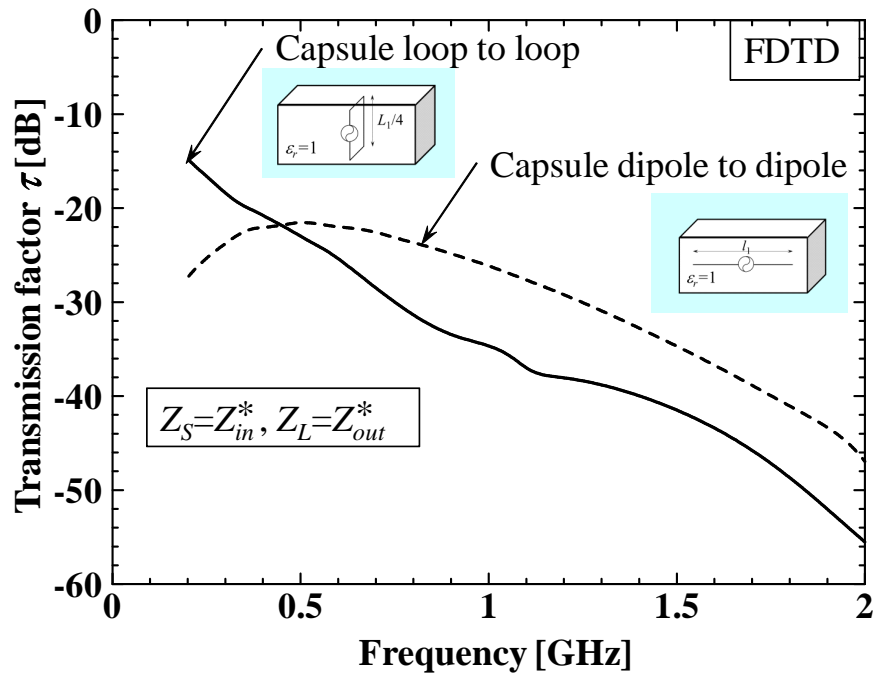


Figure 5.3: Transmission factors of capsule dipole system and capsule loop system through torso-shaped phantom.

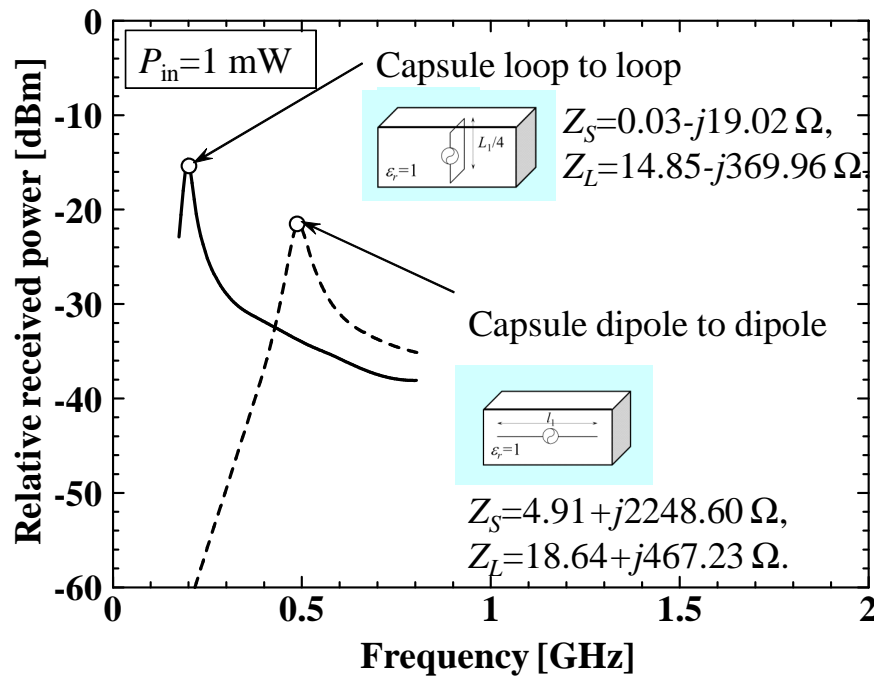
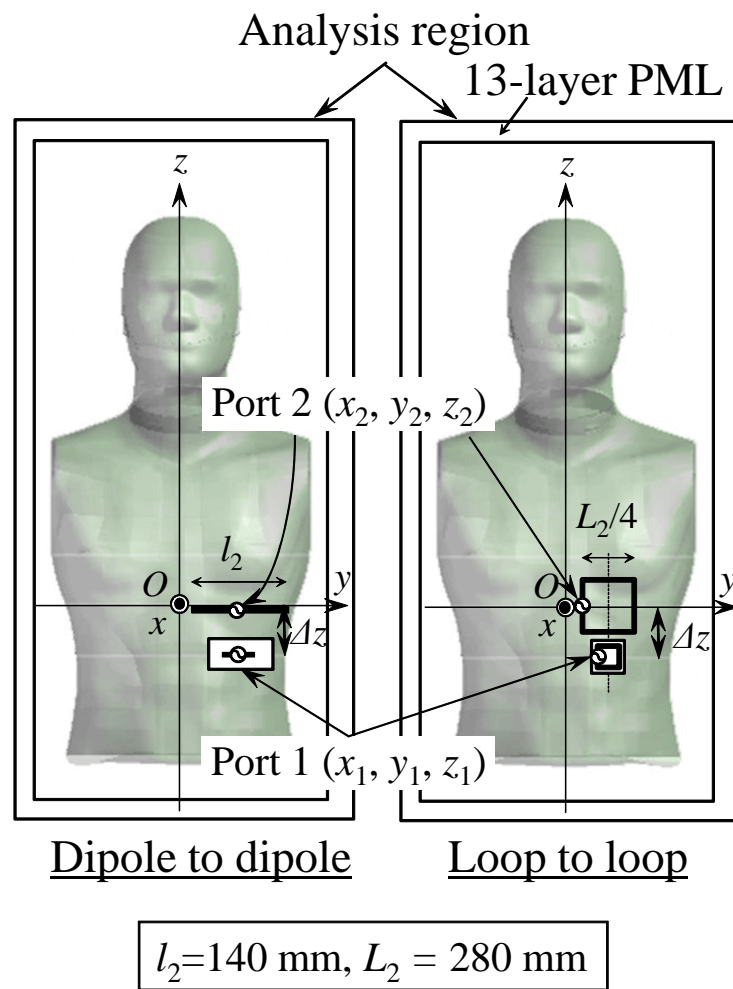
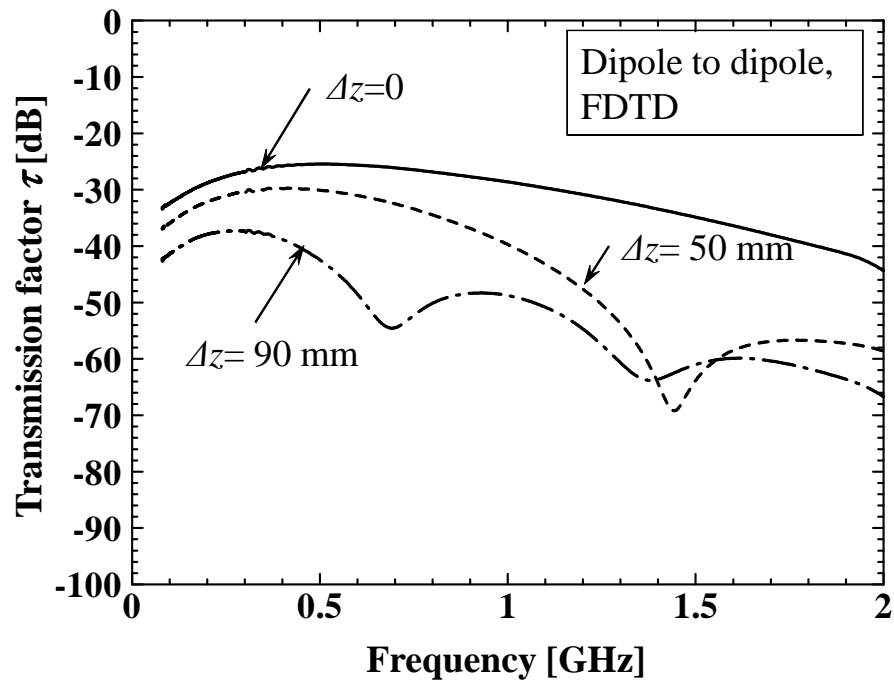
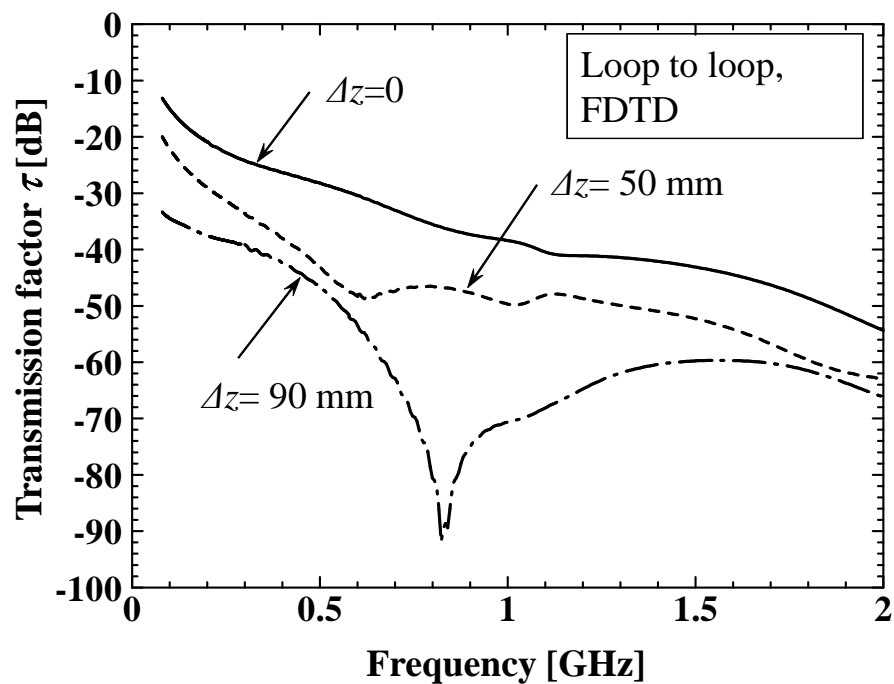


Figure 5.4: Relative received power from the capsule antenna to the outside antenna.

Figure 5.5: Analysis model of capsule antenna  $\Delta z$ .



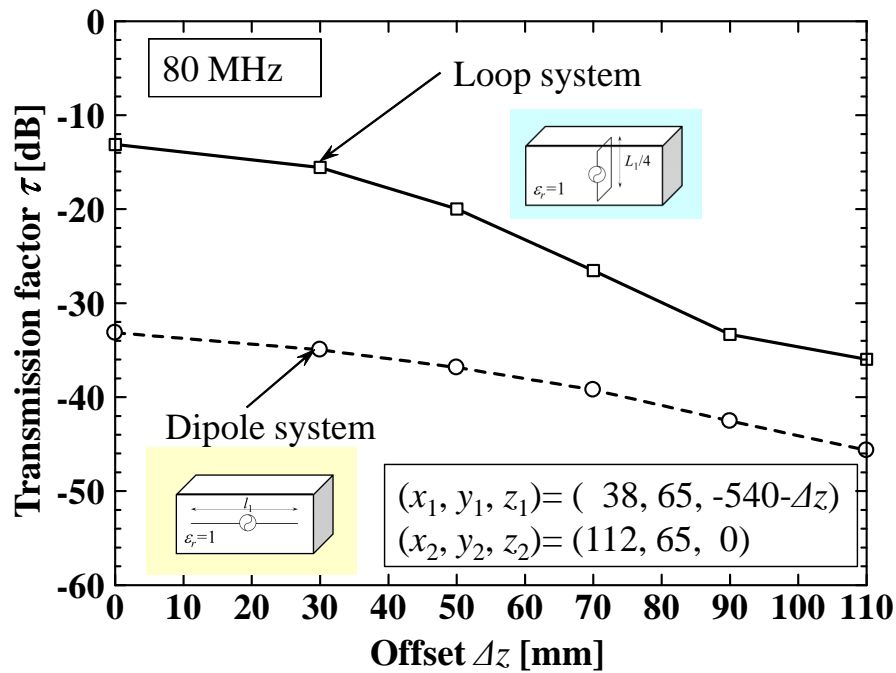
(a) Dipole to dipole.



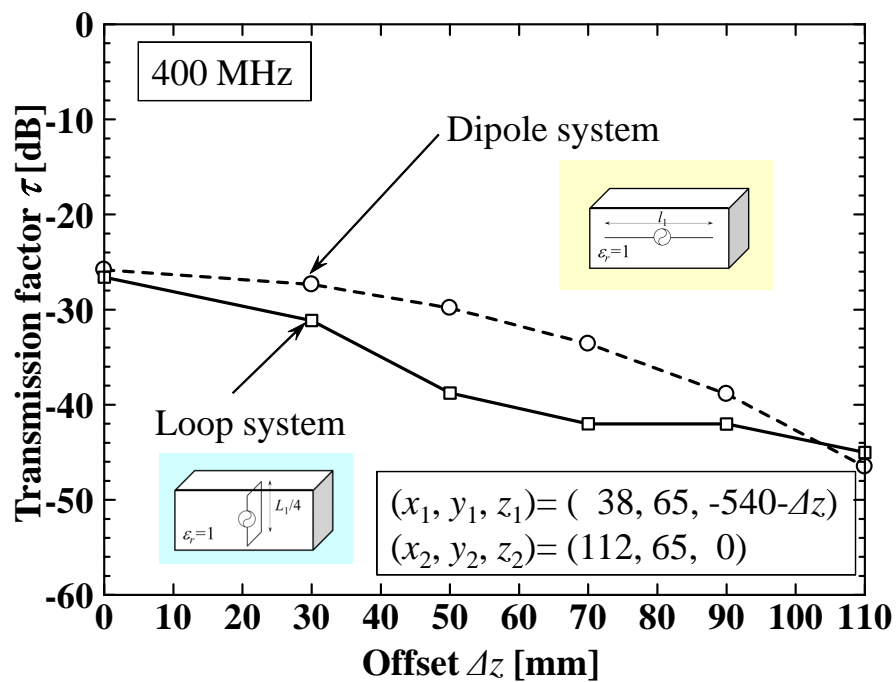
(b) Loop to loop.

Figure 5.6: Transmission factors when position of capsule antenna is offset from the outside antenna in the  $-z$  direction (function of frequency).





(a) 80 MHz.



(b) 402 MHz.

Figure 5.7: Transmission factors when position of capsule antenna is offset from the outside antenna in the  $-z$  direction (function of offset  $\Delta z$ ).

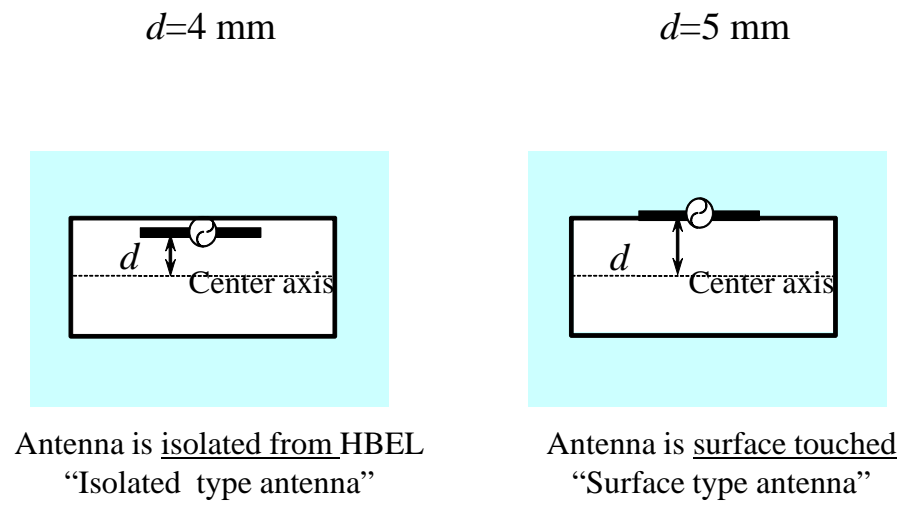
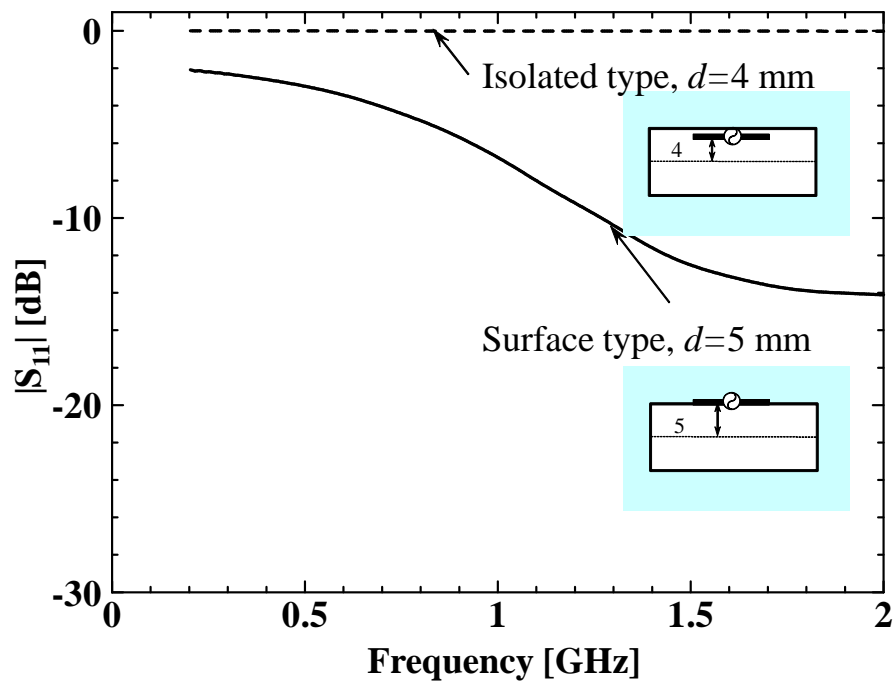
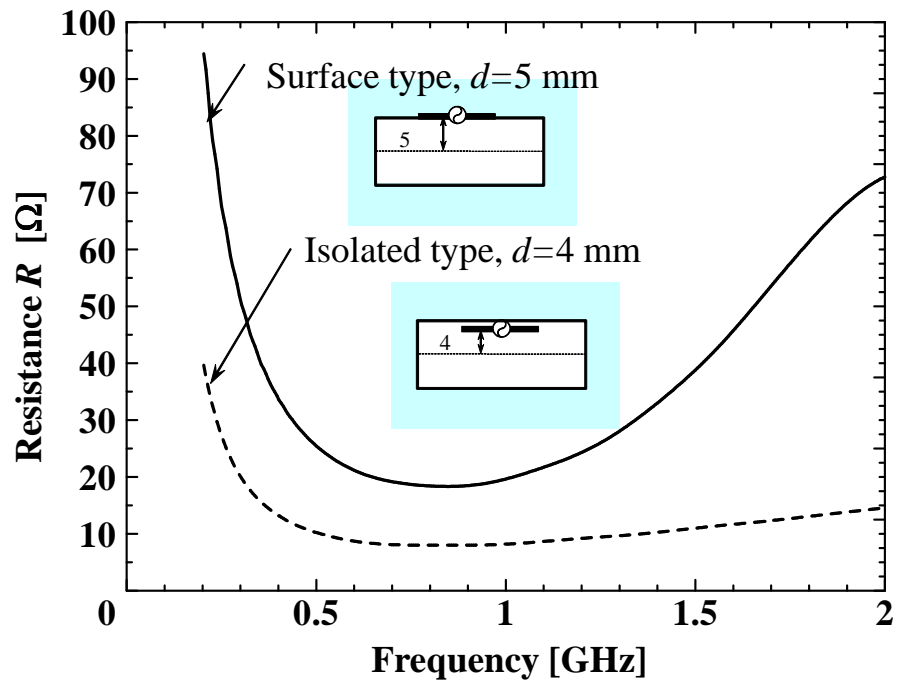
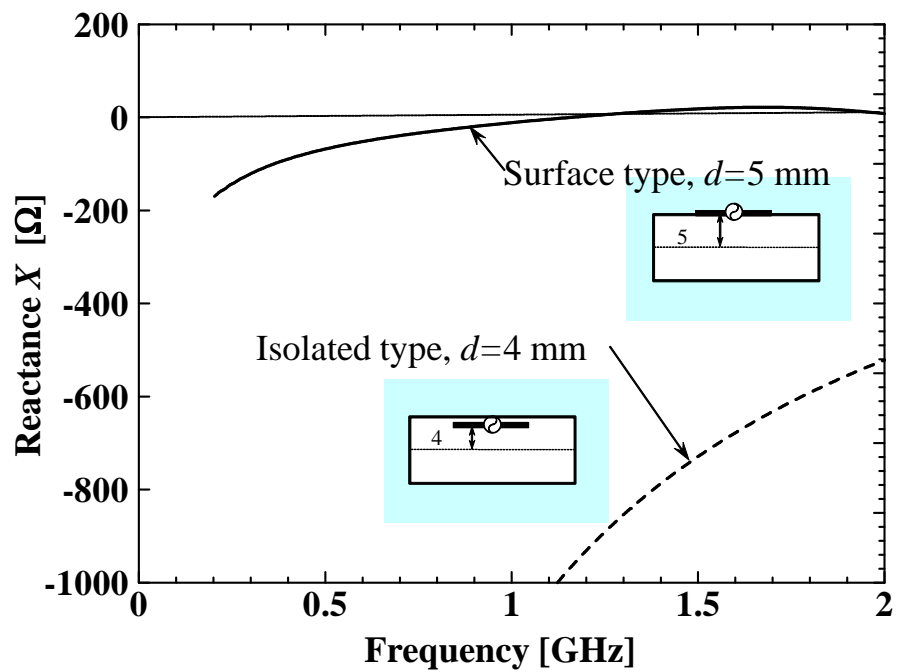


Figure 5.8: Geometry of capsule dipole antennas.

Figure 5.9:  $|S_{11}|$  of capsule dipole antenna in HBEL.



(a) Resistance.



(b) Reactance.

Figure 5.10: Input impedance of capsule dipole antenna in HBEL.

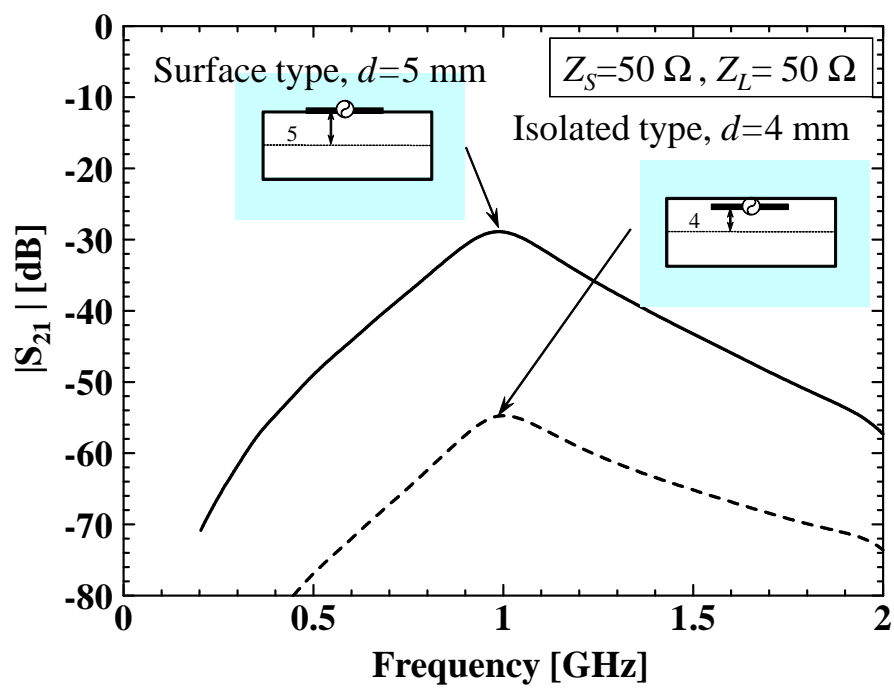


Figure 5.11:  $|S_{21}|$  from capsule antenna through torso-shaped phantom to the outside antenna.

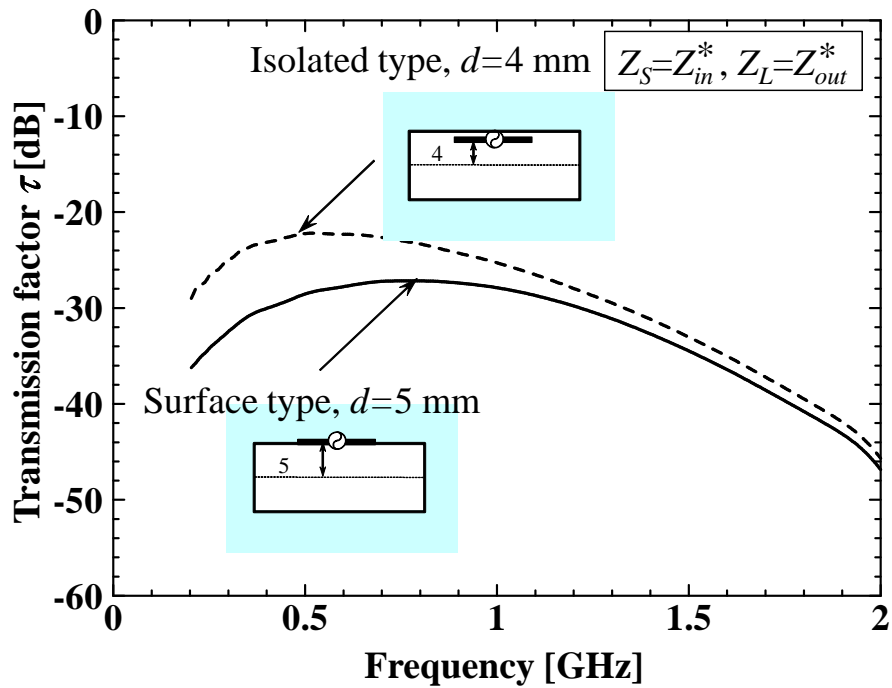


Figure 5.12: Transmission factor from capsule antenna through torso-shaped phantom to the outside antenna.

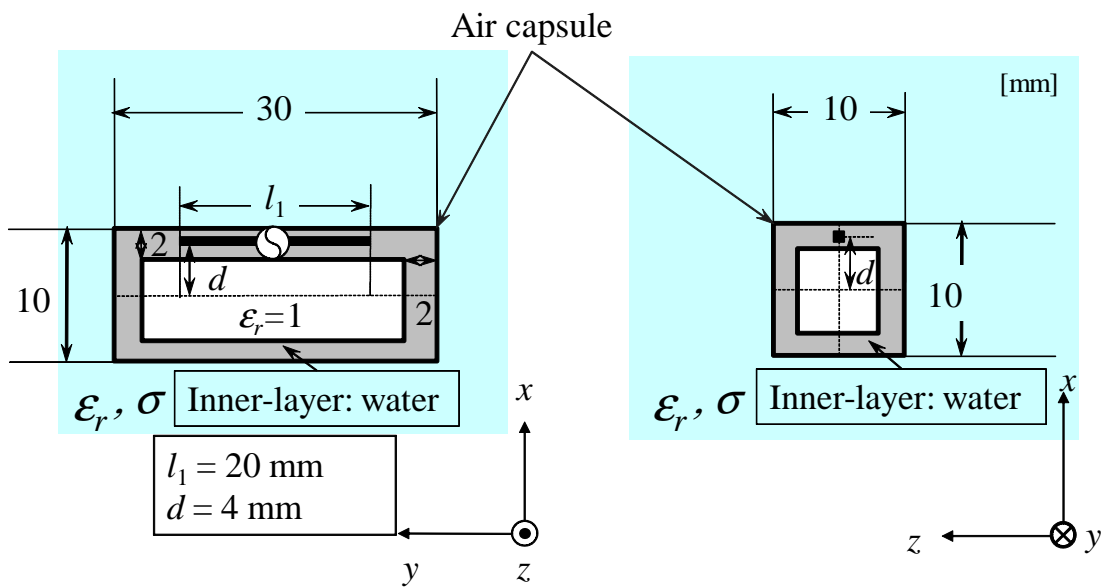
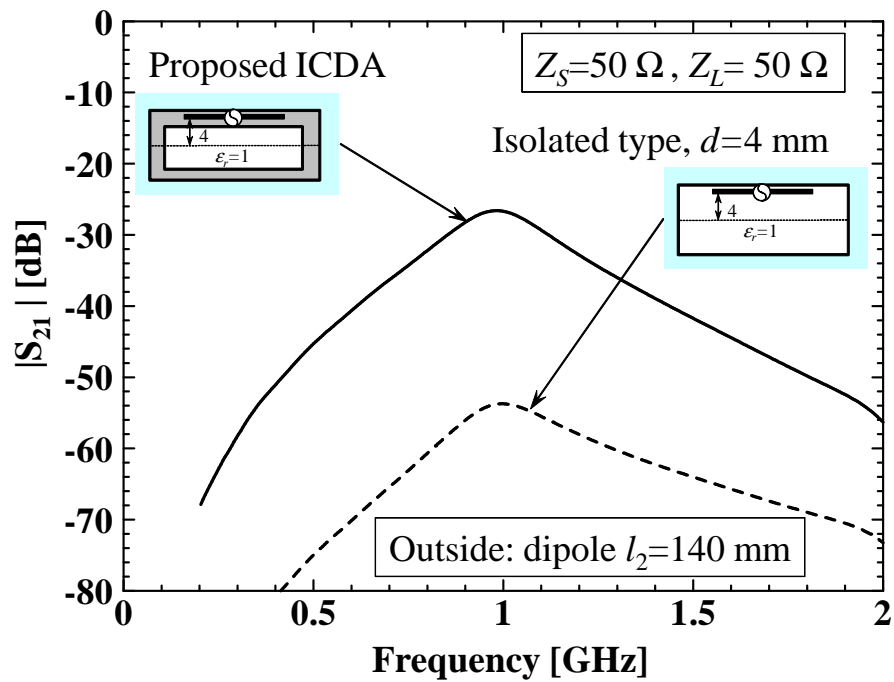
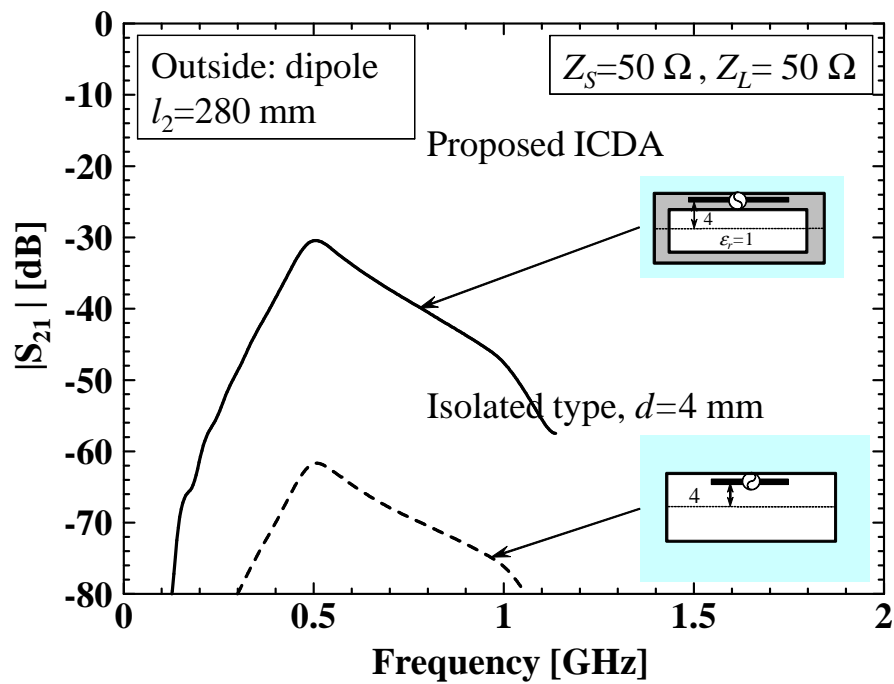


Figure 5.13: Geometry of proposed ICDA.

(a) Outside antenna: dipole  $l_1 = 140$  mm.(b) Outside antenna: dipole  $l_2 = 280$  mm.Figure 5.14:  $|S_{21}|$  from the proposed ICDA through torso-shaped phantom to the outside antenna.

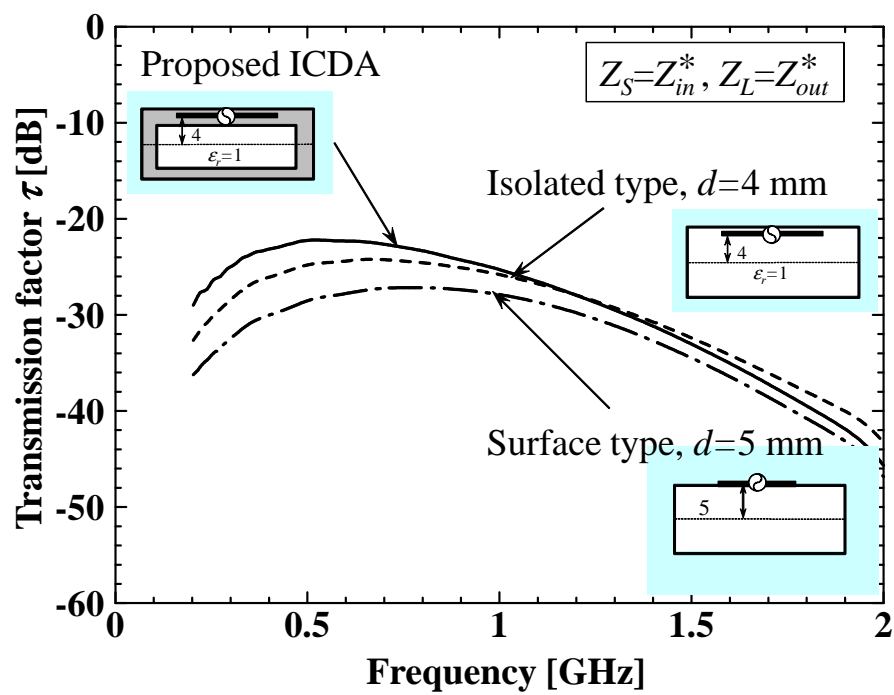


Figure 5.15: Transmission factor from the proposed ICDA through torso-shaped phantom to the outside antenna.

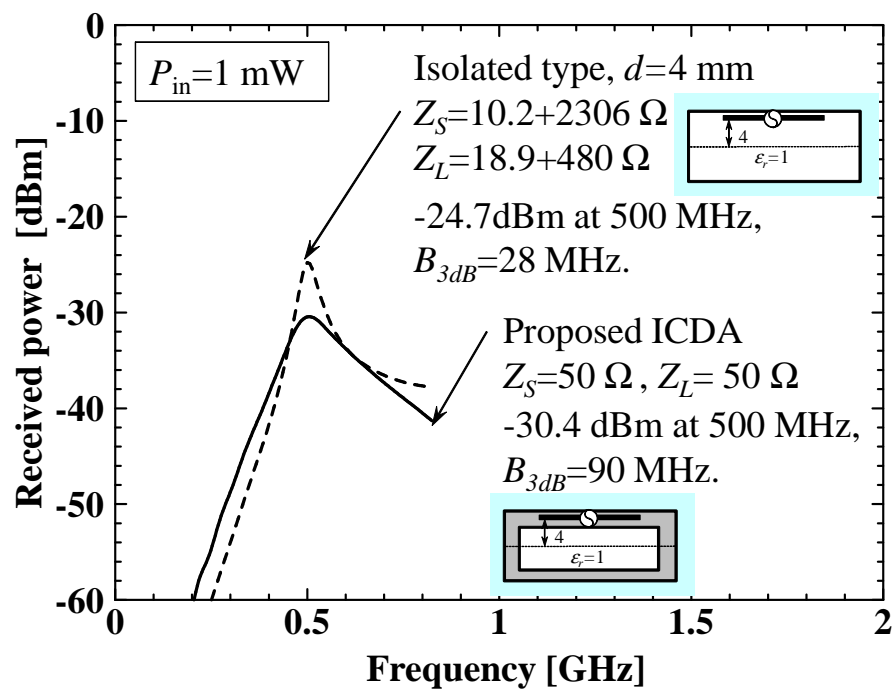


Figure 5.16: Relative received power from the proposed ICDA to the outside antenna.



# Chapter 6

## Conclusions

In this dissertation, to study a methodology to develop a wireless capsule for medical diagnostics with high transmission efficiency, the propagation loss of EM-wave pass through human body has been investigated by using numerical Finite Difference Time Domain (FDTD) method and experimental differential-mode S-parameter method. The dissertation is basically subdivided into two main themes. One is “Propagation loss of EM-wave through human body (Chapter 3, Chapter 4)”. The other is “Capsule antenna design (Chapter 5)”. In Chapter 3, a pair of dipole and a pair of loop antennas were placed inside and outside a torso-shaped phantom used, respectively, and the propagation loss excluding impedance-mismatching loss was evaluated by both the numerical and the experimental method to select the suitable antenna type. The transmission factor is the relative maximum received power under the condition that the complex-conjugate matching conditions are satisfied at both transmitting and receiving ports. Investigate propagation loss when capsule is inside some organs in Chapter 4, the propagation loss from a dipole antenna placed in a digestive system of a human body to the outside was investigated by using the FDTD analysis. In chapter 5, capsule antenna design was investigated.

Firstly, the numerical FDTD method and experiment differential-mode S-parameter method were presented in Chapter 2. In this chapter, numerical analysis and measurement of a dipole antenna placed inside deionized water to the dipole outside were performed. The measured results are compared with the numerical analysis. Under the condition that: 1) the dispersive effect of relative permittivity and conductivity of liquid was considered in

the FDTD analysis 2) differential-mode S-parameter method was used in the experiment, good agreement of S-parameters was obtained between numerical analysis and experiment results in a broadband frequency range. The reliability of both measurements and analysis were confirmed.

Furthermore, propagation loss of macrowave through homogenous human body phantom was investigated in Chapter 3. Using the validated methods in Chapter 2, the transmission characteristics of a dipole placed in the torso-shaped phantom filled with deionized water or human body equivalent liquid (HBEL) to the dipole outside were presented. In order to eliminate the effect of antenna impedance mismatching, transmission factor was used as an indicator of propagation loss. The transmission factor of a dipole to dipole system was performed and it is found that there is a local maximum in the frequency range. The local maximum was caused by the effective length of the inside antenna. It is found that in low frequency range the antenna efficiency is small while in high frequency range the media loss is large. If the wireless capsule endoscope (WCE) system operates at an optimal frequency, a relatively high received power can be obtained. If the operating frequency was decided, a relative high received power can be obtained by changing the length of inside antenna. The transmission factor of a loop to loop system was also performed and different result with dipole to dipole was obtained.

In addition, propagation loss of microwave through in-homogenous human body phantom was investigated in Chapter 4. The transmission factor from a dipole placed inside the digestive system of a human body to the dipole outside was investigated by using FDTD analysis. It is found that the local maximum of the transmission factor changes as the position of digestive system changed, almost in the frequency range of 400-600 MHz for the different organs of the digestive system. The effect of high conductivity organ (such as the heart) on the propagation loss was performed. Under the condition that the outside antenna was placed in an optimal position and polarization, a relatively high received power can be obtained.

Finally, in Chapter 5 the capsule antenna design was investigated. Two types of traditional capsule antennas, capsule dipole antenna and capsule loop antenna are compared and the guideline in designing capsule antennas by using transmission factor is also proposed. In the case of capsule dipole to dipole system, it is observed that there is a local maximum in the transmission factor at 490 MHz. In the case of capsule loop to loop

system, the value of transmission factor is large in low frequency range. The position of antenna and capsule was discussed. In the case of the antenna is isolated from the human body liquids “Isolated type antenna”, the conductivity loss is small while the impedance matching is bad in the frequency range of 200 MHz- 2 GHz. In the case of the antenna is surface touched to the human body liquids “Surface type antenna”, the impedance matching is good in the frequency range of 1 GHz-2 GHz, while the conductivity loss is large. An inner-layer capsule dipole antenna (ICDA) was proposed, it has both good impedance matching performance and the small conductive loss.

This study makes a significant contribution to the theory of microwave propagate through human body. The further deep study on the above field will certainly bring a breakthrough in genetic theory of EM-wave application on human body healthcare and significant effect on the small antenna design technology as well.

# Bibliography

- [1] J. O. Sines, "Permanent implants for heart rate and body temperature recording in the rat," *AMA Arch. Gen. Psychiatry*, vol. 2, no. 2, pp. 182-183, 1960.
- [2] R. S. Mackay and B. Jacobson, "Endoradiosonde," *Nature*, vol. 179, pp. 1239-1240, 1957.
- [3] R. S. Mackay, "Radio telemetering from within the human body," *Science*, vol. 134, pp. 1196-1202, 1961.
- [4] L.C. Chirwa, P.A. Hammond, S. Roy, and D.R.S. Cumming, "Radiation from ingested wireless devices in biomedical telemetry bands," *Electron. Lett.*, vol.39, no.2, pp.178-179, Jan. 2003.
- [5] L.C. Chirwa, P.A. Hammond, S. Roy, and D.R.S. Cumming, "Electromagnetic radiation from ingested sources in the human intestine between 150 MHz and 1.2 GHz," *IEEE Trans. Biomed. Eng.*, vol. 50, no. 4, pp. 484-492, Apr. 2003.
- [6] M.R. Yuce and T. Dissanayake, "Easy-to-swallow wireless telemetry," *IEEE Microwave Magazine*, vol. 13, pp. 90-101, September-October 2012.
- [7] E.A. Johannessen, "Biocompatibility of a lab-on-a-pill sensor in artificial gastrointestinal environments," *IEEE Trans. Biomed. Eng.* vol. 53 pp. 2333-2340 Nov. 2006.
- [8] P. Valdastri, A. Menciassi, and P. Dario, "Transmission power requirements for novel ZigBee implants in the gastrointestinal tract," *IEEE Trans. Biomed. Eng.* vol. 55 pp. 1705-1710 June 2008.
- [9] X. Chen, X. Zhang, L. Zhang, X.W. Li, N. Qi, H. Jiang, and Z. Wang, "A Wireless Capsule Endoscope System With Low-Power Controlling and Processing ASIC,"

- 
- IEEE Transactions on Biomedical Circuits and Systems, vol.3, no.1, pp.11-22, Feb. 2009.
- [10] K. Wang, G. Yan, P. Jiang, and D. Ye, "A wireless robotic endoscope for gastrointestinal," *IEEE Trans. Robot.* vol. 24 pp. 206-210 Feb. 2008.
- [11] Y.K. Moon, J.H. Lee, H.J. Park, J.G. Lee, J.J. Ryu, S.H. Woo, M.K. Kim, C.H. Won, T.W. Kim, J.H. Cho, and H.C. Choi, "Fabrication of the wireless systems for controlling movements of the electrical stimulus capsule in the small intestines," *IEICE Trans. Inf. Syst.* vol. E90-D no. 2 Feb. 2007.
- [12] H. Cao, V. Landge, U. Tata, Y.S. Seo, S. Rao, S.J. Tang, H.F. Tibbals, S. Spechler, and J. Chiao, "An implantable, batteryless, and wireless capsule with integrated impedance and pH sensors for gastroesophageal reflux monitoring," *IEEE Trans. Biomed. Eng.*, vol. 59, no. 11, pp. 3131-3139, Nov. 2012.
- [13] A. Christ, M. Douglas, J. Nadakuduti, E.B. Cooper, A.P. Sample, B.H. Waters, J R. Smith, and N. Kuster, "Evaluation of wireless resonant power transfer systems with human electromagnetic exposure limits," *IEEE Trans. Electromagn. Compat.*, vol. 55, no. 2, pp. 265C274, Apr. 2013.
- [14] A. Christ, M. Douglas, J. Nadakuduti, and N. Kuster, "Assessing human exposure to electromagnetic fields from wireless power transmission systems," *Proc. IEEE*, vol. 101, pp. 1482-1493, Jun. 2013.
- [15] X.L. Chen, A.E. Umenei, D.W. Baarman, N. Chavannes, V.D. Santis, J.R. Mosig, and N. Kuster, "Human exposure to close-range resonant wireless power transfer systems as a function of design parameters," *IEEE Trans. Electromagn. Compat.*, vol. 56, no. 5, pp. 1027-1034, Oct. 2014.
- [16] K. Na, H. Jang, H. Ma, and F. Bien, "Tracking optimal efficiency of magnetic resonance wireless power transfer system for biomedical capsule endoscopy," *IEEE Trans. Microw. Theory Techn.*, vol. 63, no. 1, pp. 295-304, Jan. 2015.
- [17] S.M. Kim, J.I. Moon, I.K. Cho, J.H. Yoon, W.J. Byun, and H.C. Choi, "Advanced power control scheme in wireless power transmission for human protection from EM field," *IEEE Trans. Microw. Theory Tech.*, vol. 63, no. 3, pp. 847-856, Mar. 2015.

- 
- [18] Q.W. Yuan and T. Ishikawa, "Effect of via-wheel power transfer system on human body," 2013 IEEE Wireless Power Transfer (WPT), pp. 238-241, 2013.
- [19] G. Iddan, G. Meron, A. Glukhovsky, and P. Swain, "Wireless capsule endoscopy," *Nature*, vol.405, no.6785, p.417, May 2000.
- [20] A. Glukhovsky, "Wireless capsule endoscopy," *Sensor Rev.*, vol.23, no.2, pp.128-133, 2003.
- [21] J. Thone, S. Radiom, D. Turgis, R. Carta, G. Gielen, and R. Puers, "Design of a 2 Mbps FSK near-field transmitter for wireless capsule endoscopy," *Sens. Actuators A Phys.* vol. 156 pp. 43-48 Nov. 2009.
- [22] <http://www.givenimaging.com/Pages/default.html>
- [23] <http://www.medivators.com/products/gi-physician-products/mirocam-capsule-endoscope>
- [24] <http://medical.olympusamerica.com/procedure/capsule-endoscopy>
- [25] <http://www.jinshangroup.com/>
- [26] S.T. Kwak, K. Chang, and Y.J. Yoon, "The helical antenna for the capsule endoscope system," in *Proc. IEEE Antennas Propag. Symp.*, vol. 2B, pp. 804-807, Jul. 2005
- [27] S.T. Kwak, K. Chang, and Y.J. Yoon, "Small spiral antenna for wideband capsule endoscope system," *Electron. Lett.*, vol. 42, no. 23, pp. 1328-1329, Nov. 2006.
- [28] S.H. Lee and Y.J. Yoon, "Fat arm spiral antenna for wideband capsule endoscope systems," *Proc. IEEE Radio. Wireless Symp.*, pp.579-582, Jan. 2010.
- [29] K. Kim, S. Lee, E. Cho, J. Choi and S. Nam, "Design of OOK system for wireless capsule endoscopy," *Proc. IEEE Int. Symp. Circuits Syst.*, pp.1205-1208, May-Jun. 2010.
- [30] S.H. Lee, J. Lee, Y. J. Yoon, S. Park, C. Cheon, K. Kim, and S. Nam, "A wideband spiral antenna for ingestible capsule endoscope systems: Experimental results in a human phantom and a pig," *IEEE Trans. Biomed. Eng.*, vol. 58, no. 6, pp. 1734-1741, Jun. 2011.

- 
- [31] S. Yun, K. Kim and S. Nam, "Outer wall loop antenna for ultra wideband capsule endoscope system," *IEEE Antennas Wireless Propag. Lett.*, vol.9, pp.1135-1138, Dec. 2010.
- [32] K. Kim, S. Yun, S. Lee, S. Nam, Y.J. Yoon, and C. Cheon, "A Design of a High-Speed and High-Efficiency Capsule Endoscopy System," *IEEE Transactions on biomedical engineering*, vol. 59, no. 4, April 2012
- [33] T.S.P. See, Z.N. Chen, and X. Qing, "Implanted and external antennas for 915-MHz capsule endoscopy," *Proc. IEEE 2011 Int. Workshop on Antennas. Tech.*, pp.29-32, Mar. 2011.
- [34] P.M. Izdebski, H. Rajagopalan, and Y. Rahmat-Samii, "Conformal ingestible capsule antenna: A novel chandelier meandered design," *IEEE Trans. Antennas Propag.*, vol.57, no.4, pp.900-909, Apr. 2009.
- [35] H. Rajagopalan, K.S. Shin, J. Kina, C.O. Chui, and Y. Rahmat-Samii, "A Smart Diagnostic Capsule with a Novel Antenna and Nano-Biosensors," 2012 6th European Conference on Antennas and Propagation (EUCAP)
- [36] Q. Wang, K. Wolf, and D. Plettemeier, "An UWB capsule endoscope antenna design for biomedical communications," *Proc. 3rd Int. Symp. Appl. Sci. Biomed. Commun. Technol.*, pp.1-6, Nov. 2010.
- [37] T. Dissanayake, K.P. Esselle, and M.R. Yuce, "Dielectric loaded impedance matching for wideband implanted antennas," *IEEE Trans. Microw. Theory Tech.*, vol. 57, no. 10, pp. 2480-2487, Oct. 2009.
- [38] T. Dissanayake, M.R. Yuce and C.K. Ho, "Design and evaluation of a compact antenna for implant-to-air UWB communication," *IEEE Antennas and Wireless Prop. Letters*, vol. 8, pp.153 - 156, 2009.
- [39] K. Ito, K. Saito, and M. Takahashi, "Small antennas for medical applications," *Proc. IEEE 2007 Int. Workshop on Antennas. Tech.*, pp.116-119, Mar. 2007.
- [40] H. Yu, G.S. Irby, D.M. Peterson, M.T. Nguyen, G. Flores, N. Euliano, and R. Bashir-ullah, "Printed capsule antenna for medication compliance monitoring," *Electron. Lett.*, vol. 43, 22, pp. 41-44, 2007.

- 
- [41] A. Alomainy and Y. Hao, "Modeling and characterization of biotelemetric radio channel from ingested implants considering organ contents," *IEEE Trans. Antennas Propag.*, vol.57, no.4, pp.999-1005, Apr. 2009.
- [42] D. Kurup, W. Joseph, G. Vermeeren, and L. Martens, "In-body Path Loss Model for Homogeneous Human Tissues," *IEEE Trans. Electromagn. Compat.*, vol.54, no.3, pp.556-564, Jun. 2012.
- [43] D. Kurup, W. Joseph, G. Vermeeren, and L. Martens, "Specific absorption rate and path loss in specific body location in heterogeneous human model," *Microwaves, Antennas and Propagation, IET*, vol.7, no.1, pp.35-43, Jan. 2013
- [44] Z.N. Chen, G.C. Liu, and T.S.P. See, "Transmission of RF Signals Between MICS Loop Antennas in Free Space and Implanted in the Human Head," *IEEE Trans. Antennas Propag.*, vol.57, no.6, pp.1850-1854, Jun. 2009.
- [45] W. Xia, M. Takahashi, and K. Ito, "Performances of an implanted cavity slot antenna embedded in the human arm," *IEEE Trans. Antennas Propag.*, vol.57, no.4, pp.894-899, Apr. 2009.
- [46] N. Ishii, T. Akagawa, K. Sato, L. Hamada, and S. Watanabe, "A Method of Measuring Gain in Liquids Based on the Friis Transmission Formula in the Near-Field Region," *IEICE Trans. Communications*, vol.E90-B, no.9, pp.2401-2407, 2007.
- [47] A. Taflove, "Application of the finite-difference time-domain method to sinusoidal steady state electromagnetic penetration problems," *IEEE Trans. on Electromagnetic Compatibility*. 22 (3): 191-C202, 1980
- [48] A. Taflove, and S.C. Hagness, "Computational Electrodynamics: The Finite-Difference Time-Domain Method," 3rd ed. Artech House Publishers, 2005.
- [49] A. Taflove and M.E. Brodwin, "Computation of the electromagnetic fields and induced temperatures within a model of the microwave-irradiated human eye," *IEEE Trans. on Microwave Theory and Techniques*. 23 (11): 888-C896, 1975.
- [50] A. Saeedfar, H. Sato, and K. Sawaya, "Numerical and Experimental Impedance Analyses of Dipole Antenna in the Vicinity of Deionized Water at Different Temperatures," *IEICE Trans. Communications*, vol. E91-B, no. 3, pp. 963-967, 2008.



- 
- [51] T. Fukasawa, T. Yanagi, H. Miyashita, and Y. Konishi, "Extended S-parameter Method Including Radiation Pattern Measurements of an Antenna," *IEEE Trans. Antennas Propag.*, vol.60, no.12, pp.5645-5653, Dec. 2012.
- [52] <https://www.speag.com/products/em-phantom/phantoms/>
- [53] S. Gabriel, R.W. Lau, and C. Gabriel, "The dielectric properties of biological tissues: II. Measurements in the frequency range 10 Hz to 20 GHz," *Phys. Med. Biol.*, vol. 41, pp. 2251-2269, 1996.
- [54] S. Gabriel, R.W. Lau, and C. Gabriel, "The dielectric properties of biological tissues: III. Parametric models for the dielectric spectrum of tissues," *Phys. Med. Biol.*, vol. 41, no. 11, pp. 2271-2293, Nov. 1996.
- [55] Y. Li, H. Sato, and Q. Chen, "FDTD Analysis of Capsule Dipole Antenna in the Digestive System of A Human Body," *IEICE Communication Express*, Vol.X6-B, No.6, pp.276-280, Jun. 2017.
- [56] Y. Li, H. Sato, and Q. Chen, "Experiment Study of Transmission Characteristics Through Conducting Human Body Equivalent Liquid," *IEICE Communication Express*, Vol.X6-B, No.6, pp.286-291, Jun. 2017.
- [57] Q. Chen, K. Ozawa, Q.W. Yuan, and K. Sawaya, "Antenna Characterization for Wireless Power-Transmission System Using Near-Field Coupling," *IEEE Trans. Antennas Propag. Magazine*, vol.54, no.4, pp.108-116, Aug. 2012.
- [58] D. Pozar, *Microwave Engineering*. Hoboken, NJ, USA: Wiley, 2011.
- [59] G. Gonzalez, *Microwave Transistor Amplifiers: Analysis and Design (2nd Edition)*. NJ, USA: Prentice-Hall, 1996.
- [60] <https://www.itis.ethz.ch/database>

# Publications

## Journal papers:

- [1] Y. Li, H. Sato, and Q. Chen, "Experiment Study of Transmission Characteristics Through Conducting Human Body Equivalent Liquid," *IEICE Communication Express*, Vol.X6-B, No.6, pp.286-291, Jun. 2017.
- [2] Y. Li, H. Sato, and Q. Chen, "FDTD Analysis of Capsule Dipole Antenna in the Digestive System of A Human Body," *IEICE Communication Express*, Vol.X6-B, No.6, pp.276-280, Jun. 2017.
- [3] Y. Li, H. Sato, and Q. Chen, "Capsule Antenna Design based on Transmission Factor through the Human Body," *IEICE Transactions on communications*, Vol.E101-B, No.2, pp.-, Feb. 2018.

## Peer reviewed international conferences:

- [1] H. Sato, Y. Li, and Q. Chen, "Measurement of dipole antenna in deionized water," in *Proc. International Symposium on Antennas and Propagation (ISAP 2015)*, S3.8.7, pp. 618-620, Tasmania, Australia, Nov. 2015.
- [2] H. Sato, Y. Li, and Q. Chen, "Experimental Study of Transmission Factor Through Conducting Human Body Equivalent Liquid," in *Proc. International Symposium on Antennas and Propagation (ISAP 2016)*, 4B2-1, pp. 990-991, Okinawa, Japan, Oct. 2016.
- [3] Y. Li, H. Sato and Q. Chen, "FDTD Analysis of Capsule Dipole Antenna in Digestive System of Human Body," in *Proc. International Symposium on Antennas and Propagation (ISAP 2016)*, 4B2-2, pp. 992-993, Okinawa, Japan, Oct. 2016.

- 
- [4] Y. Li, H. Sato and Q. Chen, "Study on Propagation Loss through Human Body for Wireless Capsule Application," in Proc. International Symposium on Antennas and Propagation (ISAP 2017). (Submitted)

## **Domestic conferences and technical meetings:**

- [1] Y. Li, H. Sato and Q. Chen, "Measurement of Dipole Antenna in Deionized Water," IEICE Society Conference, B-1-57, Aug. 2015.
- [2] Y. Li, H. Sato and Q. Chen, "Design of Capsule Dipole Antenna for Ingestible Endoscope," IEICE Technical Report, Feb 2016.
- [3] H. Sato, Y. Li, and Q. Chen, "Comparison between Capsule Dipole and Capsule Loop Antenna on Transmission Characteristics through Human Body," IEICE Society Conference, B-1-107, Sept. 2016.
- [4] Y. Li, H. Sato and Q. Chen, "Study on Propagation Loss through Human Body for Wireless Power Transfer Applications," IEICE Technical Report, Jun 2017.
- [5] H. Sato, Y. Li, and Q. Chen, "Design of Inner-Layer Capsule Dipole Antenna for Ingestible Endoscope," IEICE Society Conference, Sept. 2017.

## **Educational conferences:**

- [1] Y. Li, H. Sato and Q. Chen, "Frequency Dependence of Radiation Efficiency of Antennas Inside Human Body," 伝送工学研究会, Jun 2015.
- [2] Y. Li, H. Sato and Q. Chen, "Transmission Characteristics of EM-wave from a Capsule Dipole Antenna Located in the Human Body Phantom," 伝送工学研究会, Jul. 2015.
- [3] Y. Li, H. Sato and Q. Chen, "Maximum Received Power from a Capsule Dipole Antenna in Digestive System of Human Body," 伝送工学研究会, May 2016.
- [4] Y. Li, H. Sato and Q. Chen, "Capsule Antenna Design based on Transmission Factor through Human Body," 伝送工学研究会, May 2017.

# Acknowledgement

First and foremost, I would like to show my deepest gratitude to my supervising professor Qiang Chen, a respectable, responsible and resourceful scholar, who has provided me with valuable guidance in every stage of my research. His keen and vigorous academic observation enlightens me not only in this research but also in my future study and work.

I shall extend my thanks to Prof. Noriharu Suematsu and Prof. Yuji Matsuura for their interest in my research and taking time to join my dissertation defense meeting. I also appreciate the encouragement and elicitation from these two professors.

I wish to acknowledge Prof. Qiaowei Yuan for her support and encouragement.

I also wish to acknowledge Assistant Prof. Hiroyasu Sato for his support and advice. He had spent lots of time to discuss with me about the research.

My sincere appreciation also goes to Assistant Prof. Keisuke Konno, Dr. Kuan-hua Chen, Dr. Kaizhi Zhang, Dr. Tao Hong, Yiwen Zhu, and Sirao WU for their helpful explanations and comments in the discussions of my research.

I would also like to extend my appreciation to COI STREAM (Center of Innovation Science and Technology based Radical Innovation and Entrepreneurship Program) who supports me a lot in this research.

I am most grateful to the financial support, Japanese Government scholarship during my study and living period in Japan.

Last but not least, I would like to thank my parents, my wife Xingxing Yan, especially my daughter for their support and help.

July, 2017